-A086 268 ACUREX CORP MOUNTAIN VIEW CA F/G 16/1

DEVELOPMENT AND TESTING OF A TWO-STAGE HYBRID LAUNCHER.(U)

OCT 79 K E SUCHSLAND, J D WATSON, T J DAHM DNA001-76-C-0407

UNCLASSIFIED ACUREX-FR-79-19/AS(7386) DNA-5074F NL

1 OF 2

AD A086268

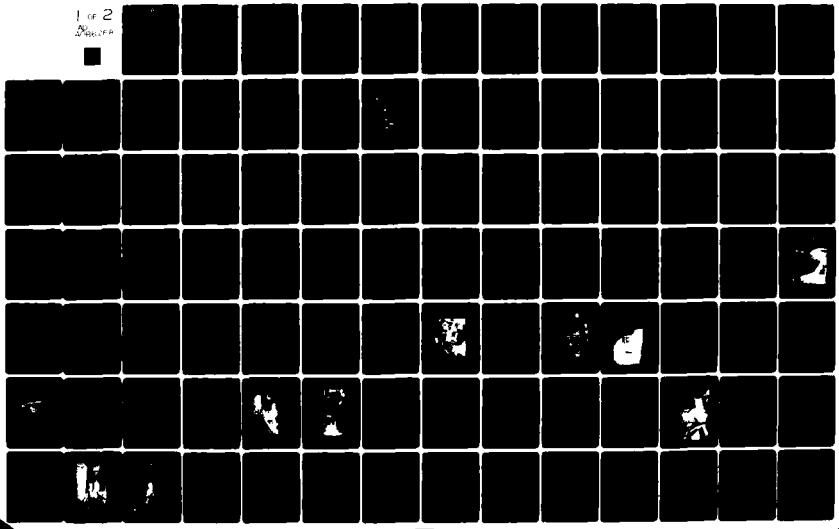

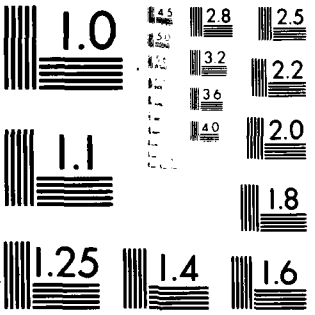

MICROCOPY RESOLUTION TEST CHART

(12) LEVEL II

AD-E300807

DNA 5074F

ADA086268

DEVELOPMENT AND TESTING OF A TWO-STAGE HYBRID LAUNCHER

Acurex Corporation/Aerotherm Group
485 Clyde Avenue
Mountain View, California 94042

31 October 1979

Final Report for Period 1 September 1977—31 October 1979

CONTRACT No. DNA 001-76-C-0407

APPROVED FOR PUBLIC RELEASE;
DISTRIBUTION UNLIMITED.

THIS WORK SPONSORED BY THE DEFENSE NUCLEAR AGENCY
UNDER RDT&E RMSS CODE B342079464 N99QAXAI12904 H2590D.

DDC FILE COPY

Prepared for
Director
DEFENSE NUCLEAR AGENCY
Washington, D. C. 20305

DTIC
ELECTE
JUL 7 1980
S D
B

80 6 11 010

Destroy this report when it is no longer needed. Do not return to sender.

PLEASE NOTIFY THE DEFENSE NUCLEAR AGENCY, ATTN: TISI, WASHINGTON, D.C. 20305, IF YOUR ADDRESS IS INCORRECT, IF YOU WISH TO BE DELETED FROM THE DISTRIBUTION LIST, OR IF THE ADDRESSEE IS NO LONGER EMPLOYED BY YOUR ORGANIZATION.

UNCLASSIFIED

SECURITY CLASSIFICATION OF THIS PAGE (When Data Entered)

12 173

REPORT DOCUMENTATION PAGE

READ INSTRUCTIONS BEFORE COMPLETING FORM

1. REPORT NUMBER: DNA 5074F

2. GOVT ACCESSION NO.: AD-A086268

3. RECIPIENT'S CATALOG NUMBER:

4. TITLE (and Subtitle): 6 DEVELOPMENT AND TESTING OF A TWO-STAGE HYBRID LAUNCHER

5. TYPE OF REPORT & PERIOD COVERED: 9 Final Report, for Period 1 Sep 77—31 Oct 79

6. PERFORMING ORG. REPORT NUMBER: 14 ACUREX-FR-79-19/AS 7386

7. AUTHOR(s): 10 K. E. Suchsland, J. D. Watson, T. J. Dahm, J. L. Hull

8. CONTRACT OR GRANT NUMBER(s): 15 DNA 001-76-C-0407

9. PERFORMING ORGANIZATION NAME AND ADDRESS:
Acurex Corporation/Aerotherm Group
485 Clyde Avenue
Mountain View, California 94042

10. PROGRAM ELEMENT, PROJECT, TASK AREA & WORK UNIT NUMBERS: 16 Subtask N99QAXAI129-04

11. CONTROLLING OFFICE NAME AND ADDRESS:
Director
Defense Nuclear Agency
Washington, D.C. 20305

12. REPORT DATE: 11 31 October 1979

13. NUMBER OF PAGES: 166

14. MONITORING AGENCY NAME & ADDRESS (if different from Controlling Office): 17 I129

15. SECURITY CLASS (of this report): UNCLASSIFIED

15a. DECLASSIFICATION/DOWNGRADING SCHEDULE:

16. DISTRIBUTION STATEMENT (of this Report):

Approved for public release; distribution unlimited.

17. DISTRIBUTION STATEMENT (of the abstract entered in Block 20, if different from Report)

18 DNA, SBIE 19 5074F, AD-E300 807

18. SUPPLEMENTARY NOTES

This work sponsored by the Defense Nuclear Agency under RDT&E RMSS Code B342079464 N99QAXAI12904 H2590D.

19. KEY WORDS (Continue on reverse side if necessary and identify by block number)

Hypervelocity Launcher
Reentry Vehicle Simulation
Light Gas Gun
Projectile
Ballistic Heat Transfer

20. ABSTRACT (Continue on reverse side if necessary and identify by block number)

This report summarizes the developments to date of a 1/4-scale launcher designed to launch a 7.2-kg model at a 6.1 km/sec in full scale. The hybrid launcher design principles are reviewed. Projected performance shows launch masses within soft-launch constraints that are 3 to 4 times larger than possible by using a conventional two-stage launcher. The results of component development tests leading to the subscale demonstration are presented. The importance of tungsten liners for obtaining

over

DD FORM 1 JAN 73 1473 EDITION OF 1 NOV 65 IS OBSOLETE

UNCLASSIFIED

SECURITY CLASSIFICATION OF THIS PAGE (When Data Entered)

H095119

Gw

20. ABSTRACT (Continued)

the projected performance is emphasized, and the results of liner bond developments are described.

PREFACE

This program has benefited through the contributions of many people and organizations. The authors take particular note of the contributions of our major subcontractors; Caral, Inc., who has provided most of the heavy metalwork; Ultramet, who has worked so cooperatively with us developing the tungsten lining processes; and Physics International (PI), who has provided construction and testing services. Timely consultations with Aerospace Corporation people, including Harry Dyner, Wally Grabowski, and Stan Channon, have been very helpful and are appreciated. Significant contributors within Acurex include Kerry Seifert, who provided the interface with PI during the last two injection experiments, Mr. Winston Lowe, who has been a principle contributor on the design of launcher and test components, and Dr. John Huntington, who has been an enthusiastic supporter of the hybrid launcher concept since its birth. Finally, we gratefully acknowledge the team spirit and professional performance of the DNA project monitor, Capt. Arthur T. Hopkins.

ACCESSION for
NTIS White Section ☑
DDC Buff Section ☐
UNANNOUNCED ☐
JUSTIFICATION
BY
DISTRIBUTION/AVAILABILITY CODES
Dist. AVAIL. and/or SPECIAL
A

CONVERSION FACTORS TO SI UNITS

To Convert From	to	Multiply By
Atmosphere (atm)	kilo pascal (kPa)	$1.013*10^{2}$
bar	kilo pascal (kPa)	$1.000*10^{2}$
British Thermal Unit (Btu)	Joule (J)	$1.054*10^{3}$
calorie (cal)	Joule (J)	$4.184*10^{0}$
centimeters (cm)	meter (m)	$1.000*10^{-2}$
degree (angle)	radian (rad)	$1.745*10^{-2}$
degree Celcius (^{o}C)	degree Kelvin (^{o}K)	$t_k = t_c + 273.15$
degree fahrenheit (^{o}F)	degree Kelvin (^{o}K)	$t_k = (t_f + 459.67)/1.8$
dyne	Newton (N)	$1.000*10^{-5}$
erg	Joules (J)	$1.000*10^{-7}$
energy unit (e.u.)	Joules (J)	$1.000*10^{5}$
foot (ft or f)	meter (m)	$3.048*10^{-1}$
foot-pound-force (ft-lb_f)	Joules (J)	$1.356*10^{0}$
gram (gm)	kilograms (kg)	$1.000*10^{-3}$
inch (in)	meter(m)	$2.540*10^{-2}$
kilobar (kbar)	kilo pascal (kPa)	$1.000*10^{5}$
kilometer (km)	meter (m)	$1.000*10^{3}$
kilo-pound-force/inch^2 (ksi)	kilo pascal (kPa)	$6.897*10^{3}$
mil	meter (m)	$2.540*10^{-5}$
millimeter (mm)	meter (m)	$1.000*10^{-3}$
pound-force (lb_f)	Newton (N)	$4.448*10^{0}$
pound-force/inch^2 (psi)	kilo pascal (kPa)	$6.897*10^{0}$
pound-mass (lb_m)	kilogram (kg)	$4.536*10^{-1}$

TABLE OF CONTENTS

Section		Page
	PREFACE	1
	CONVERSION TABLE	2
1	INTRODUCTION	9
2	DESCRIPTION OF THE SUBSCALE HYBRID LAUNCHER	13
	2.1 Hybrid Launcher Design Principles	17
	2.2 Selection of Demonstrator Ballistic Cycle	20
	2.3 Hybrid Performance Perspective	22
3	COMPONENT TESTING	24
	3.1 Explosive Driver Development Tests	32
	3.1.1 Driver Test D-1	36
	3.1.2 Driver Test D-2	39
	3.1.3 Driver Test D-3	39
	3.1.4 I-1 Drivers	39
	3.1.5 HB-1 Driver	40
	3.1.6 HB-2 Driver	41
	3.1.7 D-4 Driver	41
	3.1.8 HB-3 Driver	42
	3.1.9 I-2 Driver	42
	3.1.10 I-3 Drivers	42
	3.1.11 I-4 Drivers	44
	3.1.12 I-5 Drivers	44
	3.1.13 Driver Test Conclusions	44
	3.2 Diaphragm Tests	45
	3.3 Injection Tests	48
	3.3.1 Injection Test I-1	49
	3.3.2 "Hot Breath" Series (HB-1, HB-2, and HB-3)	55
	3.3.3 Injection Test I-2	57
	3.3.4 Injection Test I-3	66
	3.3.5 Injection Test I-4	70
	3.3.6 Injection Test I-5	70
	3.4 Component Testing Conclusions	75
4	THERMAL PROTECTION OF LAUNCHER COMPONENTS	77
	4.1 Composite Liner Options	81
	4.2 Experience With The Nominal Liner Approach	85
	4.3 Bonding Development Tests	89
	4.4 Conclusions from Launch Tube Thermal Protection Studies	105

TABLE OF CONTENTS (Concluded)

Section		Page
5	DESIGN AND FABRICATION STATUS	108
	5.1 Gun Components	108
	5.2 Gun Mounts	116
6	SUMMARY AND CONCLUSIONS	118
	REFERENCES	121
	APPENDIX A -- HYBRID LAUNCHER DEVELOPMENT SUPPORTING ANALYSES	123
	APPENDIX B -- INJECTION BLOCK METALLURGY	141

LIST OF ILLUSTRATIONS

Figure		Page
1	Performance Comparison of Hybrid versus Conventional Two-stage Light Gas Gun	12
2	General Configuration of Two-stage Hybrid Launcher	14
3	Operational Sequence of The Hybrid Launcher	15
4	Modified Mollier Diagram for Real Hydrogen Showing Conventional and Hybrid Compression Cycles	19
5	Estimated Hybrid Launch Capability	23
6	Schematic of Explosive Driver Operation	33
7	Dimensionless $\bar{x}$-$\bar{t}$ Diagram for a Long Explosive Driver	34
8	Initial Driver Design	35
9	Final Driver Design	37
10	Comparison of D-4 Sphincter with Redesigned HB-3 Sphincter	43
11	Metal Diaphragm Design	46
12	I-1 Test Injection Block	50
13	I-1 Block During Assembly	51
14	Post-test I-1 Injection Block	53
15	View Looking Down I-1 Bore	54
16	HB-1 and HB-2 Test Setup	56
17	HB-2 Target Block	58
18	HB-3 Setup	59
19	I-2 Injection Block Assembly	61
20	I-2 Test Stand and Injection Block	62
21	I-2 Injection Block Half	63
22	Redesigned Termination Assembly Used in I-3	68
23	Post-test View of I-3 Injection Block Assembly	69

LIST OF ILLUSTRATIONS (Continued)

Figure		Page
24	I-5 Layout	72
25	I-5 Test Setup During Assembly	73
26	Post-test I-5 Injection Block	74
27	Temperature Histories at The Barrel Inlet of a 10.2-cm (4-inch) Bore Hybrid Launcher with a 4.54-kg Model (Full Scale of Cycle B of Table 1) (Reference 3) . . .	80
28	Calculated Effect of CVD Process Temperature on Tungsten Lines and Launch Tube Stresses after Cooldown	84
29	Photomicrograph of CVD Tungsten on 17-4PH with Nickel Plate Layer	87
30	Representative examples of tungsten CVD at 590°C.	91
31	Representative examples of tungsten CVD at 820°C.	92
32	Photomicrographs of material interfaces, CVD at 590°C and 820°C.	94
33	Character of tungsten layer with nodules, T = 820°C . .	95
34	Effect of Initial CVD at Low Temperature on Nodule Formation	97
35	Effect of Initial CVD Temperature on Surface Cracks, 10X	99
36	Composite Photo of Worst Samples from the Matrix in Table 6	100
37	Post-bend Photomicrograph of Sample S/N 017 Showing Bond Retention During Substrate Yielding, 20X	103
38	Photomicrographs of Corners of Bent Samples, 20X . . .	104
39	Plan View of Sample S/N 032 Showing Well-bonded "Tiles," 10X	106
40	One-inch bore (1/4-Scale) Hybrid Launcher Assembly Drawing (April 1977)	110

LIST OF ILLUSTRATIONS (Concluded)

Figure		Page
41	One and a Quarter-inch Bore (1/4-Scale) Hybrid Launcher Assembly Drawing (November 10, 1977)	111
42	One and a Quarter-inch Bore (1/4-Scale) Hybrid Launcher Assembly Drawing (March 1979)	113
43	Launcher Mount Layout	117

LIST OF TABLES

Table		Page
1	Summary of Hybrid Launch Cycle Options	21
2	Summary of Component Tests	25
3	Summary of Explosive Driver Performance and Development	38
4	Relative Melt Times for Various Materials	78
5	Tungsten-nickel Bonding Development Matrix	90
6	Revised Tungsten-Nickel Bonding Development Matrix . .	96
7	Results of Bonding Development Study	101
8	Launcher Fabrication Status	114

SECTION 1
INTRODUCTION

In principle, a hypervelocity launcher can be designed on a large enough scale to permit testing of full-scale reentry vehicles in a ground-based facility. Such a launcher, based on the straightforward application of conventional two-stage light gas gun tenchology, would be extremely costly. Furthermore, a gun of such size would require development of new fabrication techniques and would involve some risk.

One of several alternative approaches for ground-based reentry testing is to develop a launcher of greatly improved ballistic efficiency. This launcher would be used on a more modest scale to test high-β* full-scale nosetips in an extended track-guided range. Such an approach would not be prohibitively expensive and could substantially extend test times to provide high-quality erosion/ablation data.

This report describes the development of a subscale launcher capable of soft launching a model two to three times more massive than can be propelled by a conventional two-stage gun of the same bore.†

The hybrid launcher uses several explosive drivers to precondition and inject high-energy hydrogen into the compressor section of a two-stage light gas gun. As a result, maximum tolerable pressures and temperatures can be developed with a very short compression cycle. Furthermore, the pressure history can be controlled independently of the peak reservoir gas temperature, making possible a very efficient ballistic cycle for accelerating high-β models.

---

*$\beta = \frac{W}{C_D A}$ = ballistic coefficient

†The subscale launcher will be referred to as the 1/4-scale launcher throughout this report.

The basic concept of the hybrid launcher is not new. Previous attempts to demonstrate such a launcher in subscale were not successful; launcher velocities were considerably below expectations (Reference 1). Reasons for this performance shortfall were identified and are briefly described below (Reference 2):

- The design relied on projectile acceleration at high launch tube length to diameter ratios, without considering heat transfer and boundary layer effects
- The design ratio of gas to projectile mass was too low. In addition, a large fraction of gas failed to be injected into the compressor section because of choking and the injection configuration.
- The first stage 75-mm gun had insufficient energy to achieve the design muzzle velocity with the proper launch tube length
- Melting occurred in the compressor section and launch tube
- The explosive drivers were overcharged, causing driver jetting and contamination of the working gas

Conclusions reached were that the basic concept does have considerable merit and is feasible with modifications to the design (Reference 2).

Detailed design analyses were conducted (Reference 3) to estimate hybrid launcher internal ballistics and to develop means of protecting the launcher components from the intense convective heating (References 2 through 4). Briefly, the features that emerged from the design study are:

- Full-scale design goal is to launch a model weighing over 4.61 kg ($\approx$10 lb_m) more than 6.1 km/sec (20,000 ft/sec). The design parameters for attaining that goal were selected to achieve calculated launch velocities of more than 6.6 km/sec within 300 calibers. Additional design margin is achieved by using a 400-caliber launch tube in a 1/4-scale demonstrator.
- Using an improved injection configuration, the second stage gas-to-projectile mass ratio will exceed 1.5 (assuming injection losses of 12 percent or less)
- Quarter-scale first stage will be an M68 105-mm gun, enabling the use of a 16-inch Naval gun in full scale

- Full-scale launch tube will be lined with a composite consisting of a tungsten heat sink with a very thin layer of tantalum carbide to reduce the peak tungsten temperature while allowing launch cycle temperatures in excess of 5800°K
- Quarter-scale launcher will use four nitromethane drivers of a proven design. Full-scale launcher will use drivers that are based on a more efficient design.

The 1/4-scale ballistic cycle that has been selected for demonstration will launch a 7.22-kg (15.9-lb_m), 12.7-cm (5-inch) diameter model at 6.1 km/sec in full scale. Alternatively, a 5.50-kg (12-lb_m), 10.2-cm (4-inch) diameter saboted model with a 20-percent higher ballistic coefficient can be accelerated with the same full-scale launcher. However, special sabot stripping techniques must be developed to couple a "superbore" launcher with a track-guided range facility. Figure 1 illustrates the performance attainable with the launcher compared to conventional two-stage light gas guns.

The objective of the current program is a subscale demonstration of the internal ballistic performance of the hybrid concept. This report documents the milestones toward this program objective that have been achieved under the current contract. It contains a review of the features of the specific design selected for demonstration. The component tests in preparation for the demonstration are reported, along with a presentation of the current design status and the status of the demonstration hardware. Thermal protection liner development results are also presented.

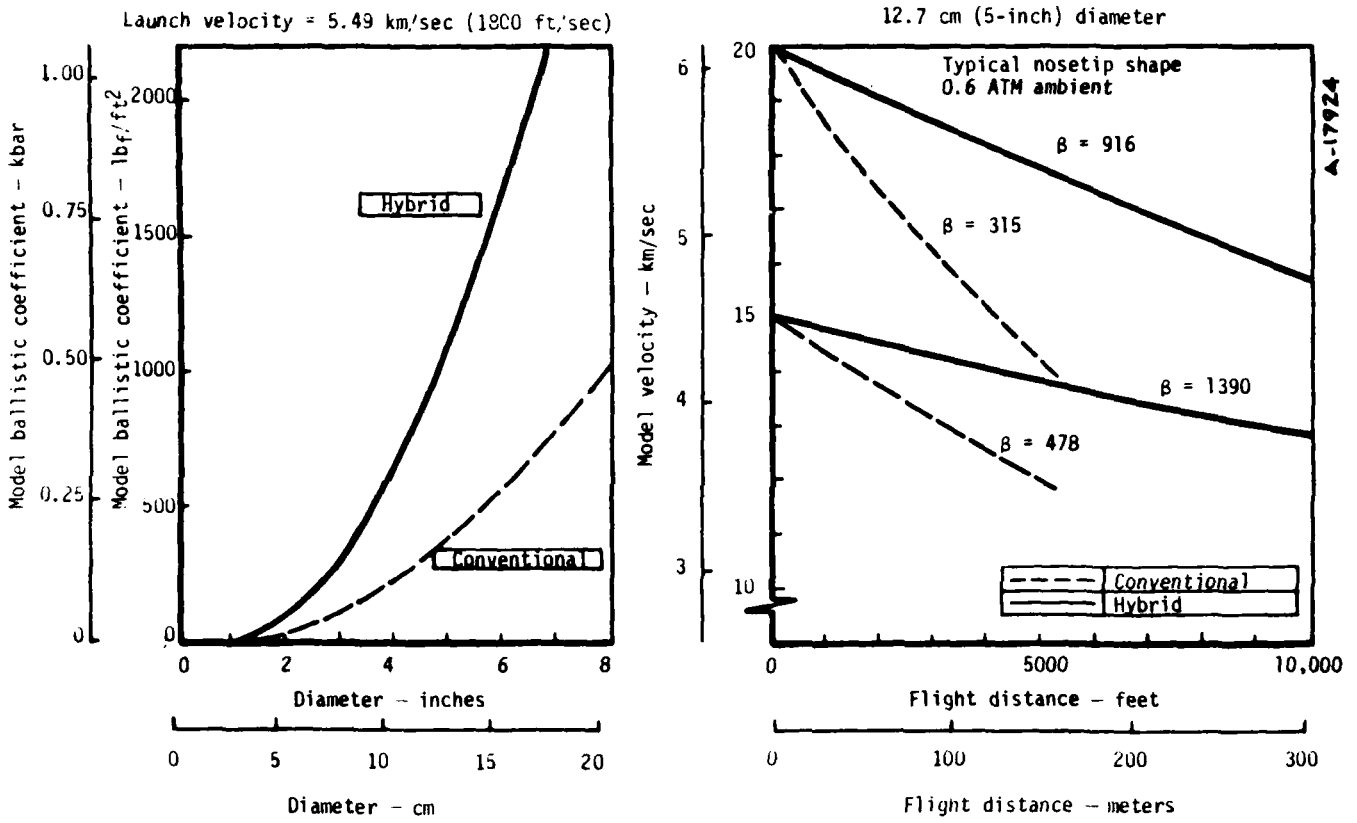

Figure 1. Performance comparison of hybrid versus conventional two-stage light gas gun.

SECTION 2
DESCRIPTION OF THE SUBSCALE HYBRID LAUNCHER

The basic design of the 1/4-scale launcher was completed in April 1977. This design (documented in Reference 3) was the end result of an analysis effort which considered several launcher concepts and identified a two-stage hybrid design as optimum. A schematic layout of this design is shown in Figure 2. The design consists of a first-stage large bore gun which fires a piston. As the piston travels down the launcher, it eventually enters the barrel extension. Subsequently, the second-stage explosive drivers are fired, injecting high-temperature, shock-heated hydrogen into the injection block. The piston enters the injection block, sweeping this high-temperature hydrogen into the compression section. This now compressed hydrogen in turn acelerates a small projectile (model) located initially downstream of the compresssion section. Late in the cycle, the piston rebounds off the hydrogen cushion, allowing the hydrogen working fluid to expand and cool. This operational sequence is illustrated sequentially in Figure 3.

The design of a gun to launch high-β models is limited to a performance envelope defined by several launcher and model material limits. In particular, the maximum pressure on the base of the model is limited to 5 kbar, a limit imposed largely by the experience gained through launching nosetip models in conventional two-stage light gas guns. For conservative performance estimation, the design is also constrained to a maximum launch tube length of 300-bore diameters.*

$$V = \left(\frac{\pi P}{2} \frac{L}{D}\right)^{1/2} \left(\frac{m_s}{D^3}\right)^{-1/2} \qquad (1)$$

*300-bore diameters selected to be conservative; however, the actual launch tube will be longer.

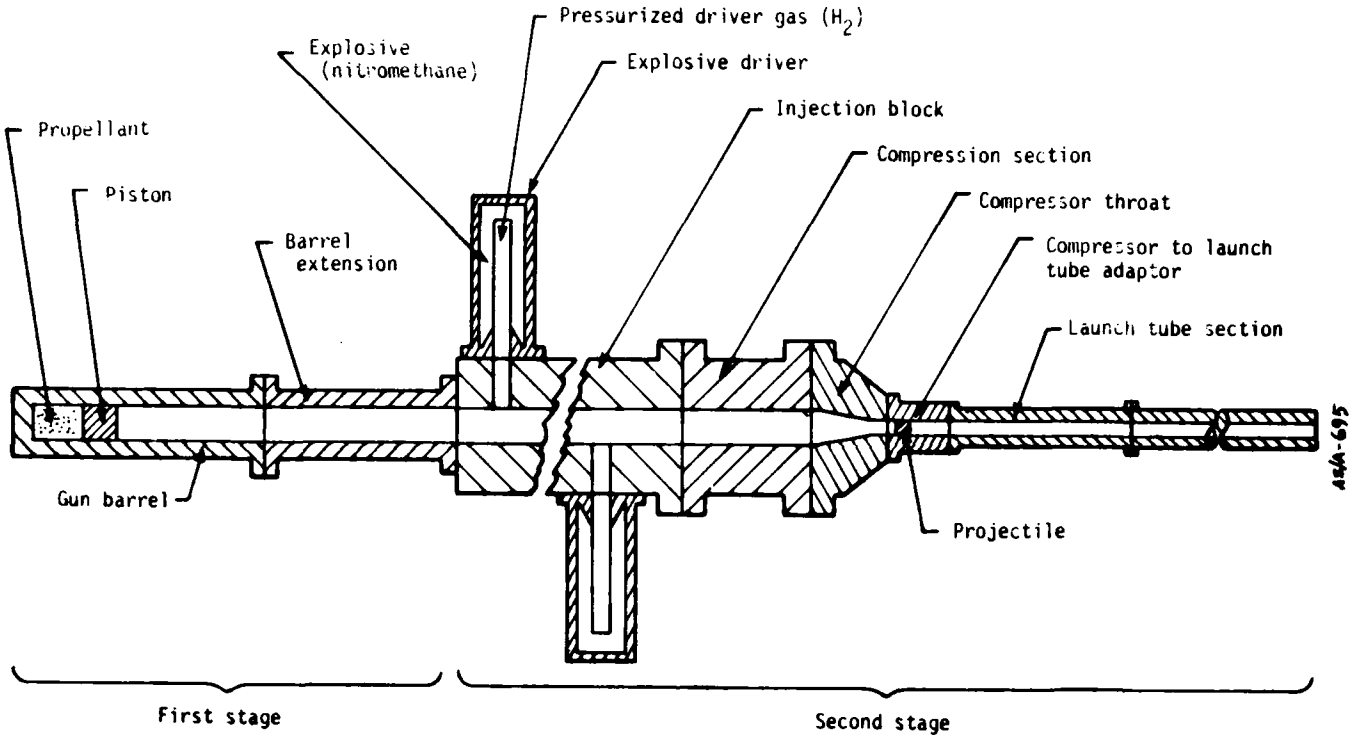

Figure 2. General configuration of two-stage hybrid launcher.

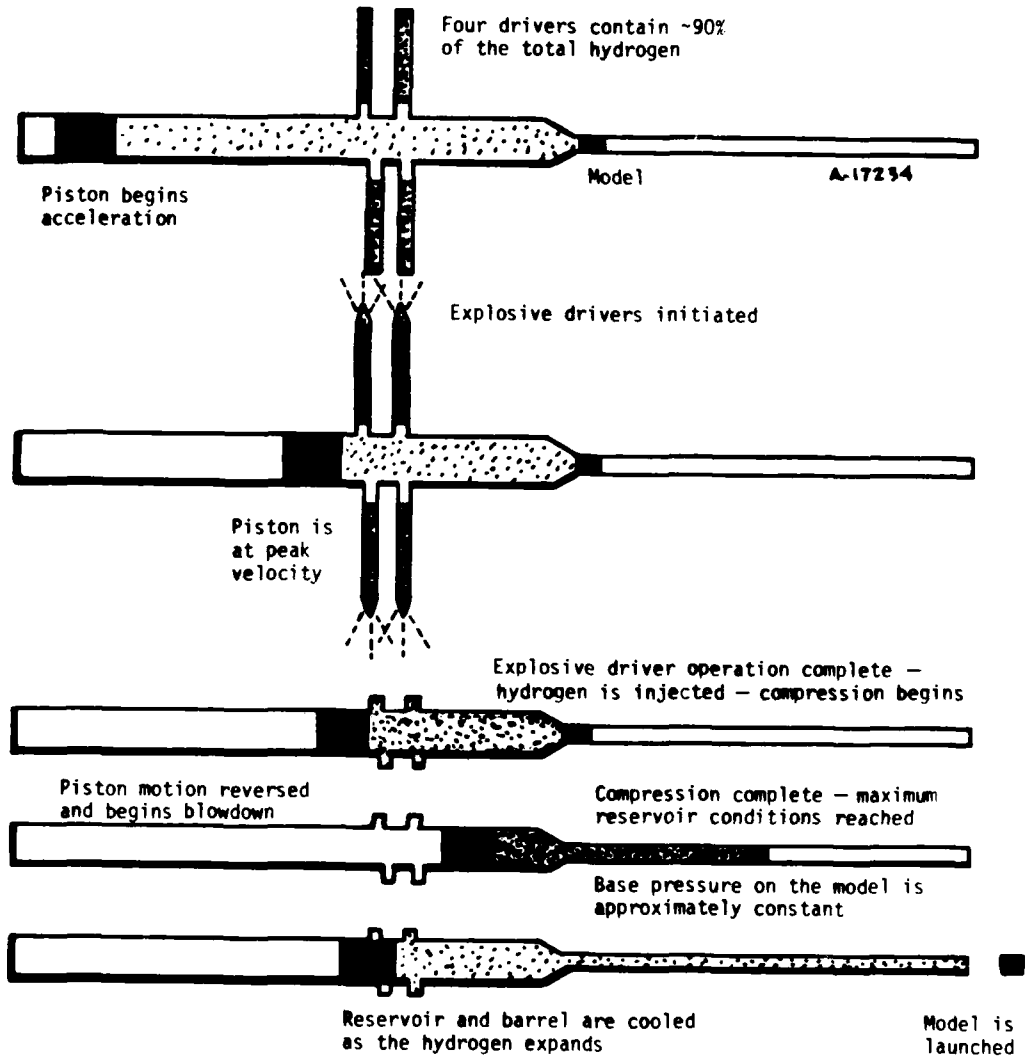

Figure 3. Operational sequence of the hybrid launcher.

Under these two constraints, the maximum possible muzzle velocity for a 7.26-kg (16-lb_m) model in a 12.7-cm (5-inch) diameter launch tube is 8.15 km/sec, with an idealized constant base pressure launch cycle.

where V = muzzle velocity

L = launch tube length

D = bore diameter

m_s = shot mass

The design velocity of 6.1 km/sec is, thus, 75 percent of the maximum possible velocity and would require an average model base pressure of 2.8 kbar during the launch cycle. Since the maximum allowable base pressure is 5 kbar, the piezometric efficiency* of the ballistic cycle must be 56 percent or more.

Such an efficient ballistic cycle requires a working fluid with the highest possible sound speed. The maximum heat load tolerated by the interior of the gun limits the peak temperatures and, hence, sound speeds that can be generated during the ballistic cycle. Hydrogen provides the highest sound speed at the highest heat loads allowable in the launcher. As will be detailed in Section 4, the practical limit on peak reservoir temperature for tantalum carbide-over-tungsten lined barrels appears to be about 5800°K.

An extended barrel 16-inch Naval gun is the largest available hardware† for use as a first stage to drive a 7.22-kg (15.9-lb_m) model in a 12.7-cm (5-inch) launch tube. This establishes an upper limit on piston energy (~540 million Joules) and piston velocity (~2.4 km/sec). For a 40.6-cm (16-inch) ID compressor section, the peak reservoir pressures are limited to about 8 kbars within the cost-effective choices of available materials, fabrication techniques, and heat treats.

---

*The piezometric efficiency is defined as:

$$\mathbb{P} = \frac{\text{constant base pressure to give the observed velocity}}{\text{peak base pressure generated during the ballistic cycle}}$$

†For example, the U.S. Army has a double length barrel (120 feet) 16-inch gun used for high altitude firings at Yuma, Arizona. A larger first stage could be manufactured at substantial extra cost.

In summary, the major design constraints are:

- Maximum model base pressure of 5 kbar
- Launch tube diameter of 300 bores
- Maximum reservoir temperature of 5800°K
- Sixteen-inch (40.6-cm) Naval gun first stage driving a 12.7-cm (5-inch) launch tube
- Maximum reservoir pressure of 8 kbar

An optimized conventional two-stage light gas gun was considered using a 16-inch Naval gun as the first stage (Reference 3). It was found that to achieve maximum tolerable pressures and temperatures (8 kbar and 5800°K, respectively) with an isentropic compression from subatmospheric pressure to 8 kbar would require an impossibly long pump tube (40.6 cm in diameter by 22.5 km long). The combination of a reasonably long pump tube and an 2.4-km/sec piston in a shock-heated compression cycle is still unable to generate peak temperatures much in excess of 2000°K without overpressuring both the reservoir and model. That is, the piston is not fast enough to provide the necessary shock heating. Conclusions regarding heat transfer (References 2 through 4) demand that the internal ballistics approximate constant base pressure behavior early in the launch cycle and approximate behavior akin to a simple wave gun late in the cycle. A fast, lightweight first-stage piston cannot achieve the required reservoir pressure tailoring; the peak pressure pulse will be much too short-lived. A conventional two-stage light gas gun of practical size is therefore not suitable for launching high-β models to the required velocities.

However, the injected or hybrid two-stage launcher avoids this dilemma by using the first-stage piston primarily to control the rate of reservoir pressure buildup and decay so as to achieve the launch objectives without melting the bore surface. The proper state of the hydrogen to achieve maximum tolerable reservoir pressure and temperatures is controlled primarily by the explosive drivers. Thus, the state of the gas and the rate of reservoir pressure buildup are independently controlled.

2.1 HYBRID LAUNCHER DESIGN PRINCIPLES

Explosive drivers are used to process the hydrogen to a high-energy density state by a single strong shock. The gas is then injected into the compressor section. This injected state (prior to compression) is

characterized by its energy density which is a function of the p V work of the drivers and by its mass density which is a function of the injection volume (see details in Reference 3).

A modified Mollier diagram (e versus S/R) for real hydrogen is shown in Figure 4. Typical compression cycles for a shock-heated conventional two-stage gun and a hybrid two-stage gun are included to illustrate the advantage of the hybrid concept and exemplify a conventional two-stage gun and a hybrid launcher of approximately the same size. The conventional two-stage gun shown has a 40.6-cm (16-inch) diameter by 68.6-m (225-foot) long pump tube and the hybrid launcher has a 40.6-cm diameter by 46.6-m (153-foot) long first-stage compessor section. The size of the conventional two-stage gun would have to be increased to an impractical value to achieve the same high-energy reservoir states as the hybrid launcher.

The energy of the gas in the conventional cycle is completely controlled by piston energy, whereas for the hybrid cycle about 60 percent of the energy of the gas is provided by the explosive drivers and 40 percent by the piston. Thus, for the same size first stage, the hybrid launcher has substantially more energy available in addition to having independent control over the state of the gas and the rate of reservoir pressure buildup.

The maximum tolerable reservoir pressure and temperature, which in practice peak simultaneously, occur at a unique entropy level. For example, from Figure 4, the dimensionless entropy, S/R, is 19.25 at 8 kbar and 5800°K. Since compression is approximately isentropic, the entropy at injection is also 19.25. Injection energy is controlled by the pΔV work of the explosive drivers, so the compressor volume at injection which controls injection density is used to control the entropy level at which compression occurs. The operational sequence of the hybrid launcher is shown in Figure 3.

A 1-D Lagrangian finite difference code (the STEALTH code described in Reference 5) was used (Reference 3) to compute the hybrid launcher inviscid, adiabatic ballistic cycle. The code includes a real hydrogen equation-of-state (Reference 2), streamwise relative area changes with 1-D

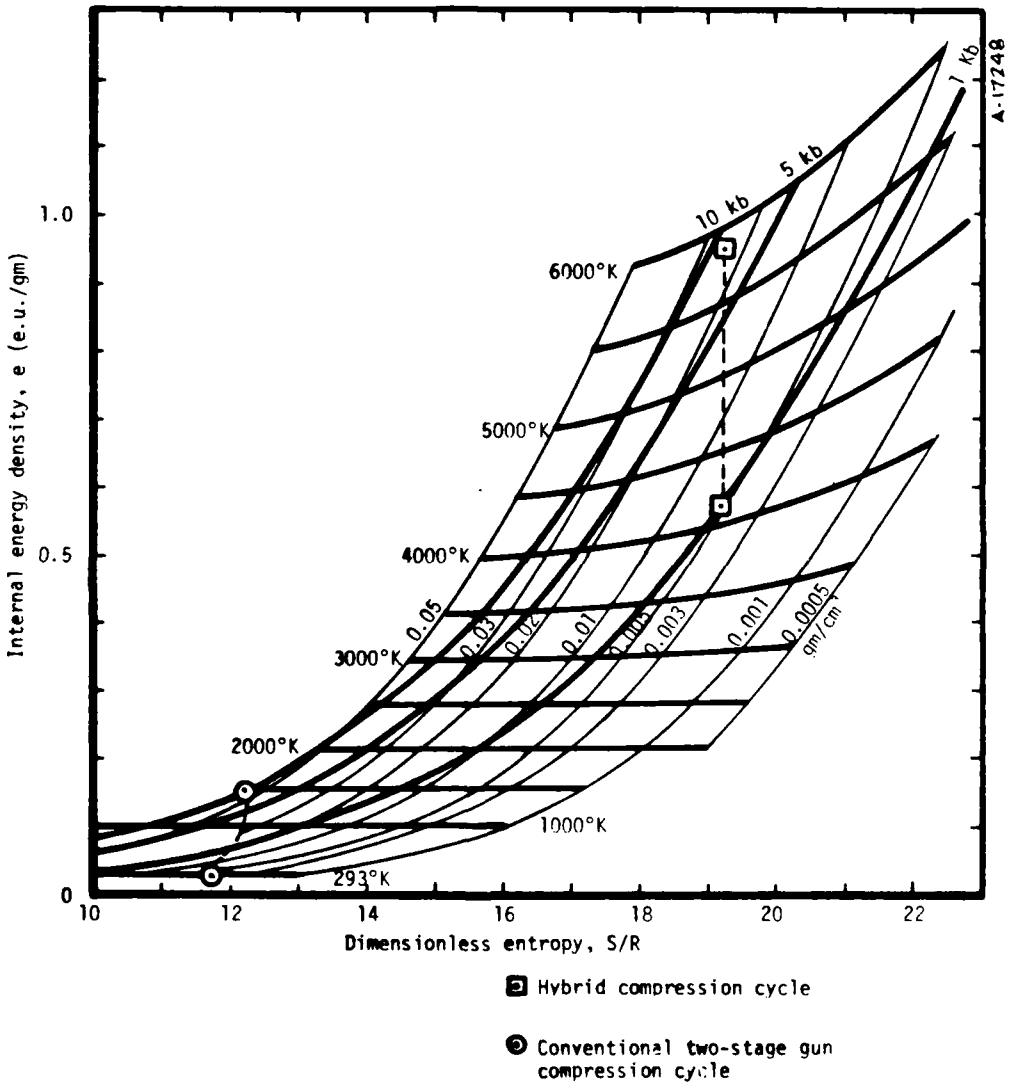

Figure 4. Modified Mollier diagram for real hydrogen showing conventional and hybrid compression cycles.

gas dynamics, and shot-start* condition. All the thermodynamic and gas dynamic variables and piston and model trajectories were calculated as functions of time and position throughout the launch cycle. Several launcher geometries, piston conditions, and initial gas conditions were evaluated in this manner to obtain the best performance within the design constraints.

To account for heat transfer losses, boundary layer losses, etc., a minimum muzzle velocity of about 6.7 km/sec for the calculated ballistic cycle is considered necessary to provide about a 10-percent margin over the 6.1-km/sec design velocity.

The calculations were carried out for a 1/4-scale of the full-scale launcher. Since the calculations assume inviscid adiabatic gas flow, results can be scaled by multiplying all times and lengths by the appropriate scale factor (4.0). The calculations resulted in a selection of four launch cycle options, which are summarized in Table 1.

2.2 SELECTION OF DEMONSTRATOR BALLISTIC CYCLE

Cycle A in Table 1 is the culmination of an extensive effort to find operating conditions that maximize launch velocity at a selected shot mass without exceeding the service temperature limits of tungsten calculated by heat transfer analyses. Since the expected maximum launch velocity is less than that desired, the necessity for a smaller shot mass was identified. Cycle B is a reflection of this modification.

Cycle C was developed in an effort to achieve the same model area density as Cycle A at the desired velocity by launching an 86-gram model using a 26-gram sabot. Cycles B and C are acceptable in terms of launch velocity. However, calculations (Reference 3) lead to the conclusion that a tungsten-lined full-scale launch tube will experience surface melting during these cycles. Calculations also show that this can be prevented by protecting the tungsten with a thin layer of tantalum carbide. It was estimated that bare tungsten would not melt (by a very small margin)

---

*The shot-start condition is usually defined as the pressure at which the projectile is released from its initial position.

TABLE 1. SUMMARY OF HYBRID LAUNCH CYCLE OPTIONS

Launch Cycle[a]	Launch Tube Dia. (cm)	Model Mass (gm)	Piston Mass (kg)	Piston Vel. (km/sec)	G/M	P_{max} Res. (kbar)	T_{max} Res. (°K)	P_{max} Model (kbar)	u_{300} (km/sec)	u_{350} (km/sec)	Full-Scale Launch Mass After Sabot Stripping (kg)	Expected Launch Velocity[b] u_{400} (km/sec)
A	2.54	86	5.68	1.48	2	8.0	5700	5.2	6.0	6.5	5.50	5.5
B	2.54	72	5.22	1.52	2	8.0	5840	5.2	6.5	7.0	4.61	6.0
C Superbore	3.175	112.5	6.36	1.52	1.56	8.1	5710	5.3	7.1	7.6	5.50	6.5
D Relaxed Superbore	3.175	112.5	5.90	1.46	1.56	6.6	5510	4.7	6.6	7.0	5.50	6.1

[a]All four of the launch cycle options make use of the same first stage, injector, and compressor hardware.
[b]Based on 92 percent of the computed velocity at L/D = 300, u_{300}.

for the conditions of Cycle D in full scale. A margin of about 350°K is expected in subscale. On this basis, Cycle D has been selected for demonstrating the hybrid launcher in subscale, thereby avoiding (at least temporarily) any complications related to coating of tantalum carbide.

2.3 HYBRID PERFORMANCE PERSPECTIVE

From basic principles, Equation (1) launch velocity capability varies with reduced shot mass, m_s/D^3, approximately independent of launcher size. Reference 6 compiled launch velocity data from eight facilities for a range in bore sizes from 5.6 to 102 mm. The performance envelope for these facilities (taken from Reference 6) is presented in Figure 5. The envelope represents the best of attempts to increase launch velocity without imposing limitations on base pressure. Thus, the envelope presented in Figure 5 presents the "hard launch" limits of conventional technology at the time (1970).

Current "soft launch" limitations are defined in Figure 5 based on the AEDC Range G data (Reference 7). The Ames launcher that was used to provide the single data point shown in Figure 5 is capable of launch velocities within 0.5 km/sec of the hard launch envelope (Reference 6); however, base pressures in excess of 12 kbar are required to do this. The performance within the 5-kbar base pressure limit noted in the figure (also taken from Reference 6) is consistent with the soft launch line indicated for Range G.

For a given bore dimension, the indicated Range G soft launch line follows a path of constant launch kinetic energy, up to velocities of about 5.5 km/sec. At smaller launch masses (higher velocities), velocities are lower than predicted using a constant kinetic energy approximation. The indicated hybrid soft launch line is an estimate that goes through the hybrid design point and provides a 65-percent higher velocity than Range G for all values of reduced shot mass. On this basis, the hybrid launcher is capable of soft launching models that are three to four times more massive than a conventional launcher of the same bore dimension. Similar factors on the conventional hard launch envelope might be anticipated for the hybrid without the 5-kbar base pressure constraint. However, this suggestion must be viewed relative to the belief that the current design will result in wall temperatures very near the service limits of tungsten.

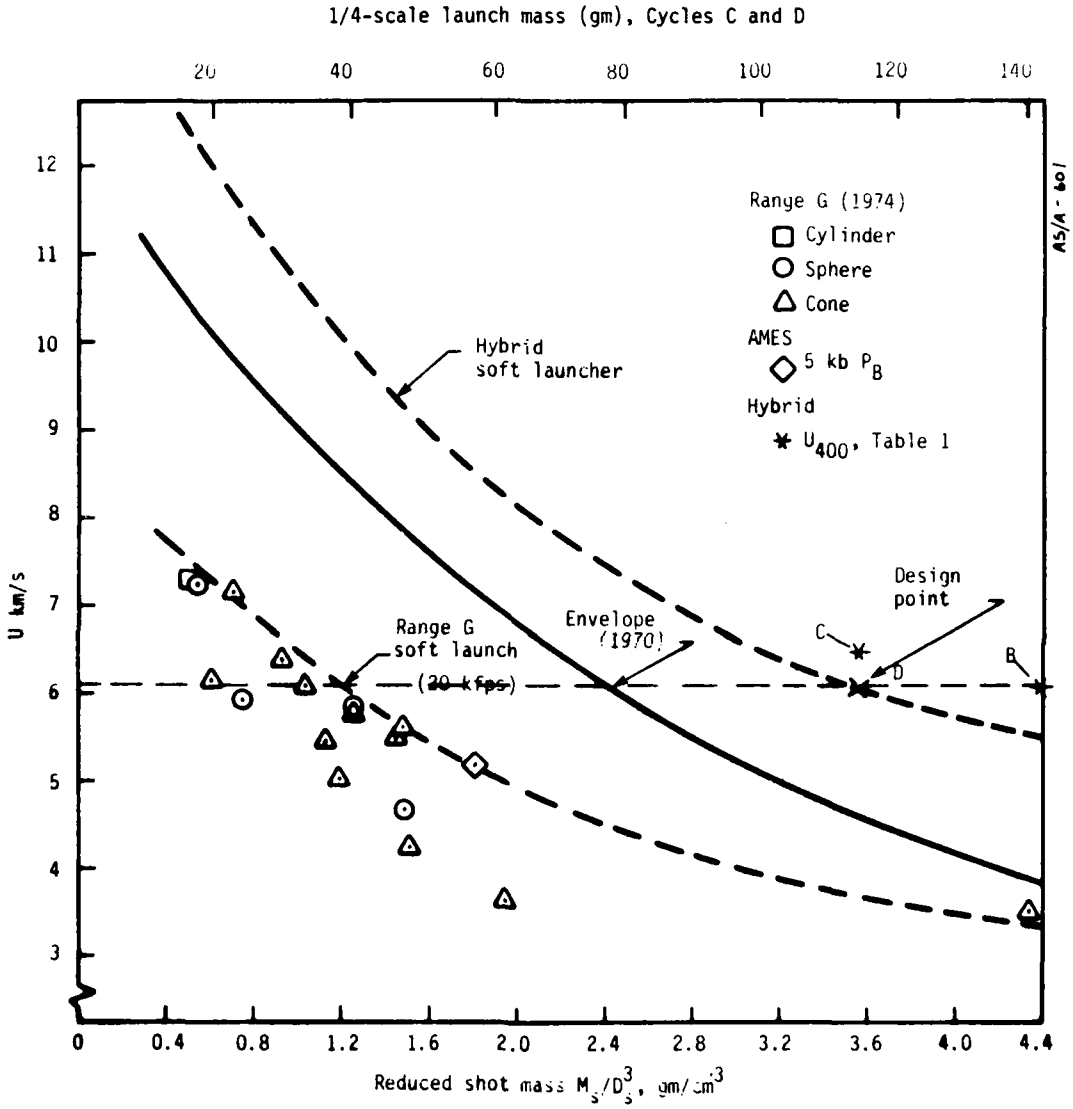

Figure 5. Estimated hybrid launch capability.

SECTION 3
COMPONENT TESTING

During the development of the 1/4-scale hybrid gun, a number of tests were required to resolve technical issues concerning injection and containment mechanics, thermal protection of the compressor and launch tubes, and launcher performance. To date, most of the testing has addressed the injection and containment mechanics. These tests will be described in the following section. A description of tests involving the development of thermal protection for the launch tubes will be deferred to Section 4, Thermal Liner Development. Tests required to assess launcher performance constitute most of the remaining testing in the 1/4-scale hybrid gun development.

The basic issues which had to be determined as a part of injection and containment mechanics were the following:

- Thermodynamic state of injected hydrogen
- Amount of hydrogen injected
- Ability to seal injection ports following hydrogen injection
- Mechanical integrity of the injection system

A large number of tests were performed to obtain data on each of the above. A brief description of each of these tests is provided in Table 2. This table chronologically lists the objective of each test, a description of the testing procedure, and the results and conclusions of each test.

The tests performed are described in more detail below. For convenience, they have been divided into three categories: driver tests, diaphragm, and injection tests.

TABLE 2. SUMMARY OF COMPONENT TESTS

Test No.	Date	Category	Objective/Purpose	Procedure
D-1	10/25/77	Driver test	To: • Collect shock and detonation velocity data • Observe pressure tube collapse • Observe sphincter sealing • Investigate ability of nylon 6/6 target to capture (embed) steel diaphragm fragments	• Built driver to design speci • Instrumented driver to measu detonation velocities • Placed nylon 6/6 target at d • Loaded driver with nitrometh to 1990 psig with H_2, then d
S-1, S-2, S-3	11/28/77 and 11/29/77	Diaphragm (plug) tests	To devise a method to seal drivers without using steel diaphragms, which add significant amounts of metal fragments to the H_2 stream in the gun. This is to be accomplished by using two nylon plugs to be released and caught just prior to driver detonation. Plugs to be caught in bore opposite injection ports, removing them from the hot H_2 stream.	• Built driver along with nylo release system, and plug cat • Pressurized driver to 2000 ps • Released plugs
D-2	12/15/77	Driver test	To: • Collect shock and detonation velocity data • Watch for shock slowdown in long driver to assess boundary layer losses • Observe collapsed pressure tube	• Built driver 156 inches long 78 inches for D-1) • Omitted sphincter • Beefed up downstream tamper • Instrumented driver and then 1350 psig H_2 in pressure tub
S-4, S-5, S-6	12/16/77	Diaphragm (opening) tests	To eliminate diaphragm material from the hot H_2 stream by initiating petaling with a small amount of High Explosive (HE), causing the diaphragm petals to open before the H_2 shock wave reaches the diaphragm.	• Machined a diaphragm with tw crossing the center at 90° t • Placed small amounts of HE o • Pressurized driver • Detonated HE
Series A	12/20/77	Diaphragm (burst) tests	To determine maximum allowable groove depth for 2000 psig stainless steel diaphragms. Maximum depth to be used at "later" date when initiating petaling with HE.	• Fabricated a small test fixt hydrostatic testing • Machined 6 test diaphragms f thick stainless steel sheet; various groove depths in eac • Machined 1 test diaphragm fr thick stainless sheet • Pressurized each diaphragm t

Procedure	Results	Conclusions
to design specifications driver to measure shock and locities 6/6 target at driver exit with nitromethane, pressurized with H_2, then detonated	• Measured shock velocity as 0.893 km/μsec • Measured detonation velocity as 0.670 km/μsec • Drove pressure tube into 1.1-inch solid bar • Over-expanded and fragmented sphincter • Destroyed nylon target	• Reduce hydrogen covolume parameter in Van der Waals equation from 11.52 cm^3/gm to 8.64 cm^3/gm to predict shock velocity • Determined pressure tube collapse adequate • Shorten drivers, lower H_2 pressure, and/or beef up driver exit to protect sphincter from over-expansion • Observed that Nylon 66 is inadequate to capture steel diaphragm fragments
along with nylon plugs, plug m, and plug catcher river to 2000 psig s	Shattered • S-1 plugs • S-2 plugs • S-3 plugs	• Cannot use nylon as it is too brittle to use as plug material • Observed large time differences in plug release times • Decided method is impractical
156 inches long (as opposed to D-1) cter stream tamper driver and then tested with n pressure tube	• Measured shock velocity as 0.885 cm/μsec • Measured detonation velocity as 0.659 cm/μsec • Observed no slowdown in shock velocity at late times • Observed that pressure tube remained intact and was driven into 1.1-inch diameter bar	• Maintain hydrogen covolume parameter at 8.64 cm^3/gm to predict shock velocity • Observed no appreciable effect of boundary layer • Appears that pressure tube collapse is adequate
phragm with two shallow grooves enter at 90° to each other mounts of HE on the diaphragm iver	• S-4, S-5: would not pierce diaphragm with small amounts of EL506 or prima-cord • S-6: pierced diaphragm with its lead-sheathed shape charge, however diaphragm failed to open	• Increase the amount of EL506 and prima-cord to pierce the diaphragm • Observed that linear shaped charge easily pierces the diaphragm • Require diaphragms to have deeper grooves to promote petaling (opening)
mall test fixture for sting t diaphragms from 0.0575-inch s steel sheet; inscribed depths in each t diaphragm from 0.087-inch s sheet ch diaphragm to burst	• Burst data indicated a uniform increase in burst pressure with decrease in groove depth • Burst the 0.087-inch diaphragm at a lower pressure than a 0.0575-inch thick diaphragm with the same thickness at the groove • Bursting of diaphragms occurred along the grooves	• Use a groove depth of 0.030 inches if 0.0575-inch thick stainless diaphragms are used • Increasing the diaphragm thickness increases the thickness necessary at the groove to prevent bursting during driver pressurization • Concluded diaphragm petaling assured if diaphragms are grooved adequately prior to piercing with HE

Test No.	Date	Category	Objective/Purpose	Procedure
D-3	12/22/77	Driver test	To: • Collect shock and detonation velocity data • Observe pressure tube collapse and sphincter closure with beefed up tamper design • Collect diaphragm petaling data	• Constructed a 78-inch driver with the tamper beefed up to prevent sphincter over-expansion • Employed a diaphragm with grooves inscribed; affixed a linear shaped charge to the diaphragm along one of the grooves • Pressurized the driver to 1900 psig • Detonated the shaped charge • Initiated driver detonation 250 μsec after detonation of the shaped charge
Series B	1/30/78	Diaphragm (burst) tests	To collect large amount of burst data on 304 stainless steel diaphragms for several groove depths and diaphragm thicknesses.	• Made 18 diaphragms using two different thicknesses and three different groove depths • Measured the diaphragms and recorded dimensions • Pressurized each diaphragm to burst in the same apparatus as used for Series A
S-7 through S-13	2/1/78 through 2/3/78	Diaphragm (opening) tests	To determine diaphragm petaling time for total opening because if, during driver operation, the shock wave arrives before petals are compietely seated, the shock wave will remove petals and ingest them into the H_2 gases.	• Placed 0.038-inch thick diaphragms with 0.01-inch deep grooves in the diaphragm burst apparatus • Placed a small pad of EL506 at the center of each diaphragm • Pressurized the test apparatus and diaphragm petaling initiated by EL506 detonation • Took X-ray photos at different times during the diaphragm opening to observe the degree of opening
S-14 through S-17	2/9/78	Diaphragm (opening) tests	Same as for test numbers S-7 through S-13, except thicker diaphragms (0.047 inches) were used to see if this caused petaling to occur more consistently along grooves.	• Burst tested S-14 for comparison with Series B burst data • Repeated the S-7 through S-13 procedure for S-15, S-16, and S-17

TABLE 2. Continued

re	Results	Conclusions
river with the tamper hincter over-expansion th grooves inscribed; charge to the the grooves to 1900 psig arge tion 250 μsec after d charge	• Measured shock velocity as 0.902 cm/μsec • Measured detonation velocity as 0.673 cm/μsec • Drove pressure tube into solid 1.1-inch diameter bar • Sealed sphincter properly (closure adequate) • Tore diaphragm petals from diaphragm	• Maintain hydrogen covolume parameter at 8.64 cm^3/gm to predict shock velocity • Beefed-up tamper design prevented over-expansion of pressure tube and sphincter • The diaphragm may not have opened adequately when the shock wave reached the diaphragm
g two different ifferent groove depths and recorded agm to burst in the for Series A	• Data indicated a great deal of scatter, especially for the larger thickness diaphragms	• Need better control of the shape and depth of diaphragm grooves to prevent large scatter in burst data • Burst pressure is a function of material thickness at the groove only for small groove depths, but at large groove depths burst pressure decreases with diaphragm thickness (for the same material thickness left at the groove)
diaphragms with in the diaphragm burst L506 at the center aratus and diaphragm L506 detonation fferent times during observe the degree	• Observed that most of the diaphragms petaled properly, but a significant fraction also tore at locations other than the grooves • Diaphragms which opened properly were fully open between 400 and 500 μsec	• Observed an adequate system of opening diaphragms with a minimum contamination of H_2 by HE detonation products • Diaphragms must be centered carefully to prevent their tearing at arbitrary (nongrooved) locations • Time shock arrival at the diaphragm for 500 μsec after piercing the diaphragm to ensure complete opening prior to the shock arrival
mparison with S-13 procedure for	• Observed that S-14 burst at a higher pressure than for the same thickness and groove depth in the Series B burst tests • Found that petaling just began at 325 μsec, but almost complete at 400 μsec • Noted that S-17 did not rip along one groove; it appears to have been off center	• Burst pressure of the diaphragms used in S-14 through S-17 may be higher than those studied in the Series B burst tests • 0.047-inch thick diaphragms petal more consistently along the groove than the 0.038-inch thick diaphragms used in tests S-7 through S-13 • Need to place the groove intersection at the exact center of the diaphragm for proper performance

TABLE 2. Continued

Test No.	Date	Category	Objective/Purpose	Procedure
Series D	2/78	Diaphragm (burst) tests	To collect more burst data on stainless steel diaphragms at various groove depths	Machined and burst twenty 304 stain diaphragms
Series E	2/78	Diaphragm (burst) tests	To determine if Niles Machine and Tool Works, Inc. can produce diaphragms with more consistent groove dimensions with better carbide cutting tool	Burst tested 12 diaphragms machined taking care to center diaphragms dur tests
I-1	2/22/78	Injection test	For hydrogen injection losses: • To determine H_2 losses during driver operation • To observe transients in injection block pressure • To determine ability of chevron seals to prevent H_2 leakage from block For injection block design: • To test injection block port design • To test sphincter retaining system • To test diaphragm petaling concept on simulated injection block • To observe sphincter termination configuration on simulated injection block For shrapnel protection system: to determine ability to prevent damage	• Machined two driver injection port 20-inch diameter block to simulate section of the proposed injection design • Capped the central bore by steel f on each end and placed pressure transducers in each flange to reco pressure histories • Placed an explosive driver at each port, pressurized to 1950 psig, an detonated drivers

[a]Following I-1, STEALTH computer program was used to estimate the initial pressure response in the bore. Details about the STEALTH code are provided in Reference 1.

Procedure	Results	Conclusions
nd burst twenty 304 stainless steel	• Observed approximately the same amount of data scatter in Series D as in Series B • Noted that Series D diaphragms tended to burst at higher pressures than Series B diaphragms of same thickness and groove depth	• Machine diaphragm groove dimensions and "shape" more uniformly to reduce data scatter • Control diaphragm centering carefully to reduce data scatter in burst tests
ed 12 diaphragms machined by Niles e to center diaphragms during	• Observed burst data was as scattered as for the Series B and D diaphragms	• Diaphragms machined by Niles burst inconsistently • Require more diaphragm development
two driver injection ports into a diameter block to simulate a of the proposed injection block he central bore by steel flanges end and placed pressure ers in each flange to record bore histories n explosive driver at each driver essurized to 1950 psig, and then d drivers	• Recorded peak pressures of 85 Ksi at each end flange with pressure transducers • Flattened crush gages in the bore beyond their calibration (i.e., they were crushed by a greater than 115 Ksi pressure) • Noted that bolts retaining the end flanges failed in tension • Cracked the mild steel block along one side causing the bolts retaining the sphincter on that side to fail in shear • Terminated sphincters adequately • Formed craters in the central bore wall opposite each injection port • Some melting had occurred at craters • Observed no diaphragm petals remaining in the sphincter which broke loose • Found no evidence of shrapnel damage on outside of injection block or on the steel plate in front of the injection block • Observed that sphincters closed adequately	For hydrogen injection losses: • Injection losses could not be determined because of catastrophic failure of the injection block resulting in no measurement of the equilibrium H_2 pressure • The peak pressure of 85 Ksi measured by the transducers at the end flange is in good agreement with computer estimates by the STEALTH code[a], of 92 Ksi • The crush gages indicate pressures in excess of 115 Ksi, slightly higher than STEALTH predicts • Could not determine the ability of the chevron seals to prevent leakage due to mechanical failure at three of the four sealing surfaces, and the inability to remove the sphincter at the fourth surface to observe the chevron seal For injection design: • Must test the injection block design using 4340 (the material selected for the gun injection block) to determine if wall cratering caused by pressure forming and/or melting is a problem • Recess bolt heads to protect them from shrapnel, and possibly bevel the diaphragm retaining ring to simplify post-test disassembly to improve sphincter retention system For shrapnel protection: 1-inch thick red quarry tile provides adequate protection from shrapnel

Test No.	Date	Category	Objective/Purpose	Procedure
HB-1	3/28/78	Injection test	To determine if the cratering observed in I-1 can be eliminated by use of flared injection ports and by replacing the mild steel test block by higher strength 4340.	• Fabricated 4340 target block and heat treated • Placed a "flared" cylinder between the 4340 target block and explosive driver as a method of reducing stagnation pressures • Fired a driver at the 4340 target block after pressurizing the pressure tube to 1900 psig
HB-2	3/29/78	Injection test	Same as above	Same as above
D-4	4/13/78	Driver test	To determine source of particles which caused craters in test numbers HB-1 and HB-2.	Built and fired a driver; as the hot H_2 gas ejected from the driver, an X-ray recorded the amount and position of particles in the H_2 gas.
HB-3	4/25/78	Injection test	To: • Determine if modification of pressure tube/sphincter design would reduce particle damage • Determine if increasing the diaphragm thickness to 0.060 inches would improve diaphragm petal retention • Determine if placing the driver/port assembly directly against the 4340 target block plus use of a momentum trap on the back of the block would prevent the target block from cracking	• Fabricated driver-port assembly similar to those of HB-1 and HB-2 except that steel spacer was made to fit between the driver nozzle and target block • Modified the driver sphincter/pressure tube assembly • Normalized the pressure tube to improve its ability to expand without rupture • Machined a 0.060-inch thick grooved diaphragm • Placed a heavy steel plate against the target block to act as a momentum trap

TABLE 2. Continued

Procedure	Results	Conclusions
) target block and d" cylinder between the ck and explosive driver reducing stagnation at the 4340 target block ing the pressure tube to	• Observed no pressure forming • Found thin film of solidified metal melt on target and nozzle • Observed small craters in target due to particle impacts • Observed two of the four diaphragm petals still on, the other two appear to have been severed by the pressure tube • Noted that the target block cracked spontaneously after several days	• Can eliminate pressure forming if 4340 is hardened sufficiently and the injection ports are flared • Could not identify the source of the thin layer of solidified metal • Origin of the small craters in the target block probably result from the pressure tube debris forming during sphincter termination • Redesign of the sphincter/pressure tube is necessary to prevent cutting of the diaphragm by the pressure tube • Make diaphragms slightly thicker to reduce the tendency of petals to tear away • Breaking of the target block was due to residual heat treat stresses or driver sphincter impact which set up internal stresses eventually cracking the block
	Same as above, except that block cracked during test.	• Same as above • The block crack was probably due to sphincter impact
driver; as the hot H_2 the driver, an X-ray nt and position of H_2 gas.	Observed: • Several small particles 2 feet from the driver exit at 400 μsec after the driver detonation • Only small nubs of the diaphragm petals remained	• The absence of large amounts of particles in the flow indicates that the particles which cratered HB-1 and HB-2 had to originate late in the driver operation (i.e., during the driver termination) • Determined that the small particles observed originated at the diaphragm when the shock wave passed based on their position in the H_2 gas flow
ir-port assembly similar and HB-2 except that a made to fit between e and target block ver sphincter/pressure ressure tube to improve xpand without rupture -inch thick grooved teel plate against the act as a momentum trap	Observed: • The target block was cratered almost as badly as in HB-1 and HB-2 • The target block did not crack • The inside of the sphincter was much less torn up than for previously tested drivers • The pressure tube was more uniform than in previous shots • Only several small diaphragm petal nubs remained	• Revision of the sphincter-pressure tube assembly appears to be an improvement • Normalize pressure tube in all future drivers • Cracking of HB-1 and HB-2 probably due to impact of the block by the sphincter • Operation of the thicker diaphragm used in HB-3 was no better than previous diaphragms; in fact, 0.060-inch thick diaphragms may be too stiff to be opened properly by the 1900 psig H_2 gas

TABLE 2. Continued

Test No.	Date	Category	Objective/Purpose	Procedure
Mylar diaphragm tests	5/78	Diaphragm (burst) tests	To determine if mylar diaphragms were a viable alternative to stainless steel diaphragms, because it is difficult to make the stainless steel diaphragms work properly.	Burst 0.14-inch thick mylar ply hydrostatically; up to 5-ply were used in each diaphragm tested.
Series I	5/78	Diaphragm (burst) tests	To determine whether chemically etched steel diaphragms would burst more uniformly than machined diaphragms; the chemically etched diaphragms are much more uniform in groove depth than previously machined diaphragms.	Burst 30 chemically etched diaphrag hydrostatically.
I-2	5/26/78	Injection test	To: • Verify structural integrity of injection block design • Observe degree of pressure forming, particle damage, and melting opposite ports • Determine amount of H_2 in drivers which actually gets injected • Test ability of W-lined launch tube to survive projectile motion and gas flow • Test clamping system proposed for hybrid gun injection block mount	• Machined a single port section of injection block from a commercial forging; the injection port was f to lower the stagnation pressure • Heat-treated injection block • Capped the injection block bore b end flange at one end, placed W-l launch tube fitted with a project at the other end • Made a test stand employing a mil steel clamping arrangement simila that proposed for the hybrid gun injection block mount • Attached an explosive driver, the pressurized and detonated it

Procedure	Results	Conclusions
thick mylar ply ; up to 5-ply were aphragm tested.	• Increased the burst pressure by ~ 285 psig with each ply used	• Estimated by extrapolation of the burst pressure that ~ 0.15 inches (or 11-ply) of mylar are required to withstand the 2000 psig H_2 pressure of the driver prior to detonation representing 17 grams of mylar contamination per driver. Each driver will hold ~ 59 grams of H_2. • Above 4-ply the burst data appears to be nonlinear; therefore, to determine the exact number of mylar ply requires burst tests employing 10-, 11-, and 12-ply
ally etched diaphragms .	• Noted that data was consistent	• Chemically etched diaphragm burst pressures were much more consistent than machined steel diaphragms
ngle port section of an ck from a commercial 4340 injection port was flared tagnation pressure injection block ection block bore by an one end, placed W-lined tted with a projectile nd and employing a mild arrangement similar to for the hybrid gun k mount plosive driver, then d detonated it	• Split the injection block into 2 halves • Normal driver operation • Observed slight pressure forming opposite the port • Measured the projectile velocity leaving the launch tube as 3300 ft/sec • Observed that the first 8 inches of launch tube tungsten liner survived • Broke mild steel clamp due to the injection block failure • Subsequent metallurgical analysis revealed -- The forging used had a cast grain structure -- The injection block forging had a very low toughness -- The forging was heat treated to too high of a hardness -- The forging used possessed large inclusions • Subsequent structural analysis revealed -- The driver termination impact is the major load on the block followed by the impact of injected hydrogen -- Design modifications are available to decrease the stress loads	• Need to reduce the structural loads encountered during the injection process • Must carefully control forging quality and heat treat • Determined that almost all of the hot hydrogen was injected (based on the projectile velocity) • Splitting of the block occurred late in the injection process; otherwise, the projectile velocity leaving the launch tube would have been much less than 3300 ft/sec • Failure of the tungsten liner was caused by its delaminating at the nickel bond during heat treat

Test No.	Date	Category	Objective/Purpose	Procedure
I-3	10/4/78	Injection test	To: • Demonstrate that reducing injection-process-induced loads with improvements in the test injection block forging and heat treat eliminates structured failure of the injection block • Test mylar diaphragms since stainless steel diaphragms have not yet performed adequately	• Revised the explosive driver des provide small drivers (i.e., lo termination loads) • Placed a mild steel spacer betw and the injection block to cushi and spread them over a large inj block area • Rounded the intersection of the block bore with the driver inject to reduce stress concentrations • Forging was -- Aircraft quality 4340 -- Triple upset -- Heat treated to a lower hardn in I-2 for a higher toughness • Used a mylar diaphragm; the numb required was determined by extra of the burst pressure of a singl • Performed in 1/8-scale (i.e., 1/ the 1/4-scale hybrid launcher) t costs • Placed a launch tube and project end of the injection block, the was capped with an end flange
I-4	11/20/78	Injection test	To determine if the spacer used in I-3 to cushion and spread the load is necessary for the injection block to survive since the spacer increases the volume of hydrogen which may be trapped in injection port regions during actual hybrid gun operations, resulting in reduced gun performance.	Honed the I-3 injection block to r thin melt layer deposited in the b retested the block eliminating the steel spacer.

TABLE 2. Continued

Procedure	Results	Conclusions
losive driver design to rivers (i.e., lower driver ds) teel spacer between drivers on block to cushion loads over a large injection ersection of the injection the driver injection port s concentrations lity 4340 to a lower hardness than higher toughness aphragm; the number of ply termined by extrapolation essure of a single ply 8-scale (i.e., 1/2-scale of ybrid launcher) to lower tube and projectile at one ction block, the other end an end flange	• The injection block survived without any damage, which was confirmed by ultrasonic testing • Observed that there were ~ 0.01-inch depressions opposite each of the two driver ports • Noted that the bore of the injection block contained a larger amount of solidified molten steel droplets than in I-2 • Found one very slight particle crater opposite one of the driver injection ports • Measured the projectile velocity leaving the launch tube at 3320 ft/sec • Metallurgical samples from the forging used in I-3 indicated it was better than the I-2 forging, but segregation of the alloying elements caused it to have soft spots due to ferrite formation during heat treat	• The mechanical problems which caused the I-1 and I-2 failures have been solved by redesigning to reduce driver loads and carefully controlling the injection block metallurgy • The I-3 success was not for an optimum quality forging as the forging used would not have met aircraft quality specs • Use of mylar diaphragms eliminated most of the remaining cratering problems • Must test the injection block in 1/4-scale to verify its success in the 1/4-scale hybrid launch design • Some attention must be given to the injection block melt problem
ection block to remove the eposited in the bore, then k eliminating the mild	Same as for I-3 except: • Observed no cratering at all opposite either injection port • Observed slightly more melting	Same as for I-3. Found that the mild steel spacers incorporated into the I-3 redesign are not necessary and they will be removed to increase the hybrid gun performance.

TABLE 2. Concluded

Test No.	Date	Category	Objective/Purpose	Procedure
Mylar diaphragm	3/79	Diaphragm (burst) tests	To determine thickness of diaphragm required for I-5.	• Purchased several types and thickness mylar sheet • Perform burst test (hydrostatically) diaphragms using various numbers of p on one of the I-5 drivers
I-5	3/26/79	Injection test	To show that a redesign of the drivers and injection block, coupled with improved metallurgy, solves mechanical failure problems associated with I-1 and I-2. The I-4 test confirmed this in 1/8-scale (1/2-scale of the 1/4-scale hybrid launcher); however, a 1/4-scale test is necessary before continuing work on this hybrid launcher.	• Used the actual forging purchased for launcher injection block, which is va melted aircraft quality 4340 • Machined two flared driver ports in t I-5 forging using the I-4 injection block design • Performed a carefully controlled heat treatment of the injection block and heat-treated block was ultrasonically tested and magnafluxed to detect crac • Placed two massive plugs in each end the injection block; one plug was fit with a section of tungsten-lined laun tube; placed a projectile in the laun tube • Placed a piece of carbon cloth opposi one port and silica cloth opposite th other to test them as thermal protection • Attached drivers of the I-3 and I-4 design but scaled-up to 1/4-scale, then detonated

Procedure	Results	Conclusions
several types and thicknesses of et urst test (hydrostatically) on s using various numbers of ply the I-5 drivers	Observed diaphragm burst pressures of approximately 400 psig per mil of diaphragm thickness	• Concluded that burst pressure is independent of mylar type • Need a 60-mil thick diaphragm for I-5
actual forging purchased for the injection block, which is vacuum-rcraft quality 4340 two flared driver ports in the g using the I-4 injection ign a carefully controlled heat of the injection block and the ted block was ultrasonically d magnafluxed to detect cracks o massive plugs in each end of tion block; one plug was fitted ction of tungsten-lined launch ced a projectile in the launch piece of carbon cloth opposite and silica cloth opposite the test them as thermal n drivers of the I-3 and I-4 t scaled-up to 1/4-scale, nated	• One of the mylar diaphragms burst during initial pressurization (after holding pressure for several minutes at 2000 psig) • Undamaged injection block • Observed slight pitting opposite each injection port • Debonding and failure of the majority of the tungsten liner in the launch tube • Noted that the projectile velocity was close to that predicted for 100% hydrogen injection • Observed resolidified melt, but the amount was less than in I-3 or I-4 • Studies of pieces of the forging which were sent through the heat treat along with the injection block revealed: -- A very good in-depth heat treat with uniform hardness was accomplished -- The toughness of the heat treated forging is good, but not as high as expected (especially in the radial direction) -- Microhardness measurements and photomicrographs indicate a very fine segregated banded structure which should have been eliminated by homogenization at 1900°F	• Design modifications made in I-4 adequate to prevent injection block failure when scaled from 1/8 to 1/4-scale • Must improve the bond holding the tungsten liner to the launch tube • Excellent driver performance in the new design; almost all of the hydrogen must have been injected • Placing simple thermal protection cloths opposite drive ports appears to reduce melt damage; carbon cloth seems to be slightly better than silica cloth for this • The forging used for I-5 should have been upset more times and homogenized at 1900°F prior to machining; however, this could not be done since partial machining had taken place prior to the I-1 failure. The forging is adequate for use in the hybrid launcher with the new injection block-driver design. • Must investigate creep failure of mylar diaphragms before specifying thickness in future tests

3.1 EXPLOSIVE DRIVER DEVELOPMENT TESTS

A schematic of explosive driver operation is shown in Figure 6 to illustrate driver terminology and features. The explosive drivers consist of two concentric tubes. The inner tube (pressure tube) is filled with pressurized hydrogen. The annulus between the pressure tube and the outer tube (tamper) is filled with nitromethane. The nitromethane is detonated at one end to initiate driver operation. As the detonation wave progresses forward, the tamper explodes while the pressure tube implodes to form a solid steel bar. The progressive implosion acts as a piston which drives a shock wave into the hydrogen, forming a slug of high-temperature, high-pressure gas. Eventually this slug of gas is ejected from the driver. The driver is closed at the termination assembly (sphincter) located at the downstream end of the nitromethane column. Proper coupling and sealing of the sphincter with an injection assembly prevents subsequent hydrogen leakage. A representation of driver performance in dimensionless $\bar{x}$ vs $\bar{t}$ is shown in Figure 7.

The design parameters for the 6-kbar hydrogen drivers were reported in Reference 3. The design was based on prior experience and on 1-D finite difference calculations of the expansion and collapse phases of driver operation. Before beginning development tests, several additional 1-D expansion-collapse calculations were made to determine the sensitivity of the design to various combinations of pressure tube, explosive, and tamper thicknesses and to various degrees of expansion prior to explosive collapses. The driver design prior to initiation of testing is shown in Figure 8.

The design was tested by itself in tests D-1, D-2, and D-3 to:

- Determine the timing of driver operation and verify repeatability
- Observe proper pressure tube collapse
- Observe sphincter closure
- Collect hydrogen shock data for equation-of-state development
- Determine the maximum driver length possible before boundary layer effects reduce performance

It was determined from the initial test (D-1) that a thicker tamper was required in the exit region to prevent overexpansion and rupturing of the pressure tube and sphincter. Test D-1 also provided the initial

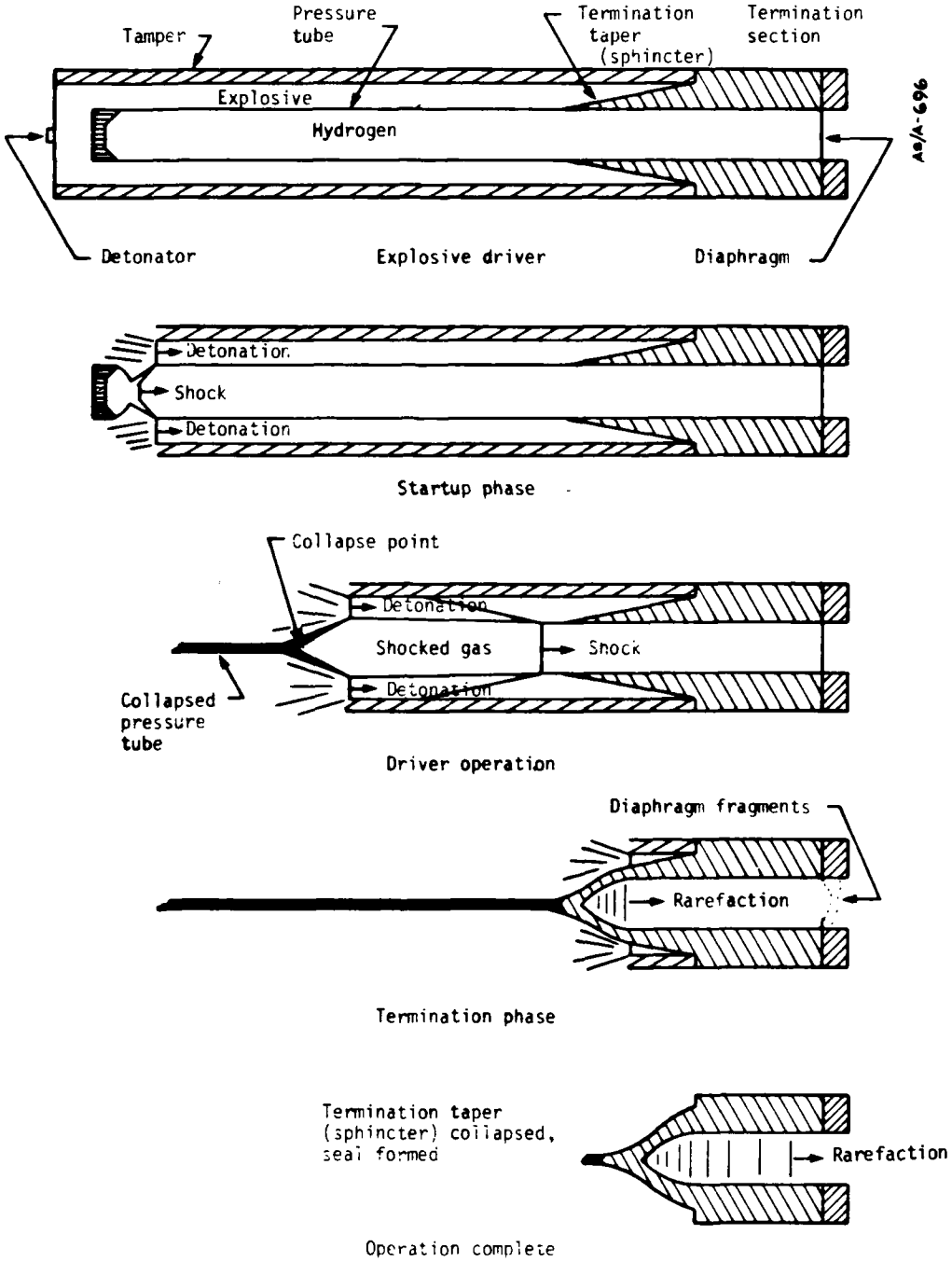

Figure 6. Schematic of explosive driver operation.

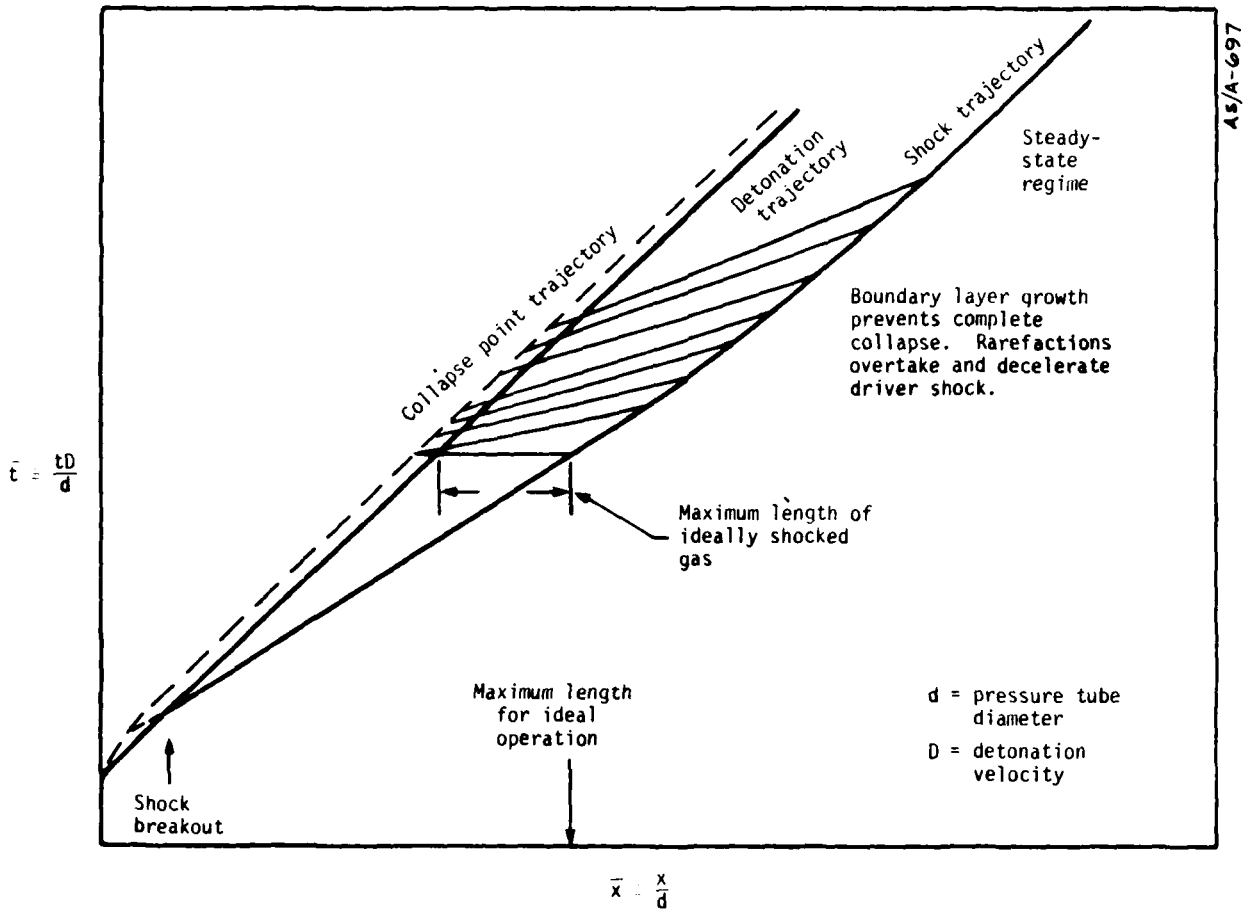

Figure 7. Dimensionless $\bar{x}$-$\bar{t}$ diagram for a long explosive driver.

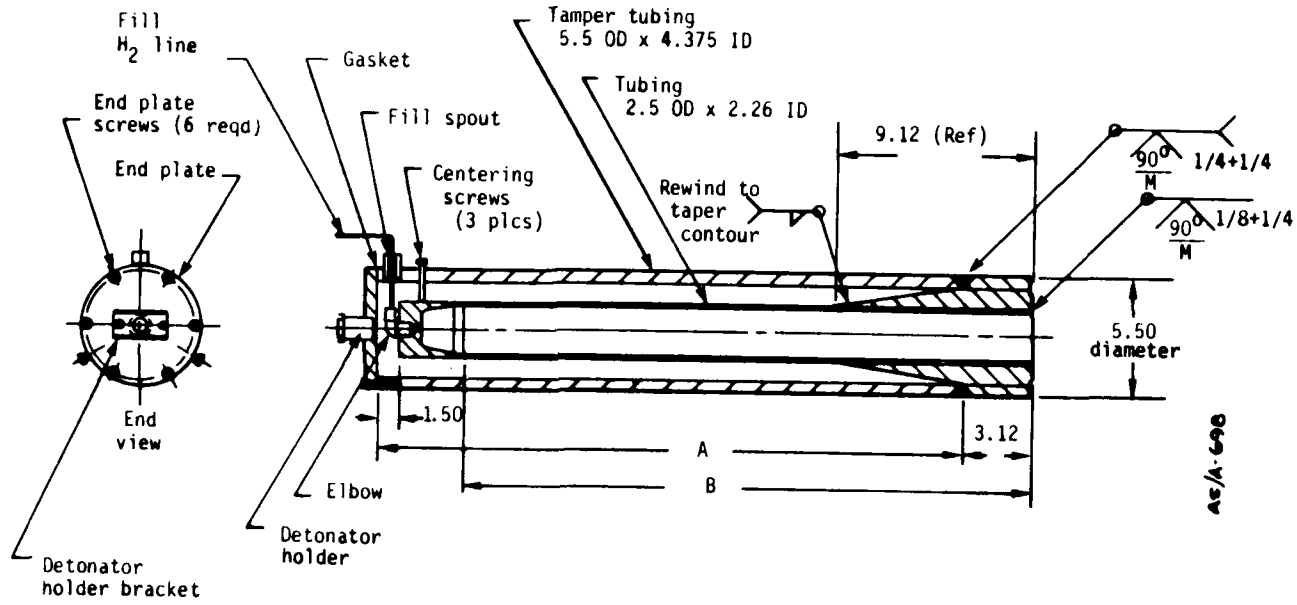

Note: Lengths A and B to be determined
(Dimensions in inches)

Figure 8. Initial driver design.

detonation and shock velocity data used to define driver timing and modify the hydrogen equation-of-state. All later drivers confirmed these data and verified driver repeatability. It was also determined in D-2 that boundary layer degradation is not significant at driver lengths of interest.

Later tests (I-1 through I-5) employed drivers as a necessary part of the injection system checkout. Photos of these drivers are provided in Section 3.3. These tests provided additional opportunities to observe driver performance. From these additional tests, it was determined that:

- The pressure tube should be annealed to facilitate expansion without rupturing
- The driver sphincter/pressure tube assembly should be modified to reduce termination debris
- The driver size had to be reduced to prevent injection block damage due to driver impact loads

The final driver design which evolved as a result of all driver testing is shown in Figure 9.

In all, a total of 16 drivers were tested. Table 3 is a tabulation of driver performance data. A brief but detailed discussion of each driver tested follows.

3.1.1 Driver Test D-1

The first driver test was made to verify the design of Reference 3. The shock and detonation wave trajectories were determined from shorting pin data. After a startup phase, the trajectories followed their anticipated x-t paths.

From Reference 3, the shocked gas conditions calculated for this driver design were:

Snock velocity = 0.935 cm/μsec
Flow velocity = 0.682 cm/μsec
Shock pressure = 6.5 kbar
Shock density = 0.037 gm/cm^3
Shock density ratio = 3.7
Shock temperature = 2483°K

According to the hydrogen equation-of-state (Reference 2), the importance of intermolecular forces is primarily determined by the covolume parameter. Based on the shock velocity observed in this test and

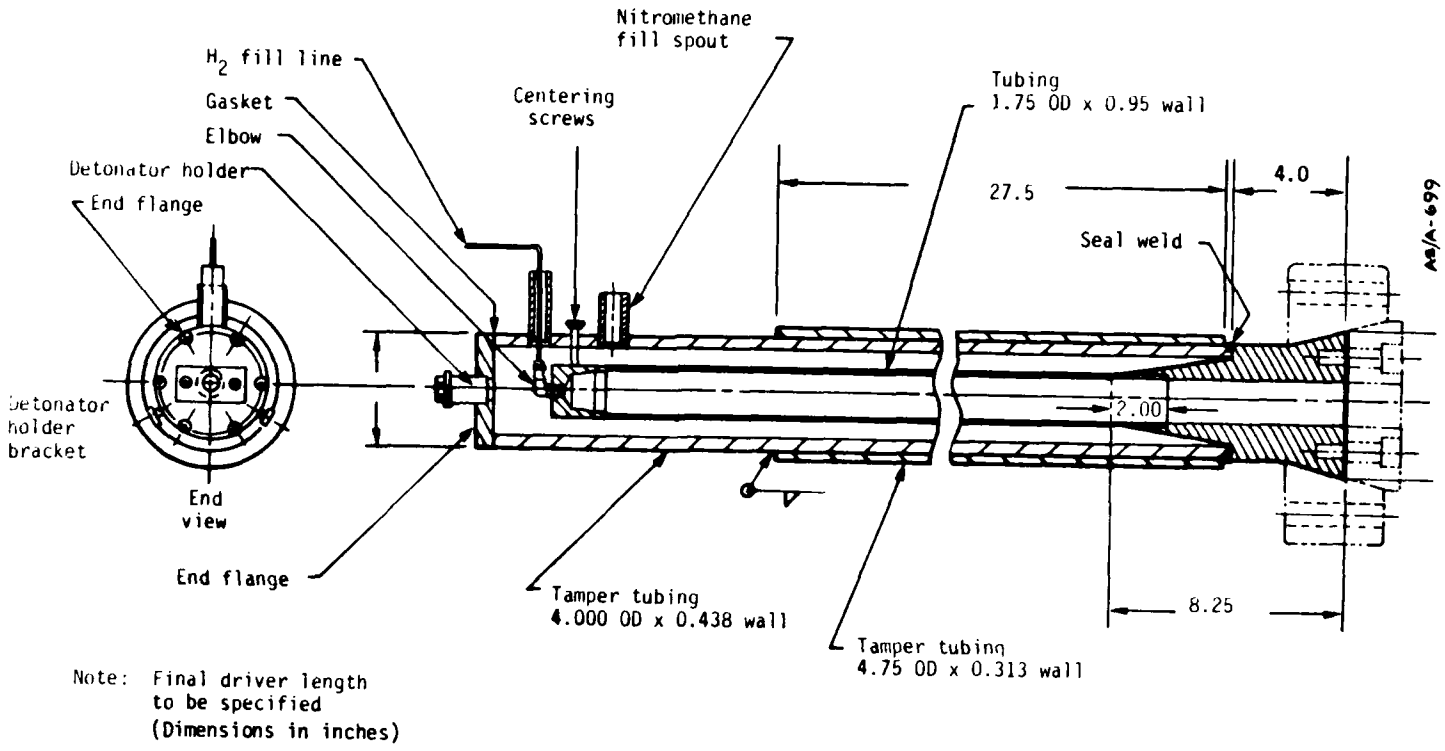

Figure 9. Final driver design.

TABLE 3. SUMMARY OF EXPLOSIVE DRIVER PERFORMANCE AND DEVELOPMENT

Driver No.	Test No.	Pressure Tube ID (cm)	Driver Length (cm)	Initial H_2 Conditions (psig/°K)	Detonation Velocity (cm/μs)	Shock Velocity (cm/μs)	Comments
1	Driver D-1	5.740	213	1990/307	0.683	0.894	
2	Driver D-2	5.740	391	1350/282	0.667	0.879	"Long driver" technology expt. (4 kbar)
3	Driver D-3	5.740	185	1900/289	0.689	0.891	Extra tamping added to control expansion
4	Injection I-1A	5.740	185	1950/294	0.687	0.930	
5	I-1B	5.740	185	1950/294	0.689	0.874	
6	Test HB-1	5.740	185	1900/296	0.678	0.934	Estimate of driver termination momentum
7	Test HB-2	5.740	185	1900/293	0.683	0.835	
8	Driver D-4	5.740	185	1900/297	0.682	0.879	1-Mev X-ray of flow
9	Test HB-3	5.740	185	1900/289	0.684	0.896	Pressure tube normalized and inserted 1 dia. into taper
10	Injection I-2	5.740	185	1900/301	0.688	0.870	
11	Injection I-3A	1.974	63.5	1900/308	0.68	0.87	Mylar Diaphragms
12	I-3B	1.974	63.5	1900/308	0.68	0.90	
13	Injection I-4A	1.974	63.5	1900/	0.68	0.9	
14	I-4B	1.974	63.5	1900/	0.68	0.9	
15	Injection I-5A	3.962	140	1900/	0.68	0.97	Anomalously high shock velocity } Final design for 1/4-scale launcher
16	I-5B	3.962	140	1900/	0.68	0.93	

subsequent driver experiments, the best value for the covolume parameter was found to be 8.6 cm^3/gm. This is 75 percent of the covolume parameter based on the critical volume ($b = V_c/3 = 11.52\ cm^3/gm$). A further description of the equation-of-state is provided in Appendix A.

The recovered pressure tube was sectioned and the collapse of the tube was judged to be complete. The driver functioned as expected until near the end of the driver cycle where overexpansion of the pressure tube and sphincter prevented proper closure.

The test results are summarized in Table 3.

3.1.2 Driver Test D-2

This was a test of a 400-cm driver (about twice as long as planned for use on the launcher) to determine the region where boundary layer growth prevents complete pressure tube collapse. When tube collapse is incomplete, hydrogen is trapped and pressure gradients develop in the shocked gas column. The accompanying degradation in shocked gas energy density would unacceptably limit launcher performance.

In this test, the driver was operated at a lower shocked gas pressure (4 kbar) to limit driver expansion during the latter stages of operation. The late-time shock trajectory showed no deceleration, so tube collapse was judged complete for at least the first 200 cm of operation. Thus, driver operation can be considered nearly ideal (except for pressure tube expansion prior to collapse) for driver lengths of about 200 cm (see Table 3 for a summary of test results).

3.1.3 Driver Test D-3

The objective of this test was to achieve proper closure of the driver termination section. Based on 1-D expansion-collapse calculations, an extra section of steel tamper was added to the end of the driver to inertially control late-time pressure tube expansion. Driver operation was normal and the additional tamping was effective. The driver termination formed in the prescribed manner and had the necessary mass to provide a good seal when attached to the launcher injection block (see Table 3 for a summary of test results).

3.1.4 I-1 Drivers

Two drivers of the same design as Driver Test D-3 were used to inject hydrogen into a test injection block. The first generation of a driver attachment and sealing system was evaluated in this test. The

pressure history in the injection block was measured to help estimate the amount of gas injected.

The shock and detonation trajectories of the two drivers were within expected limits. The driver terminations (sphincters) formed properly. However, both termination sections appeared to project some fragments into the injection block. (This was observed in later tests and subsequently eliminated; see Sections 3.1.7 and 3.1.8.) Because the injection block split open, it was difficult to evaluate the driver attachment and sealing system. Some obvious improvements, such as larger V-sealing rings and revised bolt placement, were suggested.

The first quantitative estimates of driver termination structural loads were made based on this test. The thick-walled injection block was caved in about 1.3 cm (1/2 inch) around the injection ports. Some simplified analytical structural calculations indicated a peak deflection on the order of 1.3 cm (1/2 inch) under a load of $6.7*10^{11}$ dynes (1-1/2 million lb_f) (see Table 3 for a summary of test results).

3.1.5 HB-1 Driver

The objective of this test was to use the driver design from the previous injection test (I-1) to observe the impact of the driver gas on a test block representing the internal bore of the injection block. From the standpoint of driver development, four observations were noteworthy.

First, detonation velocity was within the normal range, although the shock velocity was on the high side (see Table 3). Second, the termination closure was again judged to be very good (see Figure 10 as an example). Third, the test block was pitted, indicating that either diaphragm fragments or debris from the driver itself were entering the gas flow. The most important observation was the estimate of driver termination momentum that was inferred from this test. Prior to the test, an estimate of the explosive pressure history on the driver termination had been made from 1-D expansion-collapse calculations. The pressure-time relation was approximated by a 70-kbar peak pressure decaying linearly over 50 μsec. When applied to the available cross sectional area to accelerate the 38.6-kg (85-lb_m) termination section of this test, the resultant velocity is 76.2 m/sec (250 fps). The start of imprints of the termination bolt heads on the test block was observed, indicating the onset of local yielding of the 12-kbar heat-treated steel. The peak

Hugoniot pressure of steel on steel at 250-fps impact velocity is about 12 kbar, so 76.2 m/sec is a reasonable impact velocity. Thus, the momentum input of the termination section was estimated based on a 38.6-kg mass impacting at 76.2 m/sec. Other observations in later tests confirmed this original estimate (see Table 3 for a summary of test results).

3.1.6 HB-2 Driver

This was a repeat of test HB-1 with some modifications to the test block. Driver operation was within normal limits, however, the shock velocity was on the low side (see Table 3). Again, there was unacceptable pitting of the test block from debris in the flow, and a diagnostic test was designed to determine the source (see Table 3 for a summary of test results).

3.1.7 D-4 Driver

In this test, a 1-Mev X-ray was used to look at metallic debris in the gas flow of the current driver design. Three sources of steel fragments were hypothesized. Particles from a startup jet formed during initial collapse of the pressure tube would be out in front or near the leading edge of the shocked gas column. The tips of the diaphragm petals were expected to accelerate quickly to local flow velocity and would be found in the middle of the gas slug. Larger debris from the diaphragm or termination section would be slow and would appear later in the flow.

The driver x-t path and recovered termination section were normal. A barium titanate crystal mounted on an impact target recorded the arrival of the shocked gas as the first event. Thus, nothing was ahead of the gas pulse. The 1-Mev X-ray recorded the entire length of the gas slug and showed a group of about six small particles in the middle of the gas flow. These were taken to be the tips of the diaphragms moving at or near flow velocity (0.68 cm/ sec). Some late-term debris was just entering the field of view. This was interpreted as low velocity jet fragments emitted during the termination process. The debris was estimated to be moving at 0.2 to 0.3 cm/μsec. In general, the main body of the gas column looked very clean and free of metallic contamination.

An analysis was made of the termination process. This analysis examined the tendency for the driver to jet as the detonation wave moves

up the sphincter. From the analysis, it was determined that several inches into the sphincter the pressure tube should break loose from the sphincter, throwing fragments down the injection port. This agrees with observations of previous drivers which showed that the pressure tube pealed away from the sphincter and was bent forward at this location. A cross section of the D-4 sphincter (shown in Figure 10) illustrates this quite clearly. Based on this observation, all subsequent drivers were modified by inserting the pressure tube no more than 1-1/2 diameters into a taper section as shown in Figure 9 (see Table 3 for a summary of test results).

3.1.8 HB-3 Driver

The driver used in this experiment incorporated two notable changes. First, the drawn-over-a-mandrel (DOM) tubing was normalized to recover the ductility lost during the DOM process. Since we had observed somewhat more variation in shock velocity than desired and since recovered pressure tubes had longitudinal "stretch marks," we felt performance consistency would improve by increasing the ductility of the pressure tube. Second, the driver termination was redesigned as described in the previous section to remove a major source of late-term debris.

Driver performance was excellent and the sectioned termination showed little tendency to recirculate metal. This can be seen in Figure 10. There were small impact craters in the test block, but these were judged to be from diaphragm fragments (see Table 3 for a summary of test results).

3.1.9 I-2 Driver

One driver was used in this test and performance was well within normal range. The injection block used in I-2 split open during the test. Post-test analysis indicated driver impact loads to be the major cause of failure (see Table 3 for a summary of test results).

3.1.10 I-3 Drivers

From the analysis of the I-1 and I-2 injection block failures, it was concluded that the size of the explosive drivers relative to the injection block should be decreased to reduce structural loads to within an acceptable limit. To test this conclusion, a 1/8-scale (i.e., 1/2 size of the 1/4 scale) two-port module of the injection block was fabricated. The size of the drivers was decreased 30 percent relative to the injection

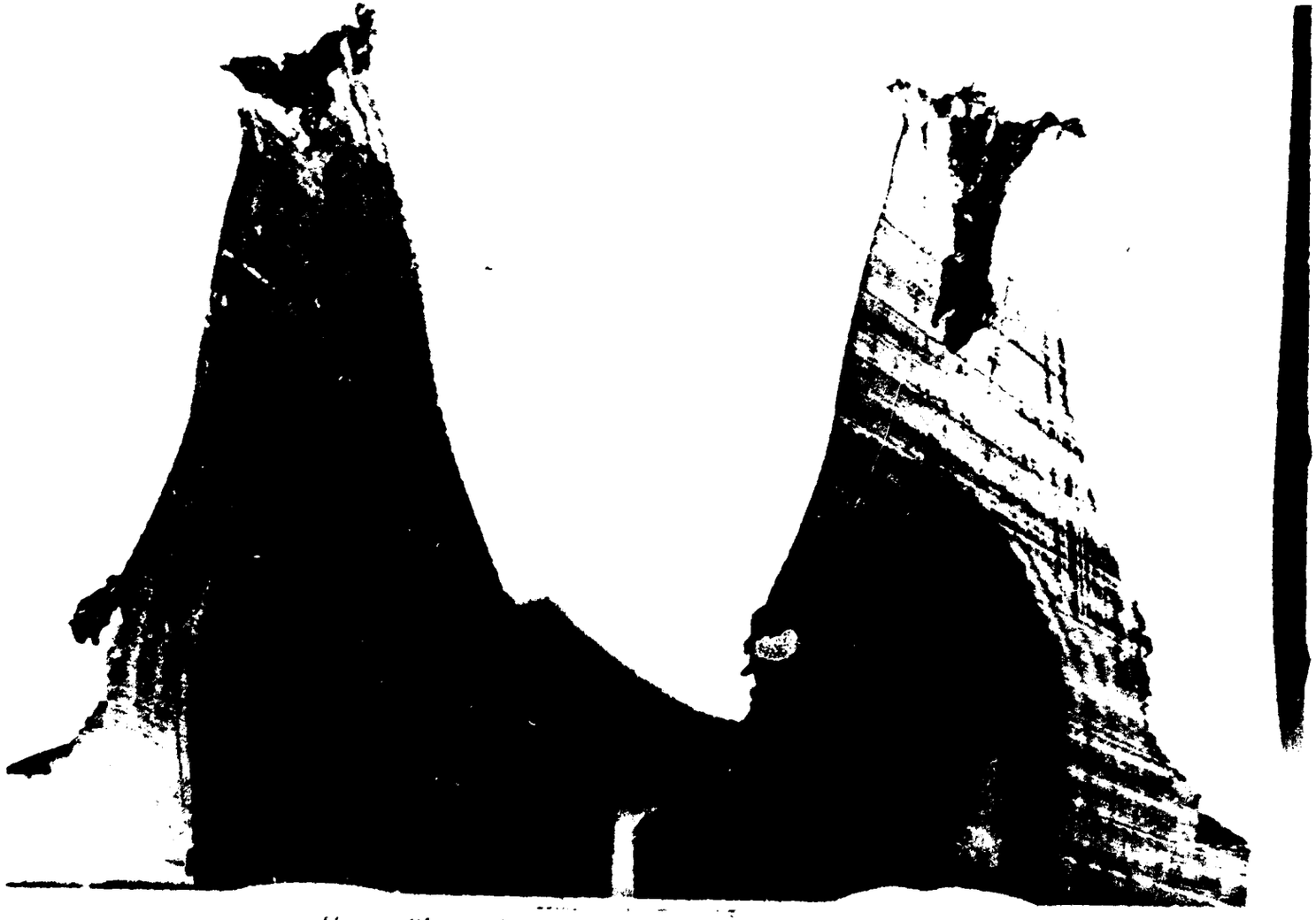

AS/H-190b

Figure 10. Comparison of D-4 sphincter with redesigned HB-3 sphincter.

block size, and the injection port diameter was decreased 30 percent to accommodate the smaller driver size. These drivers were scaled from the I-2 driver design within the constraints of available commercial tubing sizes. The driver C/M (weight of explosive to weight of pressure tube) was decreased by a small amount, and, with I-D calculations, confirmed that expansion-collapse characteristics were within acceptable limits. In addition, a change was made to mylar diaphragms eliminating metallic diaphragm debris.

Driver operation and termination mechanics were very good, and the downsized drivers did not damage the injection block. Because of the slightly lower C/M, shock breakout was somewhat later than in previous tests. Shock and detonation trajectories were otherwise normal. The terminations closed properly and the sealing system worked very well. There was negligible pitting of the injection block opposite the injection ports (see Table 3 for a summary of test results).

3.1.11 I-4 Drivers

This was, from the viewpoint of drivers, a repeat of the I-3 tests, and the results of this test were essentially the same as those of I-3 (see Table 3 for a summary of test results).

3.1.12 I-5 Drivers

After the successful I-3 and I-4 tests, the I-5 experiment was designed to test the 1/4-scale injection block with the 30-percent smaller drivers. Two drivers were used with mylar diaphragms. The results of this test were good. Gas injection appeared to be complete with the required energy. Pin data on both drivers indicated that shock breakout was later than customary, and that shock velocity of one of the drivers was higher than normal (see Table 3). Since the design was carefully scaled from the I-3 and I-4 design, this is difficult to account for. There was no evidence of driver jetting either in the injection block or in the measured performance of the injected gas (see Table 3 for a summary of test results).

3.1.13 Driver Test Conclusions

The design of the explosive driver is essentially complete. The following objectives were achieved:

- Reproducible driver performance well within acceptable limits (with one exception -- shock velocities were $\pm$ 6 percent
- Good termination (see Figure 10)

- Good quantitative data on dynamic structural loading from driver termination (see Section 3.1.5)

3.2 DIAPHRAGM TESTS

The driver designs described in Section 3.1 require a 140-bar (2000-psig) initial pressure. It was originally intended to use a thin stainless steel diaphragm to seal the downstream end of the driver. The driver shock would burst the diaphragm. Injection gas temperatures were low enough so that diaphragm fragments would not vaporize and contaminate the flow. However, the metal fragments could cause pitting and crater damage as well as deposit melt droplets in the interior of the launcher.

The initial attempts to solve this problem used a nylon disk (test D-1) into which metal fragments would be embedded, and diaphragm plugs (test S-1 through S-3) could be released and caught opposite the injection port just prior to driver operation. Neither of these techniques worked well and were abandoned (see Table 2, tests S-1, S-2, and S-3).

Subsequent work concentrated on developing metal diaphragms which could be opened prior to arrival of the 6.5-kbar hydrogen shock wave. By inducing diaphragm opening prior to shock arrival, it was hoped that no diaphragm fragments would be introduced into the flow.

Stainless steel diaphragms were developed which could be opened by detonating a small amount of high explosive (1 gram of EL506) at the diaphragm center. The diaphragm design is shown in Figure 11. Two grooves at 90o to each other were machined into the diaphragms. In subsequent tests, the grooves were etched for better depth control. These grooves caused the diaphragms to rupture uniformly along the scribe when the explosive on the diaphragm was detonated. When diaphragms were not well centered, they often failed to tear along grooves, resulting in ragged petals which would easily be removed by form drag when hydrogen gas passed over the petals.

A number of burst tests were conducted to determine the optimum groove depth and diaphragm thickness. Other tests employed a 1-Mev flash X-ray to measure diaphragm opening times. These tests revealed that the 140-bar (2000-psig) hydrogen pressure in the pressure tube cannot completely open 5.72-cm (2-1/4-inch) diameter diaphragms if the diaphragm

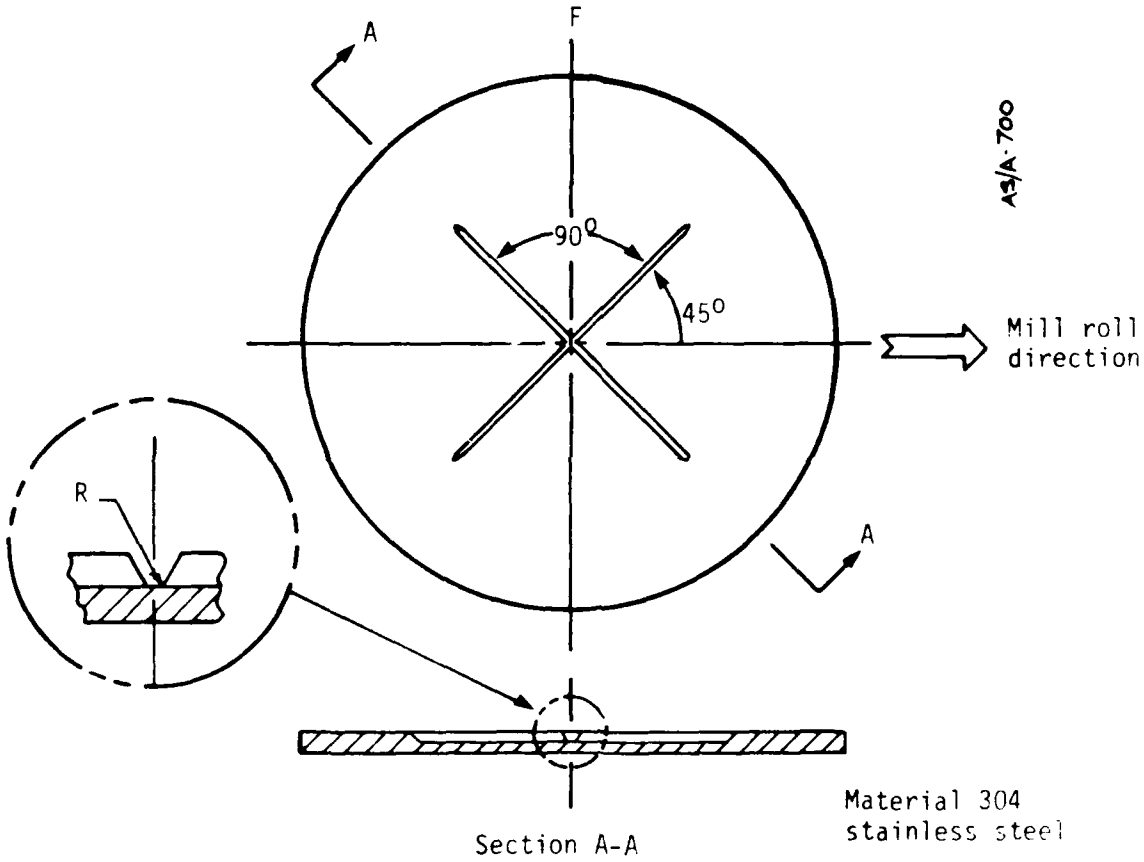

Figure 11. Metal diaphragm design.

thickness is greater than 1.5 mm (0.06 inch). It was also determined by X-ray data that diaphragms 1.0 to 1.5 mm (0.04 to 0.06 inch) thick require 400 to 600 sec, respectively, to open. The amount of hydrogen which can escape from the pressure tube prior to shock arrival is insignificant if shock arrival at the diaphragm location is timed for 400 to 600 sec after initiating diaphragm opening.

These self-petaling diaphragms were used in tests I-1, I-2, HB-1, HB-2, and HB-3. In two of these tests, two of the four petals remained after driver operation. The tips of the remaining petals were melted or torn away. The other two tests were less successful at retaining any of the diaphragm petals. After consideration of the difficulties involved in developing a satisfactory self-petaling metal diaphragm, it was decided to abandon them.

Beginning with test I-3, mylar diaphragms were used, which burst upon shock arrival. Because of the high strength to weight ratio of mylar, it is possible to seal the 140 bar (2000-psig) pressure in the driver pressure tube with a minimum of diaphragm material. Burst tests were performed to determine the minimum mylar thickness required to seal drivers.

There was concern that the mylar fragments would vaporize and contaminate the hydrogen. However, under the conditions of the injection tests, this did not appear to be a significant problem. Injection block pressure histories and test projectile launch velocities were all within a few percent of calculated values. Any substantial degradation in hydrogen temperature because of mylar contamination would have noticeably reduced the observed test projectile launch velocity.

In all of the injection tests using metal diaphragms (I-1, I-2, HB-1, HB-2, and HB-3), small craters were observed on surfaces opposite the driver discharge. These craters had been attributed to particle damage from metal fragments released during driver termination. Tests I-2 and HB-3 were performed with a redesigned termination section, which significantly reduced the particle damage. In the tests which employed mylar diaphragms, little to no cratering occurred. It must be concluded, therefore, that at least part of the cratering observed in previous tests was a result of diaphragm fragment impacts.

During the I-5 test, one of the diaphragms burst prematurely after holding 140 bar (2000 psig) for several minutes. This failure was at a pressure below that predicted by hydrostatic burst tests performed previous to I-5 to select the diaphragm thickness. This failure suggests that creep may affect the long-term mylar burst pressure.

Mylar diaphragms will be employed in the 1/4-scale launcher because they have proven to be both the simplest and the most adequate of the diaphragm systems tested. A small amount of additional development is still necessary to determine the minimum thickness required (i.e., to minimize the contamination of the injection hydrogen by mylar). This additional work will have to assess the possibility of failure due to creep to ensure that the diaphragm thickness selected is adequate.

3.3 INJECTION TESTS

To date, most testing has been directed toward developing the injection system for the 1/4-scale launcher. These tests were to determine the mechanical integrity of the injection block design and the driver coupling system and the amount and thermodynamic state of hydrogen injected into the block by the drivers. Toward these ends, two injection tests were originally envisioned. The first test (I-1) was to verify the amount of hydrogen injected by the drivers, and the second test (I-2) was to validate the injection structural dynamics. Unfortunately, in both tests the injection blocks were destroyed by the overwhelming loads placed on them during hydrogen injection and driver termination.

Analysis of the I-1 and I-2 failures suggested that a number of changes be made to improve the chances of injection block survival. These changes included the following:

- Injection ports should be flared to reduce the stagnation pressure against the bore wall opposite the injection ports
- Driver size should be reduced to lower the load at each injection port during driver termination
- Driver termination should occur at a further distance from the injection block
- The contact area between drivers and the injection block should be increased
- Care should be taken to ensure that injection block metallurgy is adequate (i.e., no large inclusions or cracks, and optimum heat treat)

These changes were incorporated into a new injection block and driver design. To minimize costs, the changes were tested in I-3 and I-4 in 1/8-scale (i.e., 1/2 size of the 1/4-scale injection system) to verify that they would indeed eliminate injection block failure. Both I-3 and I-4 were successful and were followed by a 1/4-scale injection test (I-5) which was also successful.

The success of I-3, I-4, and I-5 validated that their designs were adequate to prevent mechanical failure of either the injection block or the driver coupling system. They also indicated that nearly all of the hydrogen in the drivers was being injected into the injection block. Both I-3 and I-4, however, showed evidence of melting in the injection block bore. Such melting could be very damaging if melt from the injection block deposits on the tungsten liners of the launch tube. Calculations indicate that the most probable source of this melt was the intense but short-lived heating opposite the driver injection ports. In I-5, an ablative material was placed opposite the injection ports. The amount of melting observed in I-5 was much lower than in I-3 or I-4, suggesting that the use of ablative protection at these locations may solve the melting problem. A more detailed description of each injection test follows.

3.3.1 Injection Test I-1

The major objectives of I-1 were to:

- Determine the amount of driver gas injected into the injection block during driver operation
- Determine the time history of driver gas injection
- Test the driver coupling system and demonstrate proper sealing of the driver sphincters

A test injection block representing a two-driver module of the 1/4-scale injection block was fabricated along with two 6.5-kbar drivers and a test stand. The test block was machined from a mild steel forging to reduce material costs and to eliminate the time required to obtain and later heat treat a 4340 forging (which is the material designated for the 1/4-scale launcher injection block). A sketch of the I-1 test injection block is shown in Figure 12, and a photo of the assembly prior to firing is presented in Figure 13.

Each end of the injection block was sealed by an end flange on which pressure transducers were mounted. Crush gages were placed in the

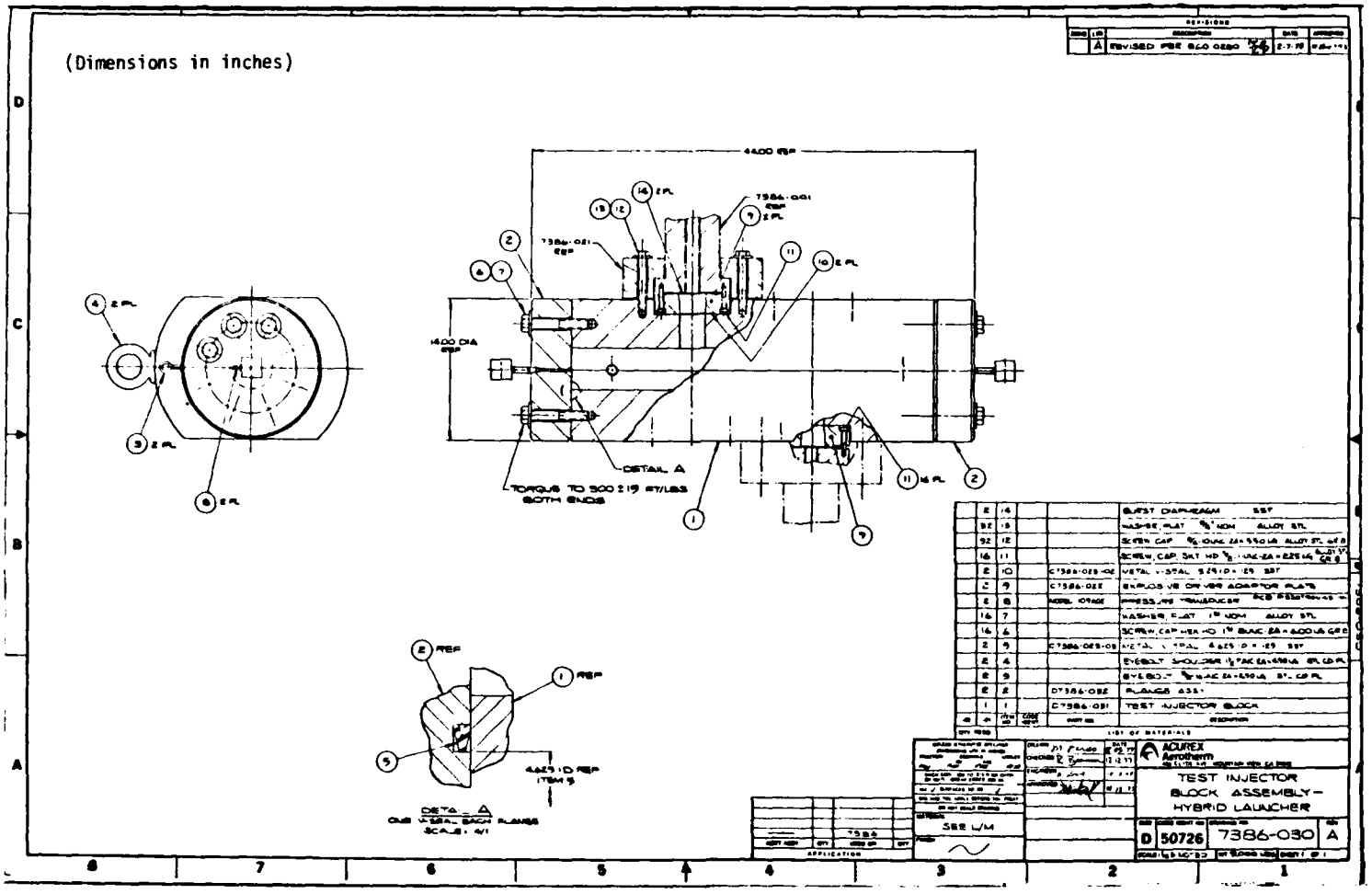

Figure 12. I-1 test injection block.

AS/H-653b

Figure 13. I-1 block during assembly.

internal bore to record the maximum pressure experienced there. Thus, pressure could be recorded and compared with the equilibrium state (1.9 kbar and 3500°K) for 100-percent hydrogen injection.

The test block split open on one side as shown in Figure 14. When this occurred, the bolts retaining the driver sphincter on the fractured side were sheared, releasing the driver and its coupling flange. However, the driver on the other side of the injection block remained in place. The sphincter which remained in place could not be removed following the test. It could not be determined whether this was because the split injection block was pinching the diaphragm clamp ring or whether the diaphragm ring had swaged itself into the driver port entrance by expanding. It was, therefore, not clear if any redesign of the driver attachment (coupling) system was necessary. The sphincter which remained in place closed adequately. Unfortunately, the internal injection block pressure was not maintained long enough to verify that the sphincter would remain closed if the block had retained the injected hydrogen.

The two end flanges were blown off. Examination of the flange bolts indicated that they failed due to a tensile loading (not shear). These, therefore, failed from pressurization of the injection block (not because the block split). Based on the ultimate strength of these bolts, it must be concluded that internal pressures of greater than 4.1 kbar (60 ksi) were attained. The pressure transducer recorded a peak pressure of 6.9 kbar (100 ksi). The crush gages were flattened beyond their calibration, indicating they felt a pressure greater than 7.9 kbar (115 ksi).

Post-test analyses using the STEALTH thermal-hydraulics code (Reference 5) were performed (assuming 90 percent of the hydrogen is injected) to estimate the initial pressure pulse felt at the end flange walls. These analyses indicated that the initial pressure would have been approximately 6.6 kbar (96 ksi) for 90 percent gas injection. Because the initial pressure peak measurements are on the same magnitude as predicted, it was concluded that the majority of the hydrogen was injected.

Opposite each injection port there was a large crater (each about 7 cm (3 inches) in diameter by 2.54 cm (1 inch deep)), and the bore of the injection block was coated with molten steel. These craters are shown in Figure 15.

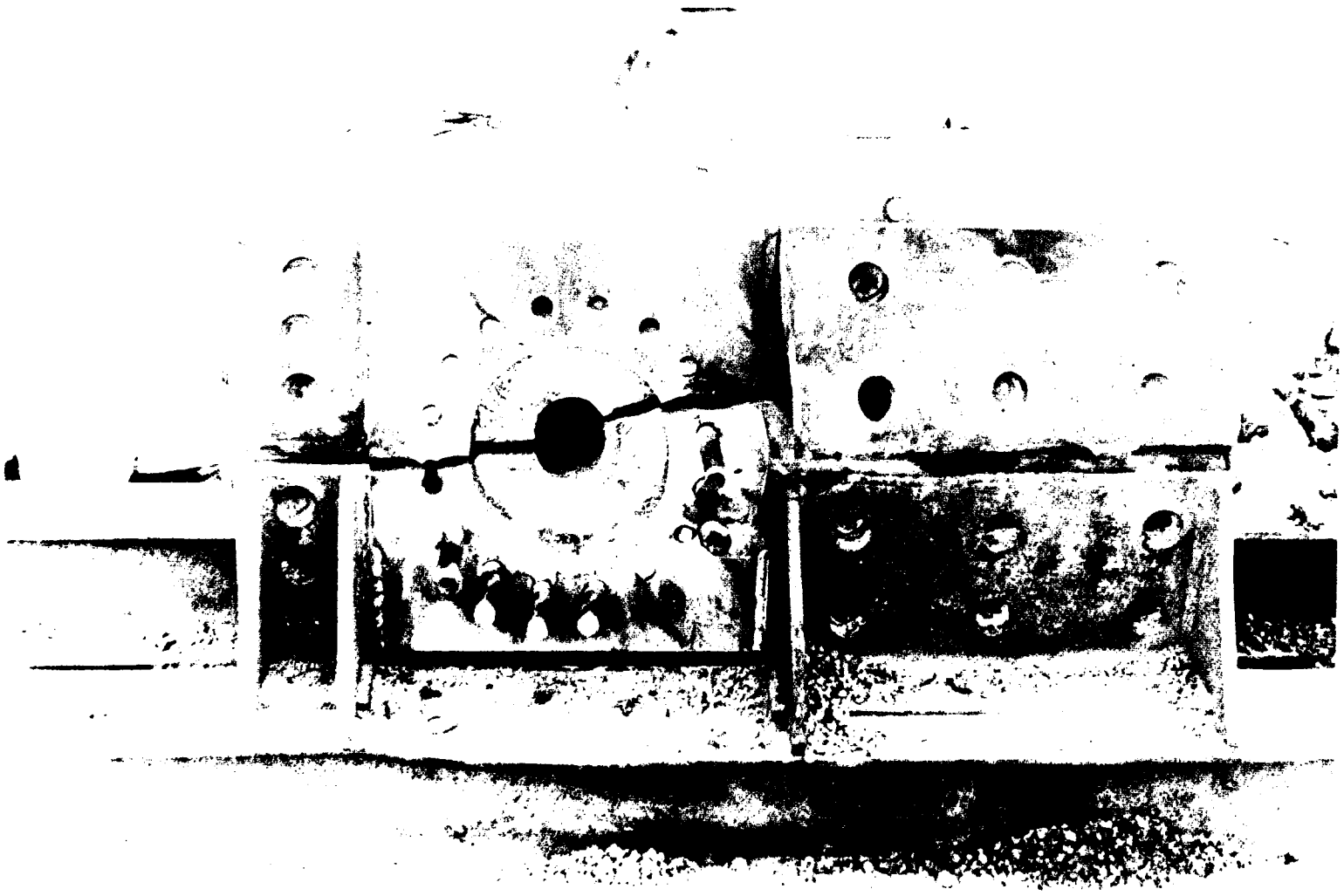

Figure 14. Post-test I-1 injection block.

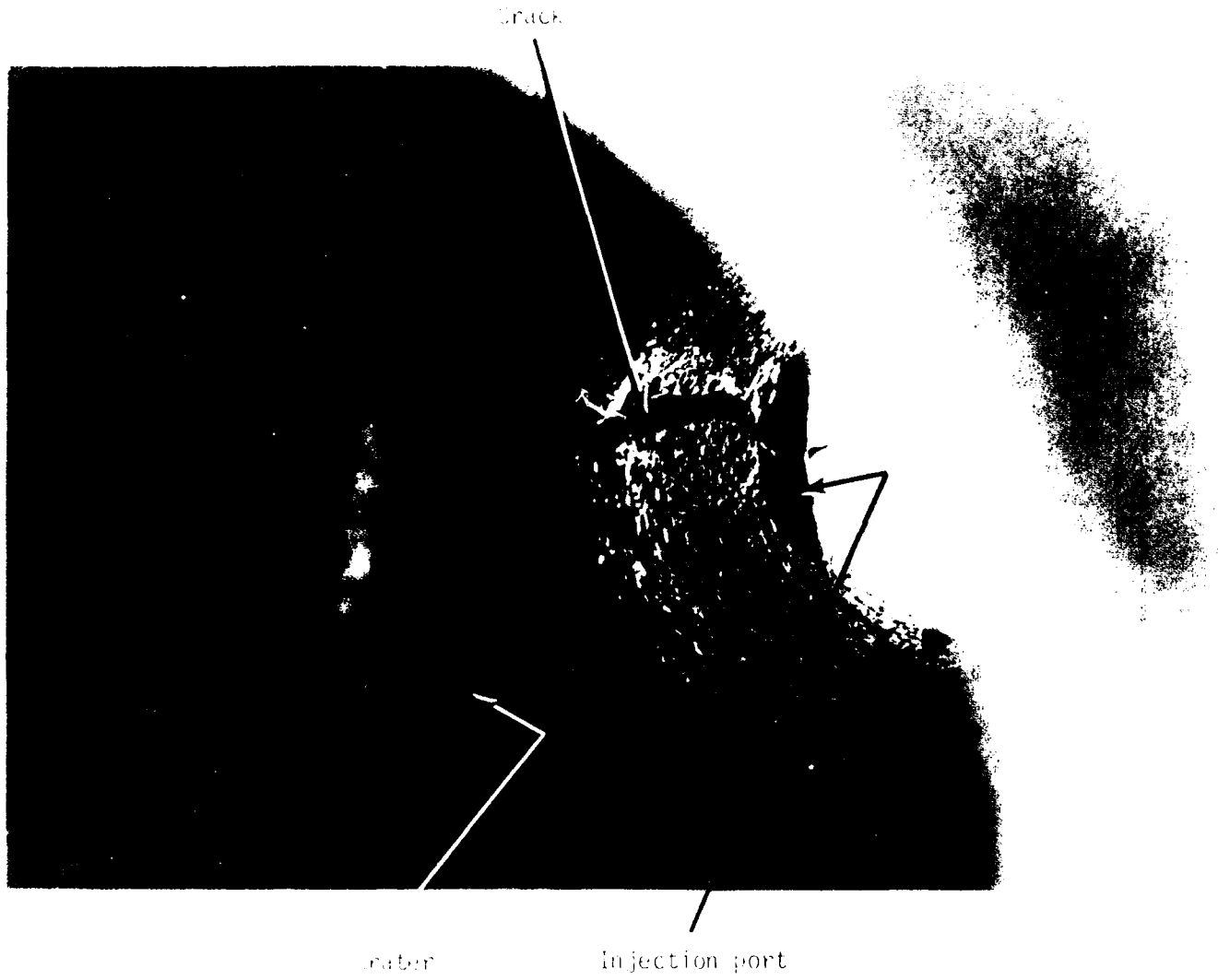

AS/H-654b

Figure 15. View looking down I-1 bore.

Heat transfer analysis showed that heat transfer-induced melting could not have produced such large craters. The STEALTH program was applied to the injection process. This analysis is explained further in Appendix A. The analysis of the injection process indicated that stagnation pressures up to 350 ksi were generated against the bore wall opposite each port. Such a high pressure would not only cause craters in the mild steel block, but would have even pressure formed craters in hardened 4340.

Preventing cratering in the actual 4340 injection block requires lowering of the stagnation pressure. STEALTH analyses indicated that the stagnation pressure could be lowered to between 8.9 to 11.7 kbar (130 to 170 ksi) if the injection ports were flared 6o to expand the flow during injection. This low of a stagnation pressure would cause at most a very minor depression in 4340, with the amount dependent on the injection block hardness. Therefore, it was decided to incorporate flared ports into the injection block design.

It was initially concluded from this test that the pressure formed craters had initiated failure, and that the use of 4340 and flared ports could prevent all injection block damage.

3.3.2 "Hot Breath" Series (HB-1, HB-2, and HB-3)

A series of inexpensive tests were conducted to test the ability of 4340 to withstand the stagnation pressure from a flared port design.* These tests (HB-1, HB-2, and HB-3) consisted of a driver aimed at a block of 4340. These blocks were heat treated to 50 Rc† for HB-1 and HB-2 (harder than would probably be desired for an actual injection block). A nozzle was placed between each block and driver to simulate the new design proposed for the injection ports. A sketch of the basic layout is provided in Figure 16 for HB-1 and HB-2.

The results of HB-1 and HB-2 verified that pressure forming was indeed eliminated. Small craters were observed in both of these tests at

---

*Flare must be a reverse flare so that port area increases as gas flows toward the bore.

†Rockwell "C" hardness

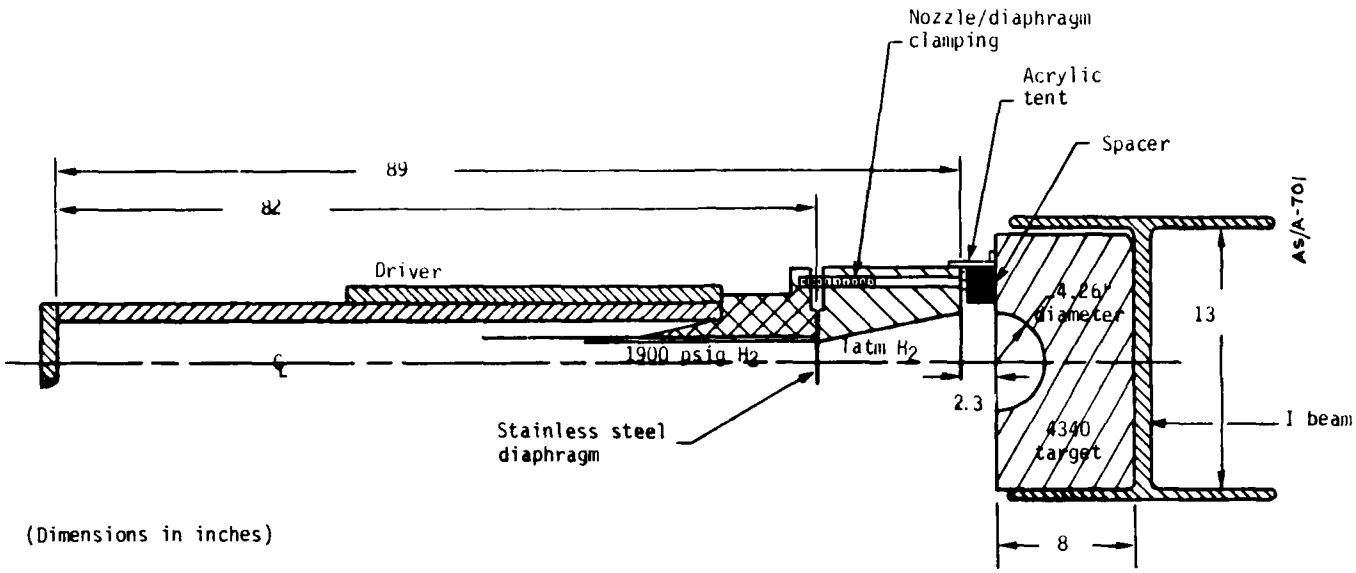

Figure 16. HB-1 and HB-2 test setup.

the gas impact location. However, these craters were the result of driver and/or diaphragm debris impacting the 4340 target block, not pressure forming. An example of this debris damage can be seen in Figure 17. In HB-2, the block cracked down the middle during the test. In test HB-1, the block appeared to be okay, but developed a visible crack several days later at the same location observed in HB-2.

The cause of these cracks appeared to be driver impact with the target block. A simple analysis of the impact force confirmed that the driver sphincter impacting the target block could easily crack the block. Therefore, in HB-3, a metal spacer was carefully fitted to the nozzle to act as a cushion and decelerate the sphincter before impact. The HB-3 target block was only hardened to 43 Rc to improve its toughness. In addition, a heavy steel plate was placed on the back of the target block to act as a momentum trap. The HB-3 setup is shown in Figure 18 with these changes.

The HB-3 target block survived the test. No cracks could be observed in the block. A magnaflux of the HB-3 target block at a much later date revealed a small crack, which ultrasonic testing indicated to be 1-1/2 inches long below the surface. This crack was on the same plane as those of HB-1 and HB-2. The amount of cratering due to debris impacts was significantly reduced. This reduction was apparantly due to a redesign of the HB-3 sphincter/pressure tube assembly to reduce termination debris.

The results of the hot breath series showed that use of flared ports and 4340 material could almost completely eliminate pressure forming. They also showed that a modified driver-pressure tube design is helpful in eliminating debris damage.

3.3.3 Injection Test I-2

Because of the I-1 failure, it was still necessary to verify the injection mechanics to determine both the amount of driver gas injected into the injection block and the mechanical integrity of the driver coupling system. In addition, it was now necessary to verify that flared ports would prevent pressure-formed craters in a 4340 injection block and that elimination of these craters would keep the injection block from splitting.

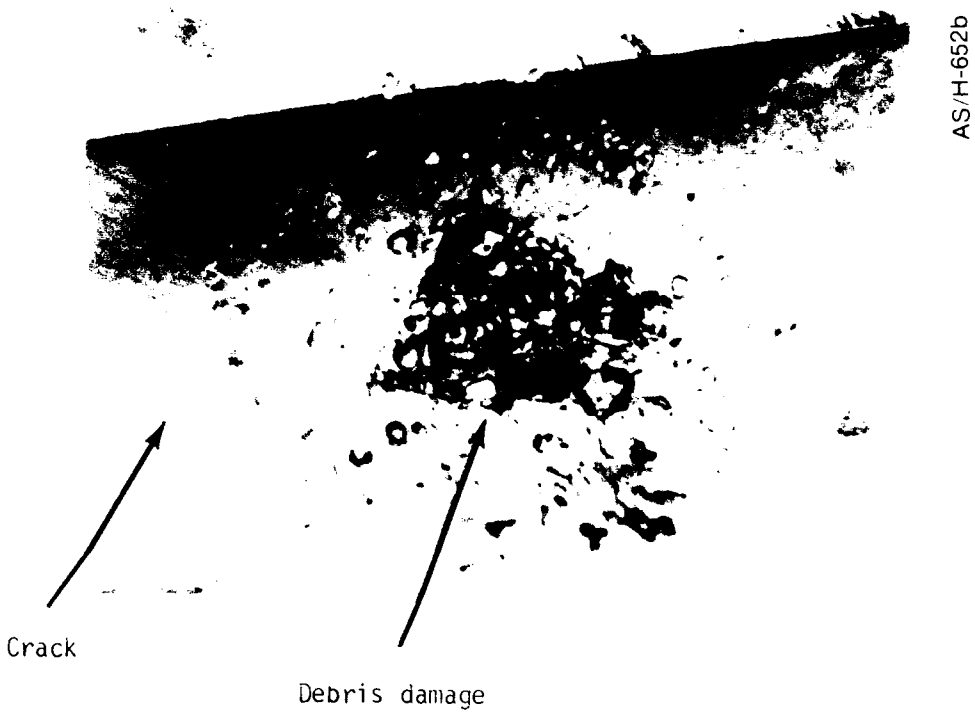

Note: photo approximately half scale.

Figure 17. HB-2 target block.

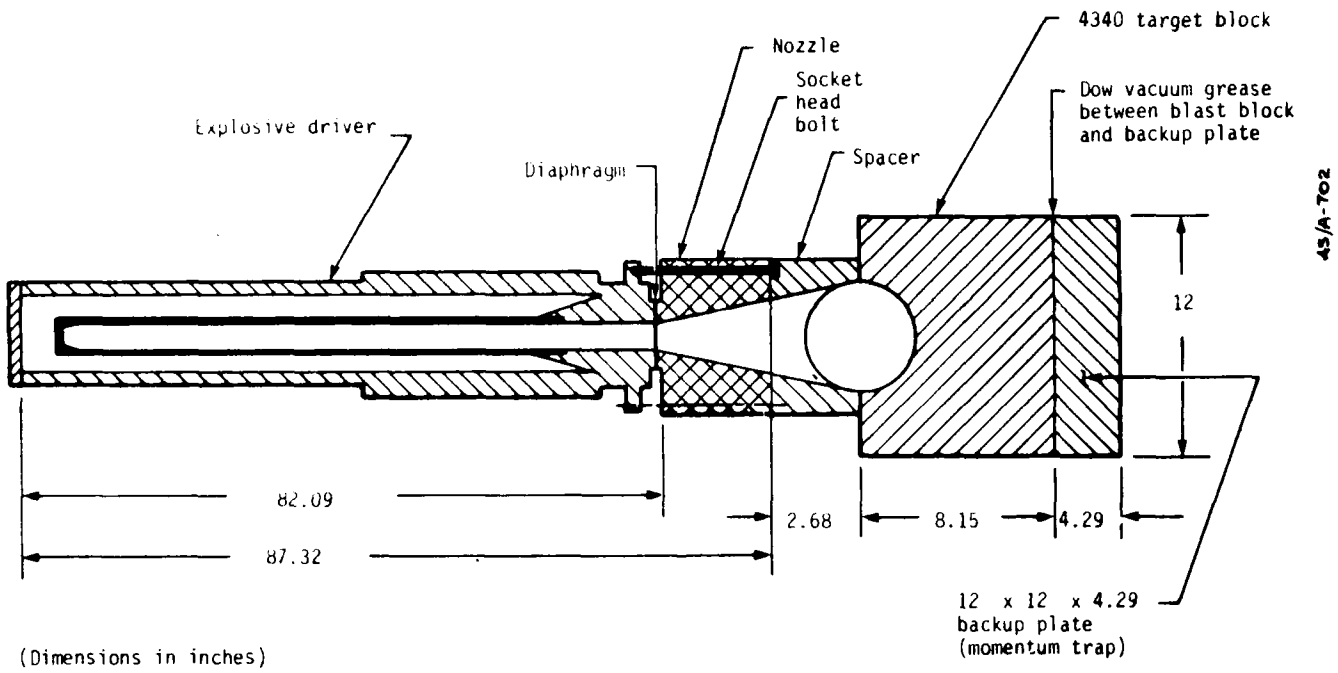

Figure 18. HB-3 setup.

To accomplish the above, a single flared injection port was machined into a 61-cm (2-ft.) long, 50.8-cm (20-inch) diameter 4340 forging. A heat treat of 43 to 44 Rc was specified. The injection block was held on top and bottom by two massive mild steel clamps of a design being considered for the launcher injection block mount system. A short launch tube section containing a 3.18-cm (1-1/4-inch) diameter, 118-gram teflon projectile was attached to one end of the injection block. The exit velocity of the teflon projectile was to be used to estimate the time-averaged pressure in the injection block. The other end of the test injecton block was fitted with an end flange containing a pressure transducer. A sketch of the I-2 injection block and driver setup is shown in Figure 19. A photo of the injection block in the test stand clamp is shown during assembly in Figure 20.

As in the first injection experiment, driver and diaphragm operation were normal, and gas injection appeared to be on schedule and complete. The teflon projectile was accelerated to within 15 percent of the calculated velocity computed assuming 100-percent hydrogen injection. However, the injection block again split open. It appears, therefore, that most of the hydrogen was injected and that the split was not complete before the projectile was accelerated to near its exit velocity.

From various observations, the injection block initially cracked along the plane of symmetry of the injection port and the main bore. This split is shown in Figure 21. The fracture plane was very flat and characteristic of a dynamic/brittle failure. The opposite side of the injection block then fractured as the hot, high-pressure gas forced open the initial fracture. Close inspection of the injection port region by materials specialists indicated that fracture initiated at the injection port approximately one inch upstream of the entrance to the main bore.

The bolts retaining the driver termination assembly failed when the injection block split. Careful inspection of the injection block, sphincter, and driver coupling system revealed that the termination assembly was in close contact with the injection block when the fracture formed. This was easily confirmed since the high-temperature hydrogen formed a distinct pattern in the shape of the crack on the termination assembly. Unfortunately, as in I-1, it could not be determined whether

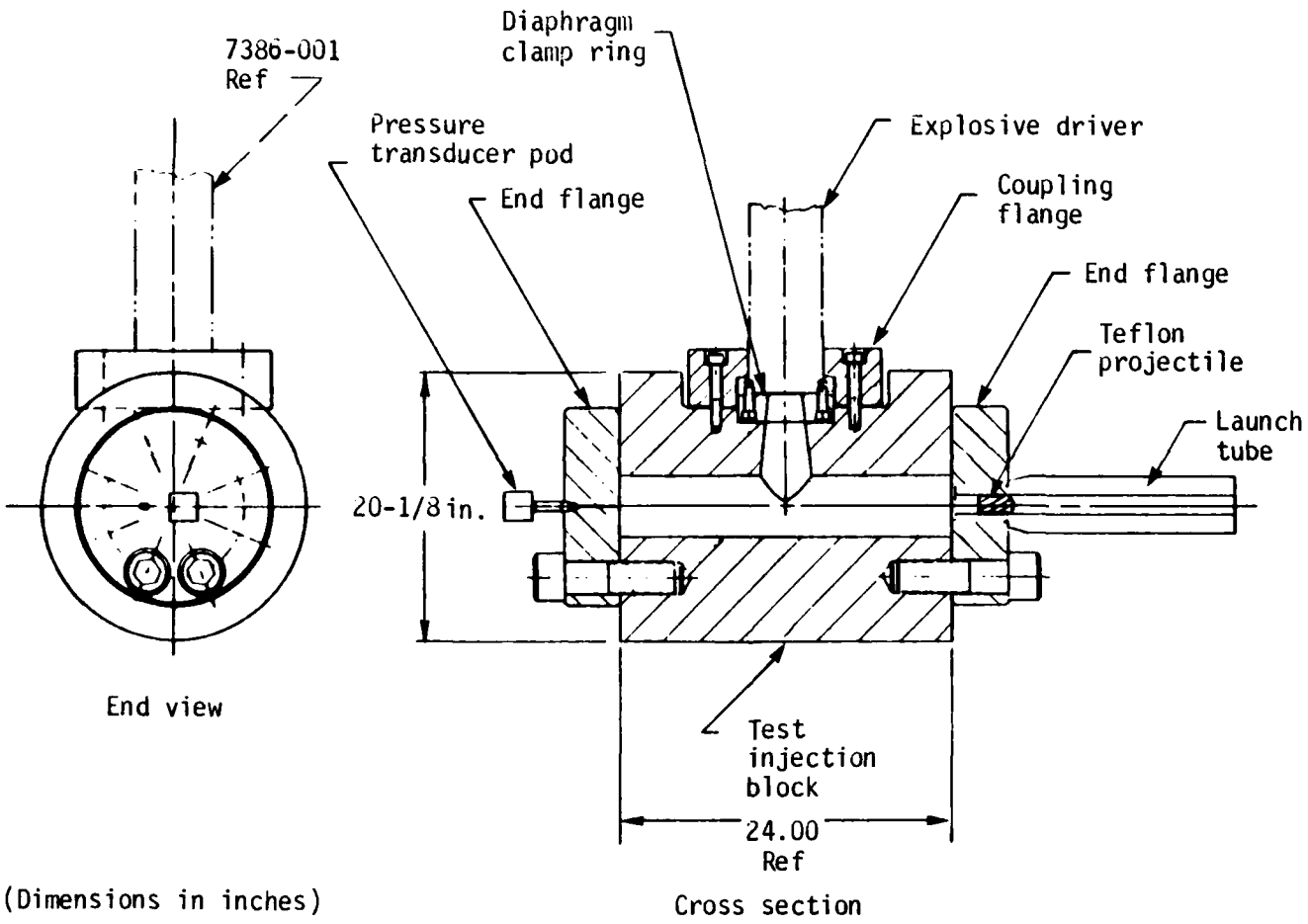

AS/A-703

Figure 19. I-2 injection block assembly.

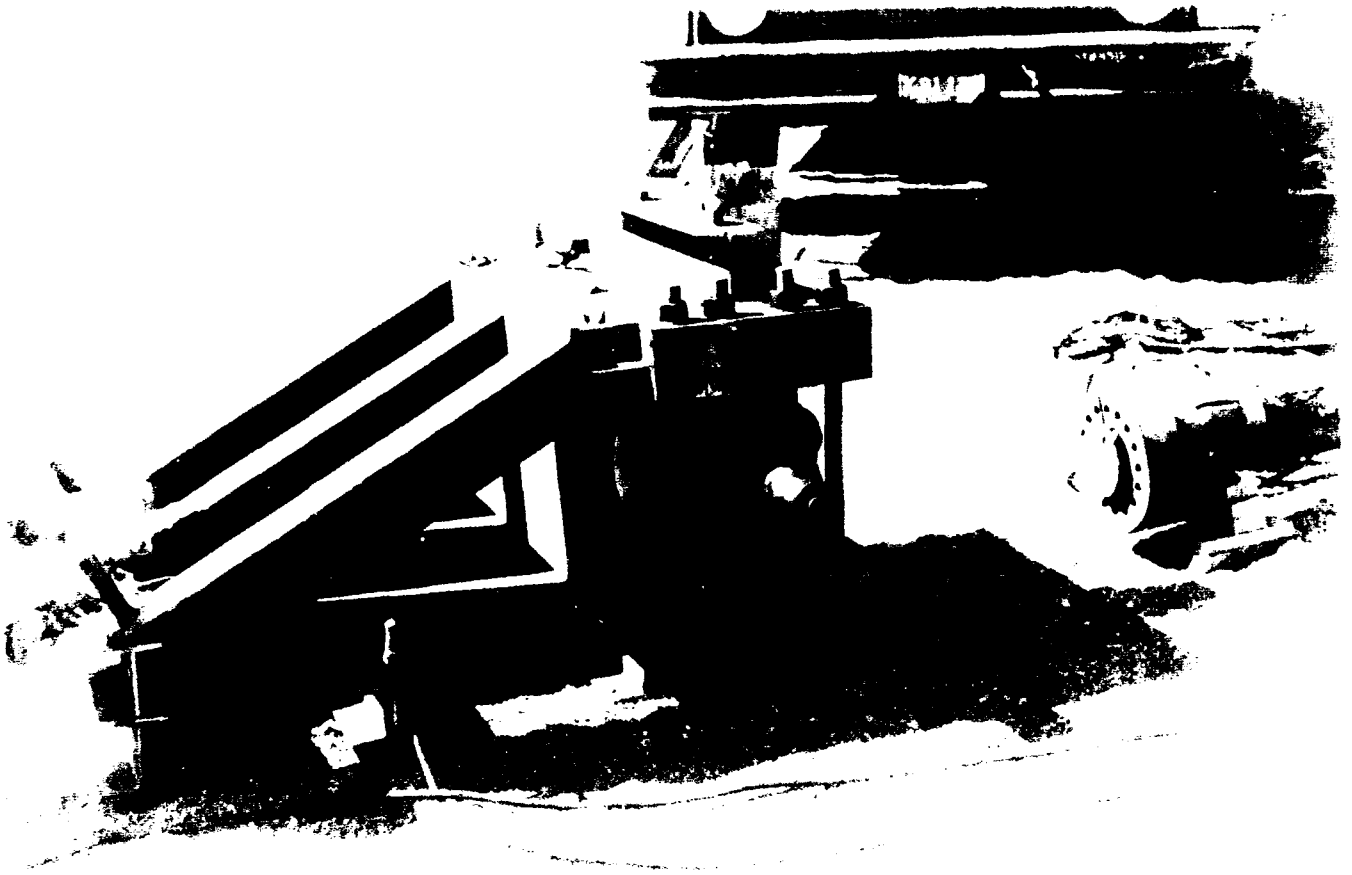

AS/H-664b

Figure 20. I-2 test stand and injection block.

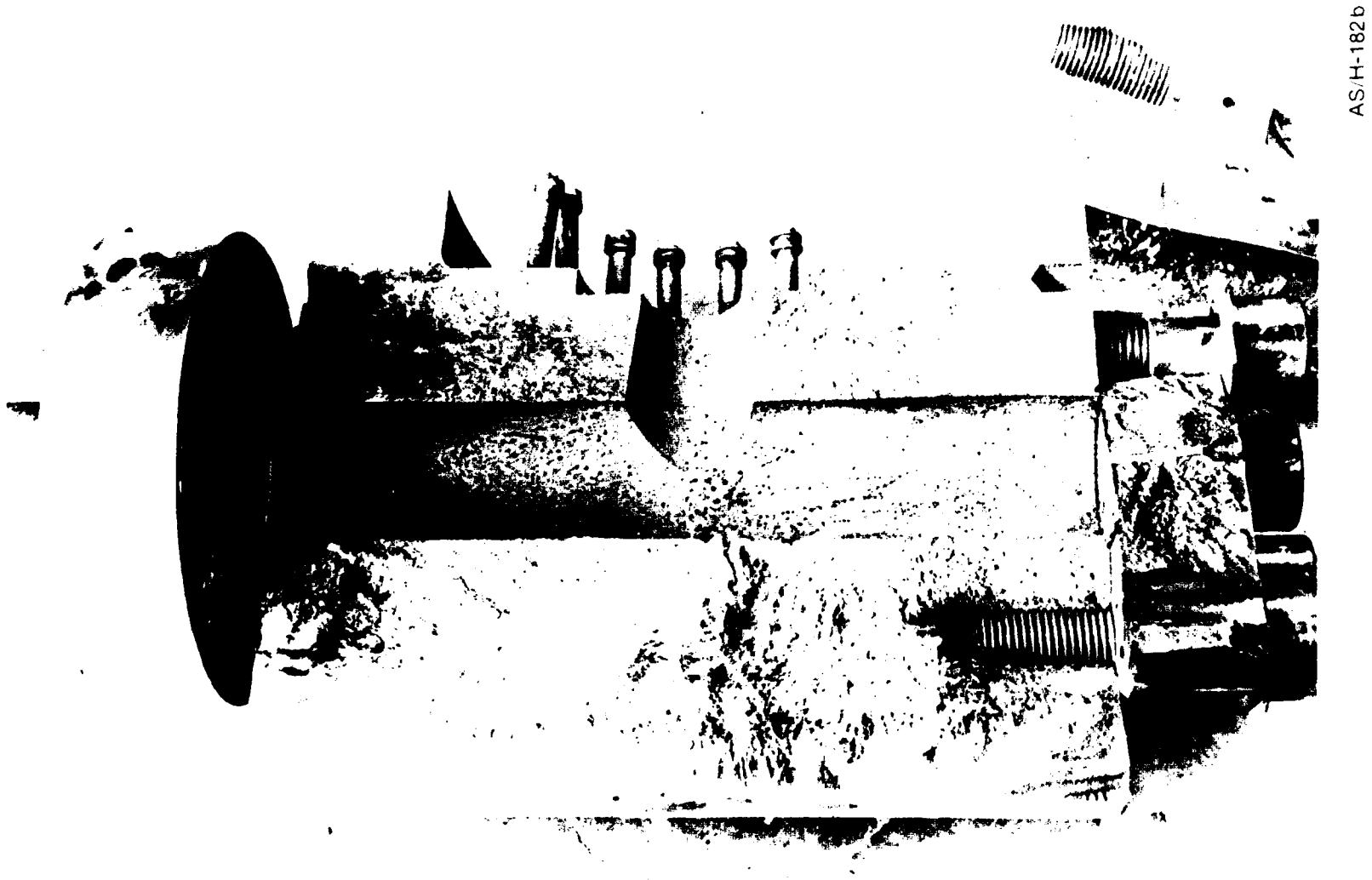

Figure 21. I-2 injection block half.

Injection Block Failure Hypotheses. Four hypotheses were put forth to explain the structural failure of I-2. They are:

1. Material failure as a result of poor material choice, heat treat, or forged properties
2. Driver termination loading -- a destructive wave interaction and/or structural failure from $3*10^8$ dyne-sec (685 lb_f-sec) momentum input over about 50 μsec
3. Internal gas pressure loading -- transient loading opposite the injection port and/or subsequent gas equilibration in the main bore
4. Any combination of the above

A combined materials testing, analytical, computational, and brainstorming attack was made to quantify each mechanism and to deduce the most likely mode or combination of modes of injection block failure.

Materials Testing. The I-2 injection block was made from a commercial grade 4340, 55.9-cm (22-inch) diameter forged round. After the experiment, the material was tested for hardness distribution, yield and ultimate tensile strengths, elongation, and fracture toughness; was examined ultrasonically; and was etched for grain structure.

The near surface Rockwell hardness values were higher than specified (45 to 47 Rc versus 43 to 44 Rc). The material strengths in the three orthogonal directions were compatible with the measured hardness, but elongation and fracture toughness (measured by Charpy impact) were substantially lower than expected. The etched specimens revealed that the dendritic cast structure was insufficiently broken down during the forging process.

The details of the materials tests are included in Appendix B. The conclusion reached is that the injection block had the required strength properties but had poor elongation and fracture toughness. With the very poor toughness of the I-2 injection block, the very minor flaws (inclusions and cracks) present in a commercial grade forging could initiate failure even prior to reaching stresses greater than yield.

Analytical. The I-2 injection block was analyzed as a static pressure vessel and was determined to be more than adequate to contain the 2-kbar equilibrium gas pressure. This is even true at the port/bore intersect where the stress may rise by a factor of 2.8.

A spring-mass structural calculation was carried out to evaluate the injection block response to the driver termination load estimated to be $3*10^8$ dynes-sec (685 lb_f-sec). (This calculation accounted for the support of the injection block clamps but neglects the injection port hole.) Converting the driver termination load to strain energy in the injection block generates bending stresses well in excess of the yield strength of heat treated 4340, and strongly suggests that the driver termination loads alone are capable of breaking the structure.

Computational. A 3-D static finite element calculation of the I-2 injection block configuration was carried out (with a 2-kbar internal pressure). This calculation verified the adequacy of the I-2 block to contain the equilibrium gas pressures. The 3-D calculation also suggested that a large radius at the injection port entrance would considerably reduce the stress concentration factor, which was found to be the same 2.8 factor as used in the analytic analysis. Details of this calculation are given in Appendix A.

A large number of 1- and 2-D analyses of the dynamics of the injection process were made using the STEALTH program. Details of many of these analyses are also provided in Appendix A. The overall results of these analyses indicate that:

1. The gas impact in the bore opposite the injection port was insufficient by itself to initiate failure
2. The driver termination impact alone probably was sufficient to initiate failure

Conclusions. Based on all information and analyses of I-2, the following conclusions were made:

- Structural failure of I-2 was caused by the driver termination load either acting alone or in concert with triggering stresses induced by various gas transients
- The I-2 block exhibited poor fracture toughness and elongation, which undoubtedly contributed to failure but was not the primary cause of failure
- The aircraft quality 4340 forging built for the launcher injection block can be used if it is properly heat treated to give good fracture toughness and if driver sizing and spacing are redesigned to more evenly distribute driver termination loads and injection gas transients

- The aircraft quality 4340 forging built for the launcher injection block can be used if it is properly heat treated to give good fracture toughness and if driver sizing and spacing are redesigned to more evenly distribute driver termination loads and injection gas transients
- The computational tools developed in the analyses of the I-1 and I-2 failures should be used in the redesign of the injection system prior to testing of the design

3.3.4 Injection Test I-3

Following the I-2 failure and analyses, a detailed set of analyses was made to determine what design changes would improve the survivability of the injection block. This resulted in the following design changes, reducing the possibility of failure:

- Decreased driver size (i.e., used more, but smaller, drivers to input the hydrogen)
- Increased surface contact area between the termination assembly and injection block
- Increased distance between nitromethane charge and injection block
- Rounded corners at the intersection of the bore with the injection port

Additionally, more care was used in the selection and treatment of the 4340 forging. Specifically:

- The forging should be aircraft quality 4340 to reduce the amount and size of flaws (cracks and inclusions)
- The forging should be upset sufficiently to break down the cast structure and improve the isotropy of mechanical properties
- The injection block should be heat treated to approximately a nominal 35 Rc (which is a compromise between the desirability of low hardness for toughness and high hardness to withstand pressure forming)

To minimize costs and lead times, it was decided to initially test the injection block design changes in 1/8-scale (rather than 1/4-scale).

An injection block representing a two-driver section of the injection block was machined and heat treated. A pressure transducer was mounted on one end flange. A launch tube containing a small teflon

projectile was attached to the other end flange. Both of these monitored pressure. The most significant change in the I-3 test assembly is that the relative dimensions of the drivers to those of the injection block were decreased 30 percent. As a result of the decrease in driver size, the 1/4-scale launcher will require 10 drivers instead of the originally conceived 4-driver design.*

A 9.53-cm (3.75-inch) mild steel spacer was placed between the driver and the injection block. The spacer increases the contact area between the driver and injection block and increases the standoff distance (i.e., distance between the injection block and nitromethane). A view of the I-3 port assembly is shown in Figure 22.

As in all previous shots, the drivers worked perfectly. For the first time in an injection "block" test, the block was mechanically unharmed. A view of the post-test I-3 injection block is provided in Figure 23. The exit velocity of the teflon projectile was within 2 percent of the preshot estimate,† indicating that nearly 100 percent of the hydrogen had been injected within the requisite time scale.

Mylar diaphragms were employed in I-3 along with the improved driver/sphincter assembly developed for HB-3. The result was that only a single, very minor debris crater could be observed opposite one of the injection ports. There were 0.25-mm (0.010-inch) depressions opposite each port, however. It could not be determined whether these depressions were the result of pressure forming or melting. The I-3 injection block exhibited much more resolidified melt than any previous injection test.

Pretest and post-test ultrasonic testing could not reveal any flaws in the forging. Large samples cut from the injection forging were sent through the heat treat with the injection block to verify that an adequate in-depth heat treat had been made. Hardness tests of these samples indicated the presence of hard and soft regions throughout cross sections of the heat treated samples. It was eventually concluded that the forging

---

*A more efficient driver design will obviate the need for more than four drivers in full scale.

†The accuracy of the pretest prediction of projectile velocity must be viewed as no better than ± 10 percent at best.

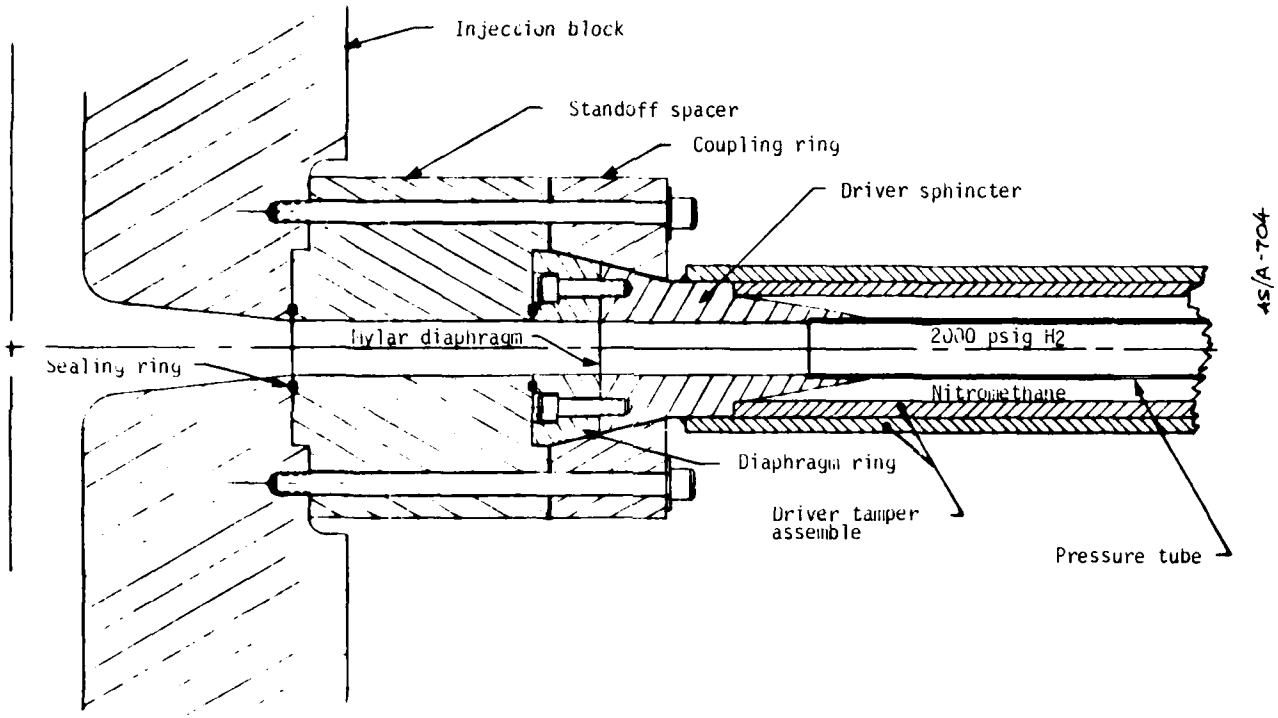

Figure 22. Redesigned termination assembly used in I-3.

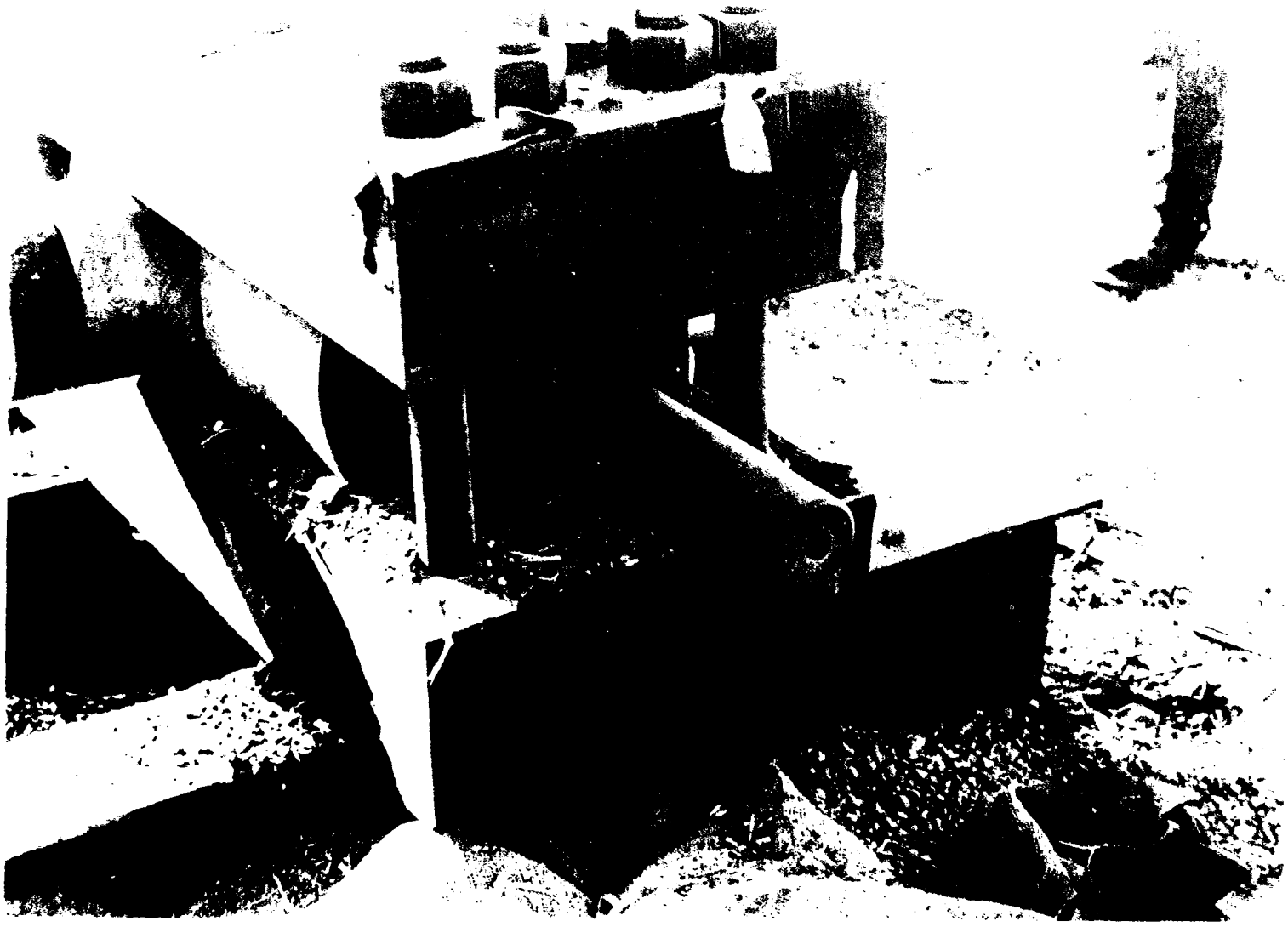

Figure 23. Post-test view of I-3 injection block assembly.

used in I-3 was not homogeneous (i.e., alloying materials were segregated throughout the forging) and should not have been classified as aircraft quality. It is important to note that the I-3 test was successful despite imperfect metallurgy. Details of the I-3 metallurgy are contained in Appendix B.

The principal conclusion of I-3 was that a design had been found which could survive the injection process. In addition, the driver coupling system was verified as adequate, and nearly all the driver hydrogen was found to be injected within the desired timeframe. Both of these were inferred in previous tests, but had required confirmation in a fully successful injection test.

3.3.5 Injection Test I-4

The I-3 injection test identified an injection block design which could survive the immense loads experienced during the injection and driver termination processes. The design, however, has a major drawback. The spacers used to increase the driver standoff and contact area significantly increase the "dead volume" in the port regions. In an actual 1/4-scale hybrid launcher firing, some hydrogen will escape compression by the piston, because of the port region dead volume. This is especially important since the number of ports must now increase from 4 to 10 because of the decreased driver size of the design developed in I-3.

Therefore, it was decided to perform an additional driver test on the I-3 injection block with the standoff spacer removed. The I-3 injection block was refurbished to remove the resolidified metal from the bore by honing. Two new drivers were prepared for the 1/8-scale injection block test.

The I-4 test results were almost identical to those of I-3. Thus, it was proven that the injection block/termination assembly design (shown in Figure 22) does not require the standoff spacer to prevent failure.

3.3.6 Injection Test I-5

The I-4 injection test demonstrated a design for the injection block which is mechanically adequate and minimizes the injection port dead volume. This design is the new design selected for the 1/4-scale launcher; however, it remained to be verified that the I-4 design would work in the 1/4-scale. The major objective of I-5 was, therefore, the 1/4-scale verification of the I-4 design.

To save time and money, the actual 1/4-scale injection block forging purchased for the hybrid launcher was used in this test. This forging is vacuum-melted aircraft quality 4340. Two injection ports were machined into one end of the injection block. The injection block was heat treated to 34 Rc on the outer surface. Details of the heat treat and metallurgical tests are given in Appendix B. A mild steel piston was placed in the bore at each end to seal off the injection gas. One piston had a 3.18-cm (1-1/4-inch) diameter hole machined along its center into which a teflon projectile was placed. As in previous tests, the injection pressure was to be monitored by the projectile velocity. As a simple test of passive thermal protection, a two-ply layer of carbon cloth was glued onto the bore wall opposite one injection port. Two-ply glass cloth was glued opposite the other injection port. The general pretest layout of the I-5 test is shown in Figure 24.

No test stand was necessary in I-5 because the 1/4-scale launcher injection block is so massive that the two explosive drivers used were not capable of moving the injection block more than a few feet. Therefore, the injection block was simply set on wooden blocks, which were used to level the injection block. Plywood-tile sandwiches containing 2.7-cm (7/8-inch) thick quarry tile were placed against the injection block just prior to testing to provide protection from driver shrapnel. Figure 25 is a photo of I-5 during assembly.

The injection block survived the I-5 test, showing that the I-4 design was indeed adequate for the 1/4-scale launcher. This was confirmed by post-test ultrasonic testing. The driver termination assembly coupling system was undamaged, verifying its 1/4-scale design. The projectile velocity was as predicted, indicating nearly 100-percent hydrogen injection. The amount of melting in the I-5 bore was less than in I-3 or I-4 with the carbon cloth providing slightly better protection than the glass cloth. A slight amount of cratering from driver debris could be observed, but the amount was much less than in any previous 1/4-scale test. No signs of shrapnel damage to the block were observed. Figure 26 is a photo of the post-test injection block.

As a result of the I-5 success, it is concluded that all major design problems associated with the injection system (drivers, coupling system, diaphragm, and injection block) are solved. It is now possible to

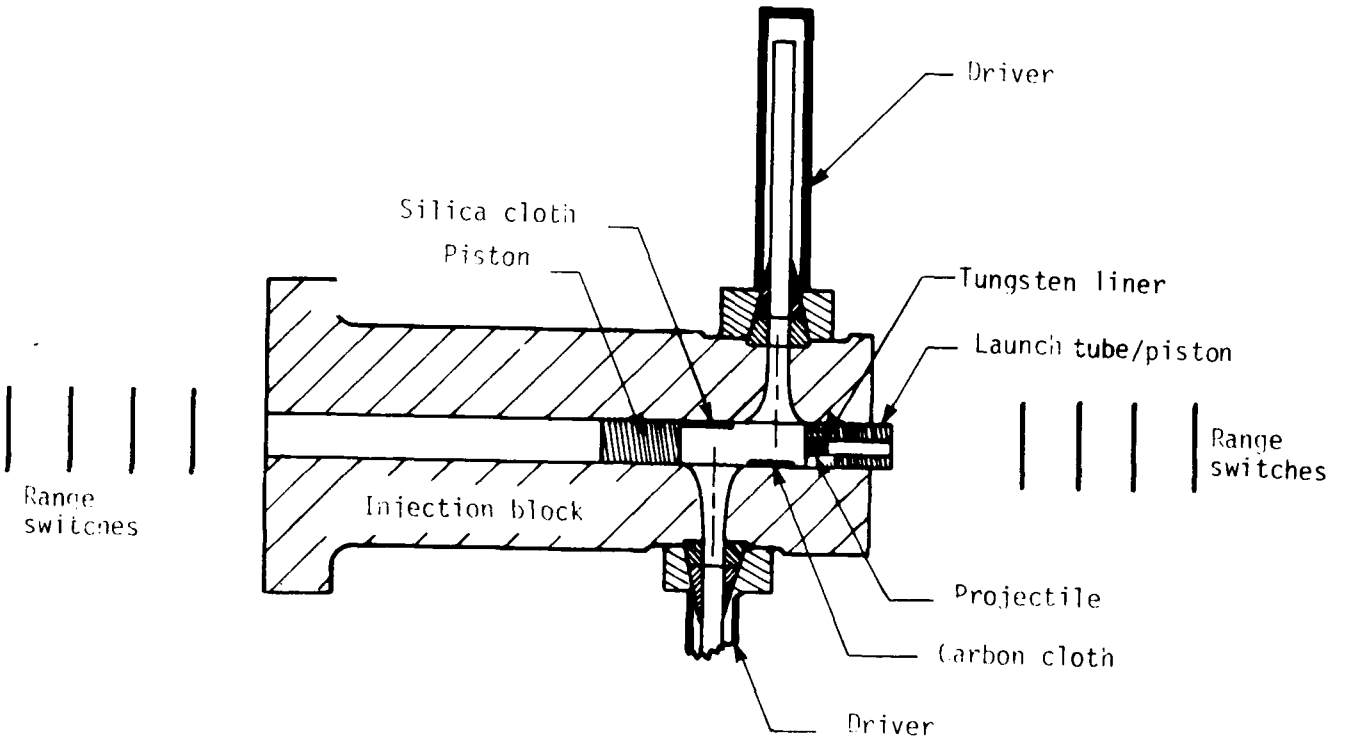

Figure 24. I-5 layout.

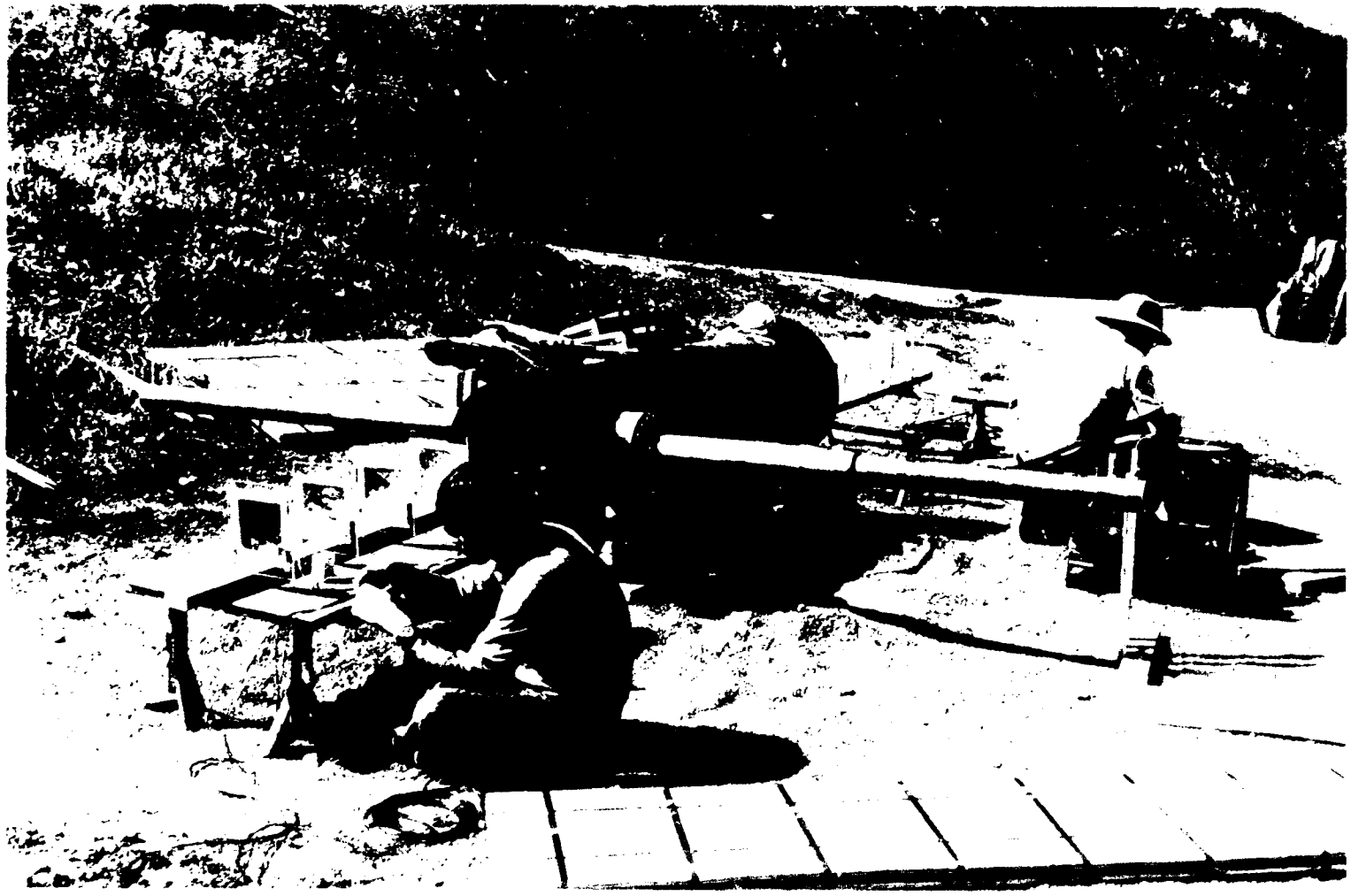

AS-H-561b

Figure 25. I-5 test setup during assembly.

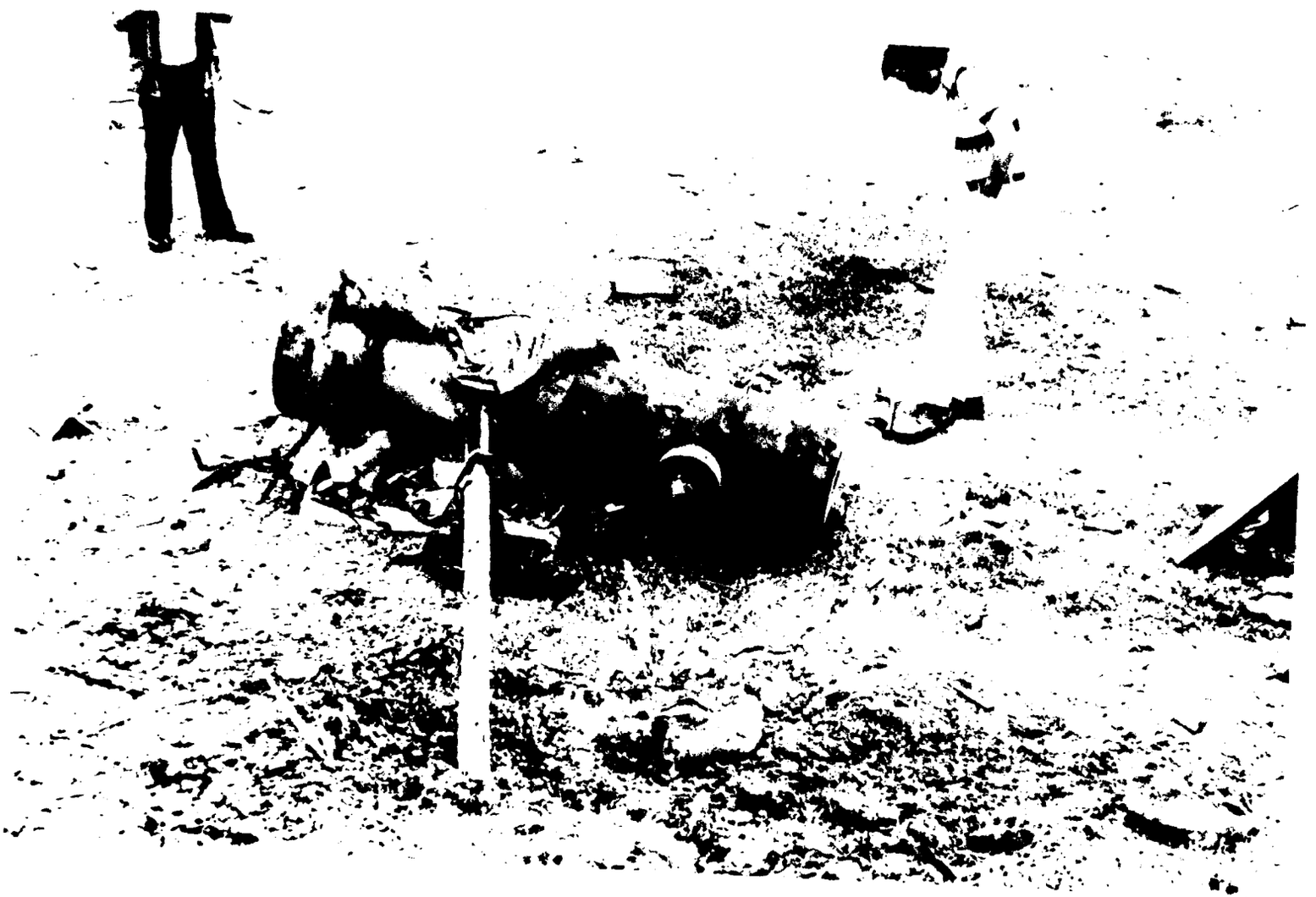

Figure 26. Post-test I-5 injection block.

finalize the 1/4-scale launcher design and complete the fabrication of the launcher.

3.4 COMPONENT TESTING CONCLUSIONS

Problems were encountered during injection and containment mechanics testing. These problems had to be resolved before the 1/4-scale launcher design could be completed. Most of these difficulties were associated with the mechanical integrity of the injection system under the severe loads encountered during injection. Specifically, two major problems were resolved by redesigning the injection system. These were:

- The injection pressures opposite the driver ports were originally so high they would have caused large pressure-formed craters in the injection block bore
- The mechanical loads associated with the driver termination were so large in the original design that the injection block could not have survived a single firing

Other less severe problems that were resolved are:

- Driver termination sections had to be modified to reduce the amount of particles ejected during termination. These particles would have caused craters in the injection block bore.
- Mylar diaphragms were determined to be the most practical method of sealing drivers despite their minor contamination of the hydrogen injection gas

Component testing has validated the design modifications. The testing also provided data necessary to determine the following:

- A simple Van der Waals model for hydrogen was verified as accurate for predicting the thermodynamic state of the high-temperature, high-pressure injection gas
- Nearly all of the hydrogen in the explosive drivers is successfully injected during driver operations. The choking problem identified in Reference 2 has been resolved.
- Driver ports are adequately sealed during the termination process
- The timing of injection events was determined. This is necessary data to select the optimum time to detonate drivers during the actual launch cycle.

- A simple method of preventing driver shrapnel damage was identified

Only one problem still remains to be resolved concerning injection and containment mechanics. During injection, a small amount of the injection block melts opposite driver ports. It may be desirable to test several thermal protection schemes. Such tests can be done inexpensively in the 1/8-scale injection block used in the I-3 and I-4 injection tests (see Table 1) or may be tested during the 1/4-scale workup tests. However, the amount of melt is such that this is not considered a serious problem in terms of the objectives of the 1/4-scale launcher, but it should be addressed for the full-scale design.

SECTION 4
THERMAL PROTECTION OF LAUNCHER COMPONENTS

Detailed studies established the severity of convective heat transfer inherent in reaching the objectives of the hybrid launcher (Reference 3). Since no existing material can survive at the required hydrogen stagnation temperatures, it is essential that the launcher components be cooled in some way. The method selected is based on using the heat sink capacity of the internal surface materials (Reference 3).

Launch kinetic energies are definitely limited by melt considerations. Attempts to increase performance once melting occurs have been frustrated even when the concept of operating with melting behavior is accepted (Reference 6, p. 42). This section estimates the limits of performance of hydrogen two-stage launchers based on material limitations.

Table 4 presents the data used in selecting tungsten as the basic heat absorption medium. The data show that tungsten can survive an arbitrary constant heat flux before melting almost two times longer than the next best choice, which is molybdenum. Tungsten can survive almost 15 times longer than steel. The design study of Reference 3 derived a number of launch cycles that more or less survive the heat loads using tungsten (see Table 1).

For materials that have a shorter time to melt than tungsten, the allowable excess of the peak cycle gas stagnation temperature over the material melt temperature decreases. For example, the maximum cycle gas temperature equals the melt temperature when time-to-melt is zero. Assuming the allowable difference between peak cycle gas temperature and material melt temperature is proportional to the relative time-to-melt, allowable peak cycle temperatures have been estimated for each of the materials in Table 4. It has been estimated that (for a limited range of temperatures) the launch mass capability for an optimized two-stage hydrogen launcher is roughly proportional to the peak absolute stagnation

TABLE 4. RELATIVE MELT TIMES FOR VARIOUS MATERIALS

Material	Melt Temperature T_{melt} (°C)	Thermal Conductivity, k (cal/hr-cm-°C)	Density (gm/cc)	Specific Heat (cal/gm-°C)	Relative Time-to-melt[a]	Estimate of Allowable Peak Cycle Temperature[b] (°F)	Estimate of Relative Launch Mass Capability[a,b,d]
Tungsten	3400	1410	19.3	0.033	14.7	10000[c]	3.0
Molybdenum	2610	1260	10.2	0.061	7.6	6700	2.1
Rhenium	3167	2140	21.1	0.033	6.5	7400	2.3
Copper	1082	3040	9.0	0.092	4.0	3000	1.0
Titanium	1690	1470	4.5	0.139	3.7	4000	1.3
Tantalum	2993	480	16.6	0.036	3.6	6400	2.0
Columbium	2415	700	8.6	0.065	3.2	5200	1.6
Rhodium	1966	760	12.5	0.059	3.0	4400	1.4
Berylium	1282	1370	1.8	0.52	3.0	3100	1.0
Silver	960	3600	10.5	0.056	2.7	2500	0.8
Gold	1063	2560	19.3	0.031	2.4	2600	0.9
Chromium	1843	580	7.2	0.110	2.2	3900	1.3
Nickel	1455	790	8.9	0.105	2.1	3200	1.1
Tantalum Carbide	3880	190	14.5	0.033	2.0	7500	2.3
Platinum	1773	600	21.5	0.031	1.7	3700	1.2
Cobalt	1496	600	8.9	0.099	1.6	3100	1.0
Palladium	1554	610	12.0	0.058	1.4	3200	1.0
Mild Steel	1510	400	7.9	0.100	1.0	3000	1.0
Vanadium	1900	270	6.0	0.120	0.98	3700	1.2
Silicon	1429	710	2.3	0.162	0.76	2800	0.9
Manganese	1245	70	7.4	0.115	0.14	2300	0.8

[a]Steel = 1.0
[b]See text
[c]Based on the design study, Reference 3
[d]Launch velocity ≈ 6 km/sec

temperature in the cycle. Relative launch masses have been estimated on this basis for each of the materials in Table 4. Note that the factor of 3 in launch mass capability indicated for tungsten over steel is consistent with the results in Figure 5, lending some credence to the performance scaling approach for melt-limited performance. Although the estimates of the melt-limited performance are crude at best*, they demonstrate, at least qualitatively, the importance of developing tungsten liners in order to demonstrate the internal ballistic potential of the hybrid launch cycle.

A composite liner that combines the heat sink features of tungsten with the high melt temperature of tantalum carbide was identified (Reference 3). Figure 27 shows the reduction of maximum tungsten temperature due to a thin layer of tantalum carbide. Note from Table 4 that tantalum carbide by itself would be expected to melt almost as quickly as unprotected steel. In this respect, tantalum carbide is fairly representative of a number of carbide and nitride refractories. Several alternate materials could potentially serve the function of tantalum carbide in the composite liner concept.

The heat sink concept requires tungsten liner thicknesses of only about 0.064 mm (0.025 inches). However, liners this thin require bonding to the launch tube should cracks develop in the liner. Heavy-walled tungsten tubing is not available commercially. Consequently, either bonding techniques needed to be developed in order to demonstrate this hybrid cycle or some cost-conscious way of making heavy-wall tubes had to be developed. The thin-wall approach was chosen.

Several methods exist for making the desired liner, including electrodeposit, metal spray, and chemical vapor deposition (CVD). The CVD technique has been selected based on the demonstrated ability to achieve high quality tungsten forms. In addition, the CVD process is a feasible way of plating tantalum carbide on tungsten, or vice-versa.

---

*If needed, refined estimates can be derived based on the analysis method of Reference 3.

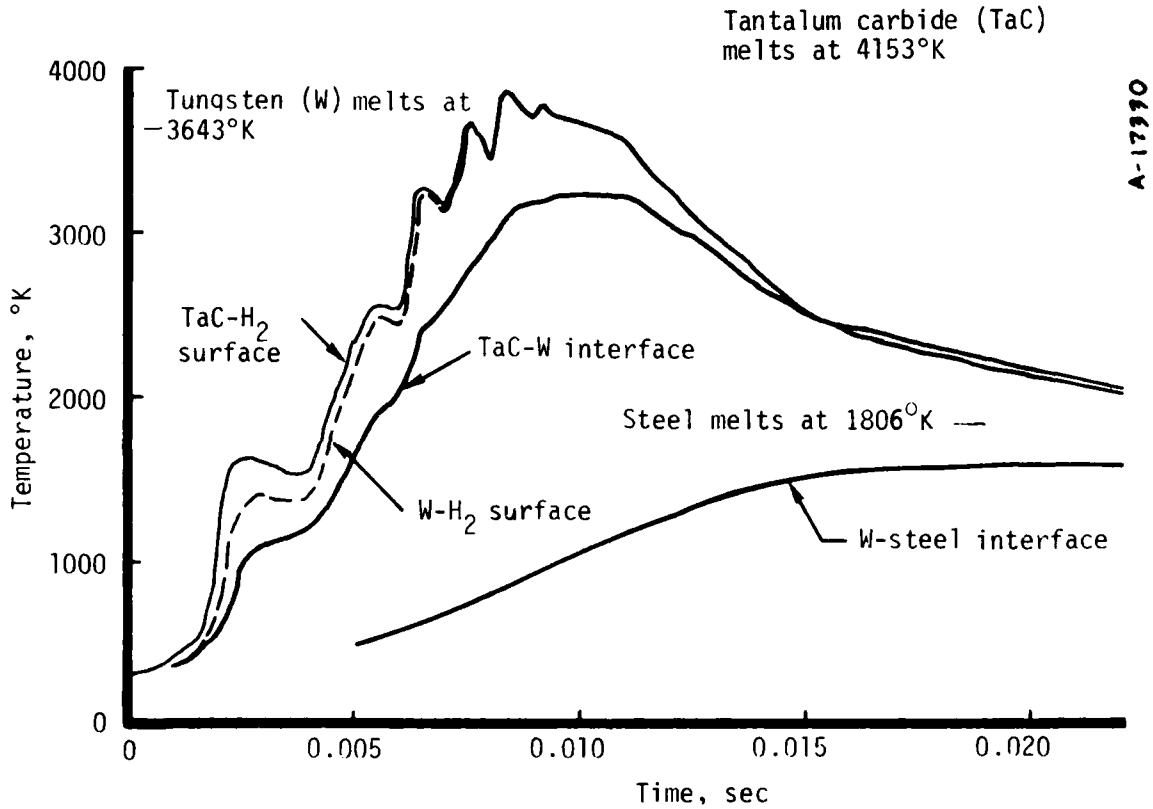

Figure 27. Temperature histories at the barrel inlet of a 10.2-cm (4-inch) bore hybrid launcher with a 4.54-kg model (full scale of Cycle B of Table 1) (Reference 3).

4.1 COMPOSITE LINER OPTIONS

Tungsten does not provide a good bond with steel by the tungsten CVD process or diffusion bonding techniques. However, both copper and nickel can achieve good diffusion bonding with both steel and tungsten. Nickel is known by its property of high strain-to-failure, suggesting the possibility of bond retention under high strain situations. Tungsten is a fairly brittle material, so that liner cracking is to be expected under the dynamic loads of the launch event. Consequently, nickel has been selected as the bonding medium since high strains might be expected should tungsten cracking occur. Tantalum carbide bonds very well to tungsten. It is expected that if cracks occur in tungsten they will occur at the same place in the tantalum carbide, and that the tantalum carbide will not peel from the tungsten surface.

The nominal composite liner then consists of tantalum carbide that is bonded to tungsten, tungsten that is bonded to nickel, and nickel that is either bonded to steel or is quite thick so that the liner can be shrink-fit into the launch tube or clamped between the two halves of a split clamp launch tube (the nominal concept of Reference 3).

It appears that the composite can either be developed from the inner surface outward, or vice-versa. The scenario to build from the inside-out might go as follows:

- CVD tantalum carbide on molybdenum
- CVD tungsten over the tantalum carbide
- Grind the outside of the tungsten to the desired dimension and to be concentric with the molybdenum mandrel
- Dissolve the molybdenum mandrel using nitric acid
- Electroplate a thin layer of nickel on the tungsten (nickel plating thicknesses greater than about 0.05 mm (0.002 inch) are not reliable)
- Shrink fit the composite either into a nickel tube or into the launch tube. Diffusion bond the composite to the substrate (either nickel or steel).

If the nickel tube approach is selected, diffusion bonding is not required. If the composite is to be diffusion bonded to the steel, a number of complications arise, such as:

- Tolerances of the launch tube ID and the composite liner OD
- Selection of the shrink-fit temperatures for the launch tube and the composite liner
- Selection of the diffusion bonding temperature, which may be the same as the launch tube shrink-fit temperature only if the composite liner is chilled to accomplish the fit
- Influence of the selection of launch tube shrink-fit and diffusion bonding temperatures and times on launch tube properties or heat-treat requirements

The scenario to build a liner from the outside-in might go as follows:

- CVD tungsten on the inside of a heavy-walled wrought nickel tube
- Hone the tungsten to the desired dimension, and CVD the thin layer of tantalum carbide inside the tungsten
- Shrink-fit the composite liner into the launch tube

This approach eliminates the requirement for diffusion bonding the liner to the launch tube, perhaps alleviating concerns about the launch tube heat treatment. However, additional concerns about the thick-walled nickel tube concept include:

- The potential for longitudinal plastic flow of the nickel in the downstream direction due to the pressure differential across the projectile. Nickel has a fairly low yield strength ($\simeq$ 55 kpsi). The tendency and extent of longitudinal plastic flow increases with nickel thickness, however, large thicknesses are desired to minimize the likelihood of failure of the unbonded nickel tube if the tungsten cracks.
- The convergent region upstream of the launch tube needs tungsten protection. A number of fabrication methods exist for making a suitable nickel shell to fit the entrance contour, but none of them are simple.

Many of the difficulties with approaches discussed so far could be minimized using the following approach:

- Plate nickel directly on the inside of the launch tube and convergent section
- CVD tungsten on the nickel plate
- Hone the tungsten to the desired dimension, and CVD a thin layer of tantalum carbide inside the tungsten

The apparent difficulty with this approach is that tantalum carbide application is most reliable at temperatures near 1038°C (1900°F). This means that subsequent heat treatment would be required in order to obtain an appropriate balance between launch tube tensile strength and toughness. A shrink-fit liner allows independent control of deposition temperatures and launch tube heat treatment temperatures. Although the subsequent heat treatment is not necessarily problematical, it might be advantageous to minimize the number of significant thermal cycles at the tungsten-nickel-steel interface prior to completing fabrication because of the disparity of thermal expansion coefficients between tungsten and steel. On the other hand, 1038°C (1900°F) processing almost guarantees good diffusion bonding at all interfaces if they are appropriately prepared (cleaned).

Calculations were made to estimate the stresses in the launch tube and tungsten assuming a zero stress condition at the CVD processing temperature, T_p. The combined properties of the launch tube and tungsten dictate a small tensile stress in the launch tube after cooldown from the CVD process condition and a large compressive stress in the tungsten. The results in Figure 28 show that compressive stresses increase rapidly with processing temperature. The compressive yield strength in tungsten is unknown, and it is not clear what will happen when it is exceeded (plastic deformation or crumbling). One potential benefit of high processing temperatures is that the tungsten liner may never get into a tensile state as a result of internal ballistic pressures. For example, Figure 28 shows that at 100 kbar, tungsten stresses in the absence of thermal effects are approximately zero if the CVD processing is done at slightly less than 700°C.

Tungsten becomes quite plastic at high temperatures. High temperatures will exist near the internal surface of the tungsten both during the launch event and during cooldown after expulsion of the projectile. It is expected that some yielding will occur near the internal surface with perhaps a very negative effect on a tantalum carbide layer. Subsequent pressurization will then drive the internal surface into tension with possible tensile failure near the surface (cracks). It is not clear what effect the processing temperature has on the subsequent behavior near the tungsten surface.

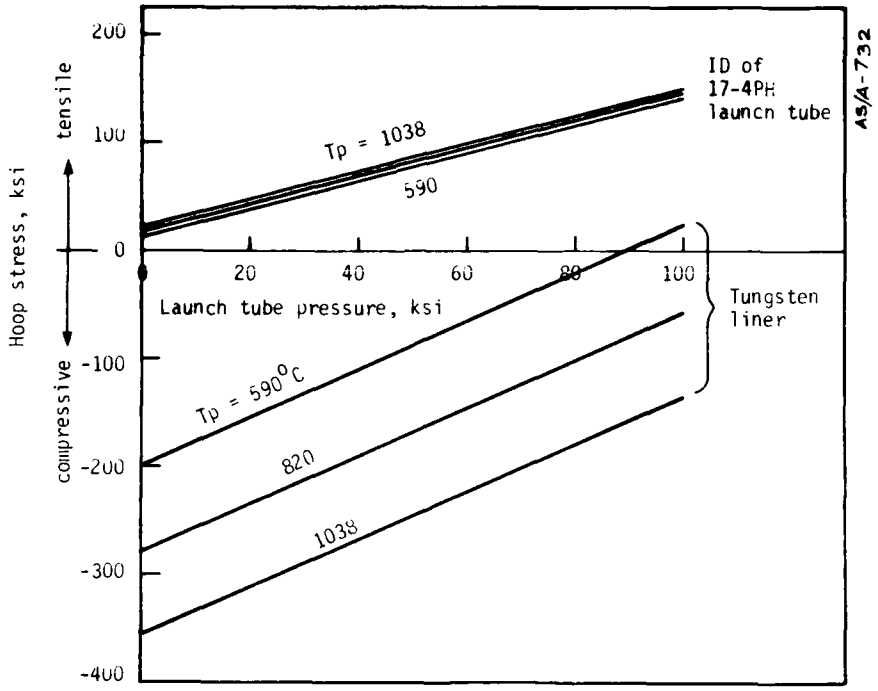

Liner

$\sigma_\theta = 25.0\ (\sigma_{ri}\ P)$

17-4PH @ inner radius

$\sigma_\theta = -\sigma_{ri}\ (1.422)$

where

$$\sigma_{r_1} = \frac{\Delta t(\alpha_{st} - \alpha_w) + \dfrac{Pr_i}{E_w \tau}}{\dfrac{1}{E_{st}}\left[\left(\dfrac{r_o^2 + r_1^2}{r_o^2 - r_1^2}\right) + \nu_{st}\right] + \dfrac{r_1}{E_w \tau}}$$

= Stress state at interface between 17-4PH & W (ignoring Ni)

Δt = Difference between CVD temperature and room temperature

α = Coefficient of thermal expansion $\approx 2.6 \times 10^{-6}$(in./in./°F) for W

$\approx 6.3 \times 10^{-6}$(in./in./°F) for 17-4PH

P = Internal pressure

r_i = Internal radius = 0.651 in.

r_o = Outer radius = 1.559 in.

E = Youngs modulus = 28.5×10^6 for 17-4PH

= 58×10^6 for W

τ = Thickness of W = 0.026 in.

ν_{st} = Poisson's ratio for 17-4PH = 0.272

$\sigma_{r_i} = \Delta t(7.807) + P(0.911)$

Figure 28. Calculated effect of CVD process temperature on tungsten liner and launch tube stresses after cooldown.

The approach selected for the 1/4-scale launcher based on the foregoing considerations is the following:

1. The original launch tube split clamp design was rejected on the basis of costs and the selected method of fabricating the liner
2. 17-4PH stainless steel was selected for the launch tubes and convergent section. This selection is based on the flexibility and subsequent fabrication reliability afforded by being able to quench in air from both the solution treatment temperature (condition A, 1038°C (1900°F)) and typical precipitation hardening temperatures 482°-621°C (900°-1150°F)
3. Launch tubes are to be bored, honed, and plated within the bore with nickel before the tungsten CVD process
4. CVD temperature is selected at a minimum of 482°C (900°F) to enable solution hardening of the launch tube during the CVD process and to allow diffusion bonding between nickel and the adjacent steel and tungsten materials
5. A demonstration cycle has been selected that eliminates the need for the tantalum carbide layer

4.2 EXPERIENCE WITH THE NOMINAL LINER APPROACH

While considering the approach to fabricating the liner, our CVD contractor (Ultramet, Pacoima, California) conducted a number of trial platings to evaluate processing temperatures and the feasibility of heat treating after plating. At that time, both 4340 steel and 17-4PH were being considered. Platings that have been done on configurations other than flat samples include:

1. A section of 17-4PH tubing that was intended to be used as an insert in the compressor-to-launch-tube adapter (see Section 5)
2. A short section of 4340 tubing
3. The insert for the compressor throat section (see Section 5)
4. A 244-cm (8-foot) long 17-4PH launch tube
5. Two 91-cm (3-foot) long maraging steel launch tubes that were completed for AEDC under separate contract

The bores of all of these samples, except item 2, were electroless nickel plated prior to plating tungsten.

Item 1 above was not tungsten plated to sufficient thickness on the first try, so the part was subjected to the CVD process a second time.

-A086 268 ACUREX CORP MOUNTAIN VIEW CA F/G 10/1
DEVELOPMENT AND TESTING OF A TWO-STAGE HYBRID LAUNCHER.(U)
OCT 79 K E SUCHSLAND, J D WATSON, T J DAHM DNA001-76-C-0407
UNCLASSIFIED ACUREX-FR-79-19/AS(7386) DNA-5074F NL

2 OF 2
AD
A086268

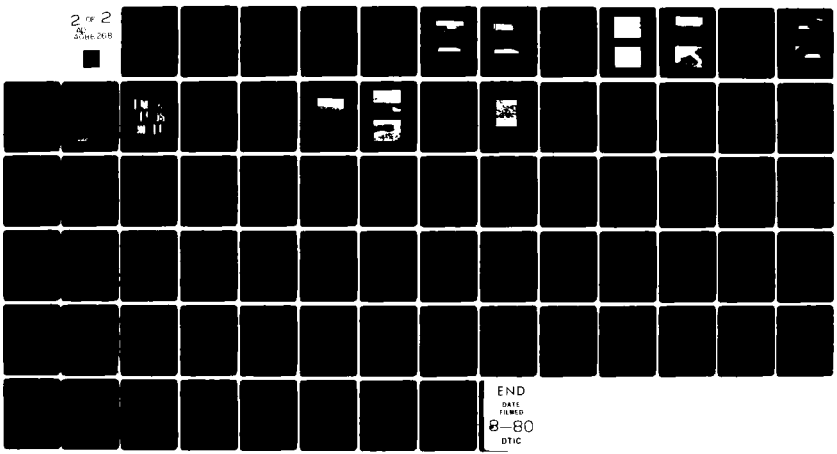

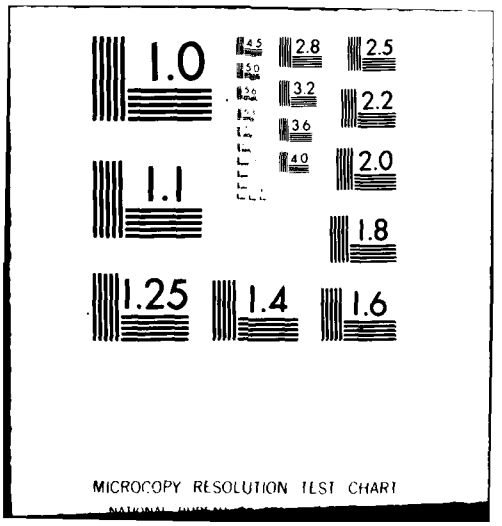
1.0
4.5
5.0
5.6
2.8
3.2
3.6
4.0
2.5
2.2
2.0
1.8
1.1
1.25
1.4
1.6
MICROCOPY RESOLUTION TEST CHART

Because of the time-at-temperature for the two processing events, it was judged that the part was over-aged. Thus, it was heated to condition A, air quenched, and then precipitation hardened at 482°C (900°F) and air quenched. The finished part showed debonding at the nickel interface. The debonding was attributed to the tensile stresses at the bond line due to differential expansion in going from the processing temperature to condition A. In addition, the tungsten-to-tungsten interface from the second CVD attempt showed poor bonding and some regions of separation. This part was used as a short launch tube in the I-2 firing. Portions of the liner failed during the firing, as expected based on the quality of the part. However, a large percentage of the liner was intact in spite of its poor quality.

Item 2 above resulted in an apparently high quality tungsten tube within the outer tube, but minimal bonding. Although good bonding was not expected for tungsten on steel, this failure was in part attributed to the post-process heat treat. This experience enforced the idea of avoiding raising the tube to temperatures higher than the CVD process temperature.

The throat section, item 3 above, was the first attempt to plate over a large surface area. Most of the tungsten liner appeared to be of high quality. A bubble was formed in one area. This might be due to the need for better surface preparation prior to plating.

The plating at approximately 482°C (900°F) and subsequent honing of the 8-foot launch tube (item 4 above) appeared to be quite successful. The tube was cut into a number of 10-cm lengths in preparation for hydrostatic tests. The hydrostatic test hardware has been fabricated but not used to date. Microscopic examination of the parts shows excellent diffusion between the nickel plate and the steel, as shown in Figure 29. Minimal diffusion is apparent at the nickel-tungsten inferface. Some of the tube sections show minor longitudinal slippage at this interface, no doubt due to the greater longitudinal shrinkage of the steel relative to tungsten during the cooldown. Even though the bonding was less than perfect, a major milestone had been achieved by the successful uniform growth of an apparently high quality tungsten liner by the CVD process in a high L/D tube (~ 77). In addition, the honing of the liner was successful and less difficult than had been anticipated.

Note good diffuse bond between Ni and 17-4PH
but sharp bond line between Ni and W

Tungsten: 0.025" thick
CVD @ ≈480°C

Nickel: 0.00025" thick
electroless deposition

Magnification: 800X

No etching

Figure 29. Photomicrograph of CVD tungsten on 17-4PH with nickel plate layer.

At the time of this success, it was quite clear that because of the I-2 injection block failure, it was going to be some time under this program before we could subject a tungsten-lined tube to representative loading conditions. With the objective of early proof-testing of the concept, the two tubes indicated in item 5 above were fabricated for AEDC. Maraging steel was used for this application because of the extreme high-pressure conditions where the tube was to be used (Range S1 at AEDC). The CVD process was carried out at tube temperatures of $540^{o} \pm 20^{o}C$. This is a good precipitation hardening temperature for both maraging steel and 17-4PH, and also is a condition conducive to better diffusion bonding than in the 8-foot tube. The platings were apparently successful. Final machining of the part was done by AEDC. The 5/8-inch diameter bore required the first tube to be cut in half in order to do the honing. The liner has not yet been examined with photomicrography.

Liner performance during the firing was partially successful.* The two honed halves of the tube were used in a series arrangement. During the first firing, the downstream section lost part of the lining and ballistic performance was lower than normal for the launcher. The upstream section was intact with some cracking noted on the inside diameter, as expected. The launcher was fired again using the good launch tube section, but approximately 5 percent of the liner was lost and ballistic performance was lower than normal. The region of lining that cracked in the first firing remained intact during the second firing. The second launch tube has not been tested.

Subsequent to the AEDC tests, one of the short lengths of the 8-foot tube was used in the I-5 firing. Consistent with the AEDC experience, a small portion of the liner failed (approximately 10 percent). The conclusions from these experiences are:

- Thin tungsten liners can be formed successfully by the CVD process in long tubes

---

*Exact internal ballitic conditions for the test in Range S1 are unknown. First-stage kinetic energy was higher than typical.

- A thin, high-quality tungsten liner will not survive representative internal ballistic loads unless the liner is well bonded to the launch tube
- Internal ballistic performance is degraded when liners fail. It is, therefore, essential that the liner not fail during the demonstration firing of the hybrid launcher.
- It follows, by analogy to our experience with failed liners, that gun barrel melting will degrade internal ballistic performance. Tungsten liners are essential to achieving full performance of the hybrid concept.

4.3 BONDING DEVELOPMENT TESTS

Since it is clear that better bonding is required, a bonding development effort has been conducted. Rather than continuing to try to obtain a high quality liner that is well bonded to a long steel tube having all the desired structural properties, attention is being focused on developing a good bond. Nickel type, nickel thickness, and tungsten CVD temperature have been systematically varied in the tungsten plating of flat samples. The nominal material study matrix is presented in Table 5.

It has been our presumption that the key factor that dictates bond quality is the degree of diffusion at the tungsten-nickel bondline. This improves as melt temperature is approached during processing. On the other hand, if tungsten CVD is at higher temperatures than in the past, the heat treatment of the launch tube becomes complicated. Samples processed at 590°C to assess the possibility of good bonds at a reasonable 17-4 pH heat treatment temperature are shown in Figure 30. Sample 01 with 2.54 micron (0.1 mil) electrolytic nickel as the bonding medium resulted in bondline failure sometime during the processing, no doubt during cooldown. However, aside from the fact that it is broken, the tungsten layer appears to be of high quality. Sample 11 with a 5 times thicker nickel plate survived the processing satisfactorily. Two representative samples processed at 820°C are shown in Figure 31. Processing at this elevated temperature results in the formation of large nodules of tungsten and a large variation of tungsten thickness over the sample. Flow of CVD reactants is lengthwise along the sample, with the heaviest tungsten deposition near the sample leading edge. The gradients in tungsten thickness suggest diffusion control of tungsten deposition at

TABLE 5. TUNGSTEN-NICKEL BONDING DEVELOPMENT MATRIX

TEST SAMPLE INVENTORY

WATTS PROCESS Ni THICKNESS	SAMPLE #'s
0.0001"	01 --- 08
0.0005"	09 --- 017
0.001"	018 -- 026
0.002"	027 -- 034

ELECTROLESS Ni THICKNESS	SAMPLE #'s
0.00025"	035 & 036

NO TREATMENT	SAMPLE #'s
-0-	037 & 038

TUNGSTEN CVD TEMPERATURE	SAMPLE #'s
510°C	S/N 09, 018, 035 & 036
590°C	S/N 01, 02, 010, 011, 019, 020, 027 & 028
820°C	S/N 03, 04, 012, 013, 021, 022, 029 & 030
1038°C	S/N 05, 06, 014, 015, 023, 024, 031 & 032
CVD SET-UP/CHECK OUT	S/N 07, 08, 016, 017, 025, 026, 033 & 034

TEST MATRIX

NICKEL PLATE/CVD TEMP

FLAT PLATES 1/4" X 1" X 5 1/2"

17-4 PH, CONDITION A

CVD TEMP	NICKEL TYPE: ELECTROLESS THICKNESS 0.00025"	ELECTROLYTIC THICKNESS 0.0001"	ELECTROLYTIC THICKNESS 0.0005"	ELECTROLYTIC THICKNESS 0.001"	ELECTROLYTIC THICKNESS 0.002"
510°C	2 SAMPLES (BASELINE) S/N 035 & 036		1 SAMPLE S/N 09	1 SAMPLE S/N 018	
590°C		2 SAMPLES S/N 01 & 02	2 SAMPLES S/N 010 & 011	2 SAMPLES S/N 019 & 020	2 SAMPLES S/N 027 & 028
820°C		2 SAMPLES S/N 03 & 04	2 SAMPLES S/N 012 & 013	2 SAMPLES S/N 021 & 022	2 SAMPLES S/N 029 & 030
1038°C		2 SAMPLES S/N 05 & 06	2 SAMPLES S/N 014 & 015	2 SAMPLES S/N 023 & 024	2 SAMPLES S/N 031 & 032

8 SPARES REQUIRED FOR CVD CHECKOUT: S/N 07, 08, 016, 017, 025, 026, 033, 034

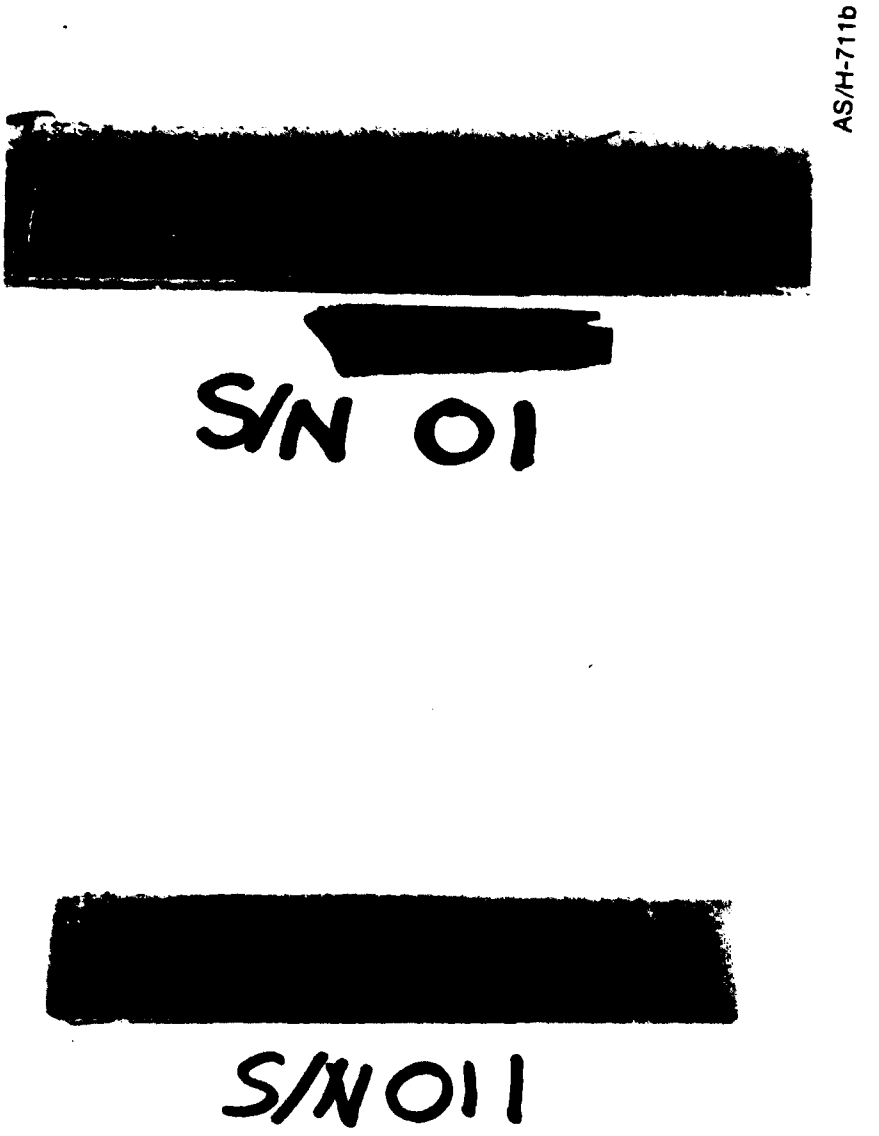

Figure 30. Representative examples of tungsten CVD at 590°C.

AS/H-710b

S/N 030

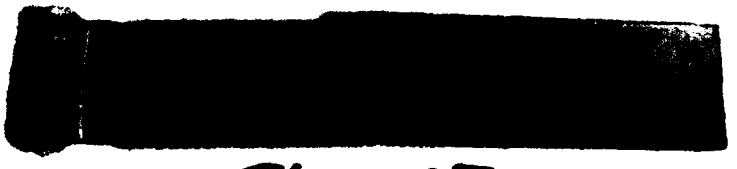

S/N 013

Figure 31. Representative examples of tungsten CVD at 820°C.

elevated temperatures, in contrast to kinetic control at lower temperatures.

Photomicrographs of representative cross sections in Figure 32 show excellent diffusion across the nickel-steel interfaces. Sample number 17, processed at 590°C, shows a sharp discontinuity at the tungsten-nickel interface, and sample 30, processed at 820°C, shows a somewhat more diffuse interface. Thus, the higher temperature is accomplishing be desired result in terms of tungsten-nickel diffusion, but a quite unacceptable result in terms of tungsten layer character. The nodules that are formed are easily broken away from the tungsten, resulting in the general features shown in cross section in Figure 33, sample 33. The photomicrograph of sample 30 in Figure 33 shows cracking of the tungsten in the nodule cavity with some extrusion of the nickel between the cracks in the tungsten. It is clear that deposition of tungsten to the required thicknesses at high temperature is not practical. However, trials with samples 33 and 34 that were plated to about 180 microns (7 mils) at 820°C showed nodules in their early stages of growth that would probably be acceptable.

Thus, the material study matrix was revised as shown in Table 6. The table includes those samples that were processed according to the original plan. We felt that it was necessary to expose the tungsten-nickel interface to high temperatures for a period of time to achieve good diffusion, but that it was not necessary to do all of the CVD deposition at high temperature. This thought is reflected in most of the revisions in the matrix. One concept we explored was to deposit a thin layer of tungsten at high temperature, and then hold the sample at that temperature for a long period (~1 hr) without further deposition. Subsequently, temperature is reduced and CVD deposition completed at the lower temperature. Elements of this scenario had already been proven on our first samples. We also briefly explored the idea of starting at low temperature and completing the tungsten deposition at high temperature.

The results of this latter concept are shown in Figure 34 where sample 25, which was processed according to the concept, is compared to sample 29 that was processed at a constant 820°C. The results are about as expected, with smaller nodules being formed through the variable

S/N 017 T = 590°C, 800X

S/N 030 T = 820°C, 500X

Figure 32. Photomicrographs of material interfaces, CVD at 590°C and 820°C.

S/N 033, 100X

S/N 030, 400X

Figure 33. Character of tungsten layer with nodules, T = 820°C.

TABLE 6. REVISED TUNGSTEN-NICKEL BONDING DEVELOPMENT MATRIX

		Nickel Type				
		Electroless	Electrolytic			
		Thickness	Thickness			
		0.00025"	0.0001"	0.0005"	0.001"	0.002"
CVD Temperature (°C)	590		2 SAMPLES S/N 01 & 02	4 SAMPLES S/N 010 & 011 & 016 & 017	2 SAMPLES S/N 019 & 020	2 SAMPLES S/N 027 & 028
	820			2 SAMPLES S/N 012 & 013		4 SAMPLES S/N 029 & 030 & 033 & 034
	820/510	2 SAMPLES (BASELINE) S/N 035 & 036		1 SAMPLE S/N 09	1 SAMPLE S/N 018	
	820/590			1 SAMPLE S/N 015	2 SAMPLES S/N 022 & 024	1 SAMPLE S/N 032
	1040/590			1 SAMPLE S/N 014	2 SAMPLES S/N 021 & 023	1 SAMPLE S/N 031
	590/820		3 SAMPLES S/N 03 & 04 & 07		1 SAMPLE S/N 25	

4 SAMPLES NOT PLATED WITH TUNGSTEN: S/N 05, 06, 08, 026

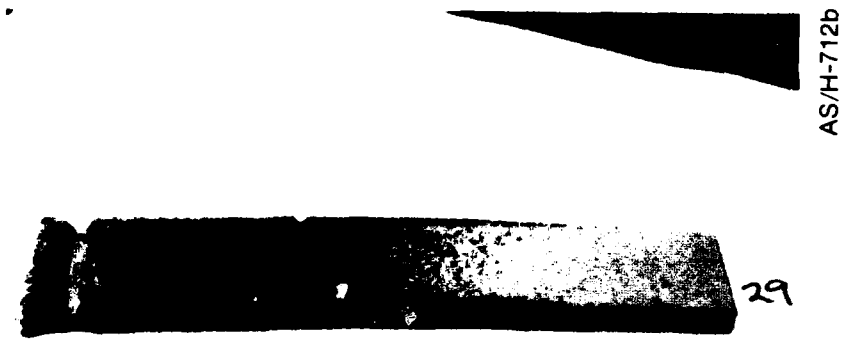

CVD at 820°C

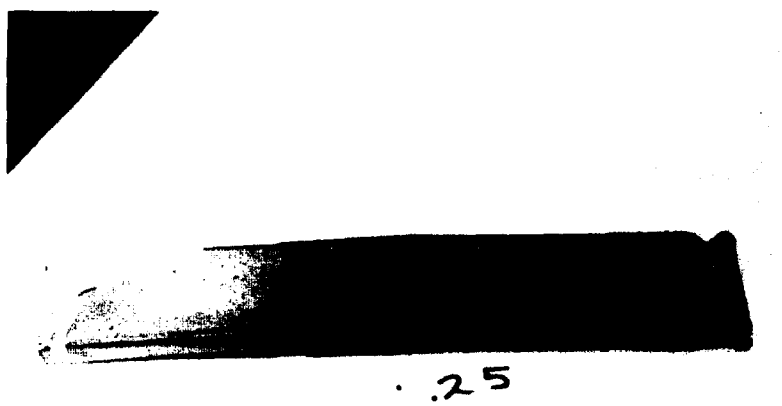

CVD at 590° to 820°C

Figure 34. Effect of initial CVD at low temperature on nodule formation.

temperature process. However, the tungsten layer is of nonuniform thickness and the bondline failed on sample 25 sometime in the process.

The concept of variable temperature being high during early deposition worked very well. No bond failures were noted at the completion of the process. However, cracks are formed in the tungsten, apparently during the deposition process. These are illustrated by the surface photomicrographs presented in Figure 35. The sizes of the cracks appear to increase with initial temperature. The surface distance between cracks appears to decrease slightly with increasing initial temperature. The cracks are attributed to expansion of the steel at the final plating temperature following the nonequilibrium shrinkage during cooling from the initial high temperature. This hysteresis in thermal expansion is characteristic of 17-4 pH stainless steel in the precipitation hardening temperature range.

All but two of the samples with ostensibly acceptable quality following the CVD process were subjected to bend tests (the two excluded samples are being held for later tests). Samples with nodules, debonding, or large cracks were not subjected to bending tests.* All samples survived deflections normal to the bar thickness direction of about 1 cm without evidence of debonding. However, the tungsten cracked in all of the samples at deflections that are roughly consistent with expectations considering the ultimate tensile strength of tungsten. Since a deflection of 1 cm was not sufficient to assess bond quality, all bend samples were placed in a vice and bent through approximately 90°. This test provided the desired discrimination.

A composite photograph of the worst appearing samples from each of the points in the matrix of Table 6 is presented in Figure 36. Certain results for all samples are presented in Table 7. From Figure 36, it is clear that bonding is poor (but not consistently so, see samples 19 and 28 in Table 7) when CVD deposition is done entirely at 590°C. This is slightly higher than the process temperature for the AEDC tubes. In light

---

*Tungsten plated samples bend naturally during cooling because of the disparity of tungsten and steel thermal expansion coefficient. As a consequence, we believe that flat samples are more prone to tungsten or bondline failure than tube samples.

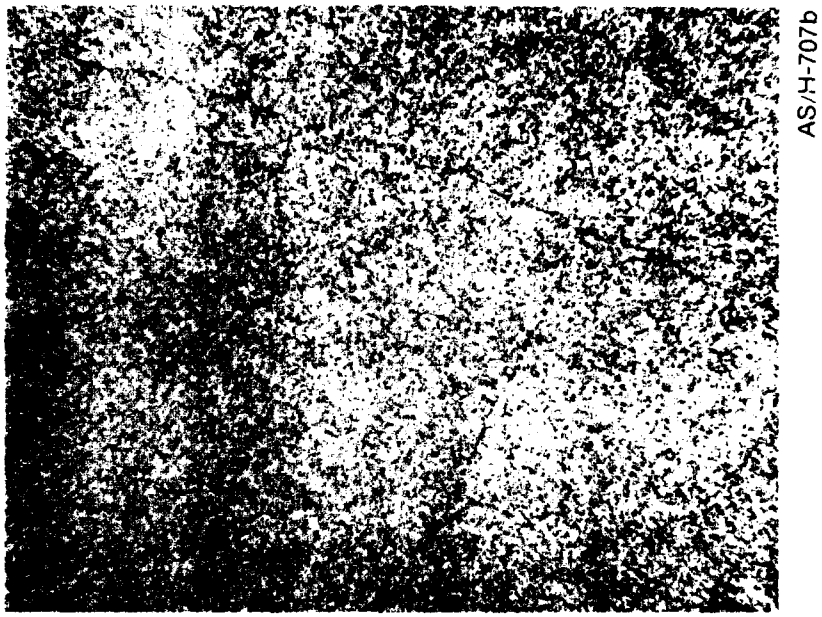

T = 820° to 590°C

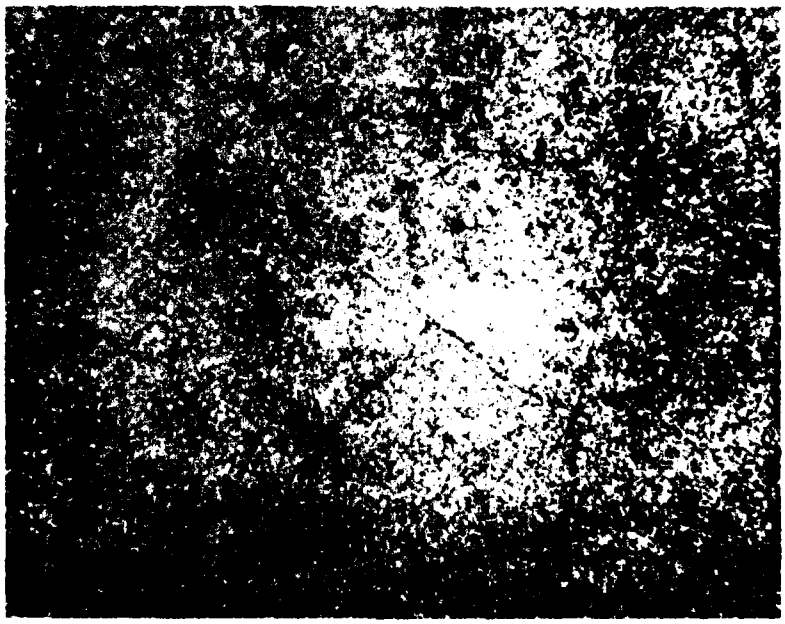

T = 1040° to 590°C

Figure 35. Effect of initial CVD temperature on surface cracks, 10X.

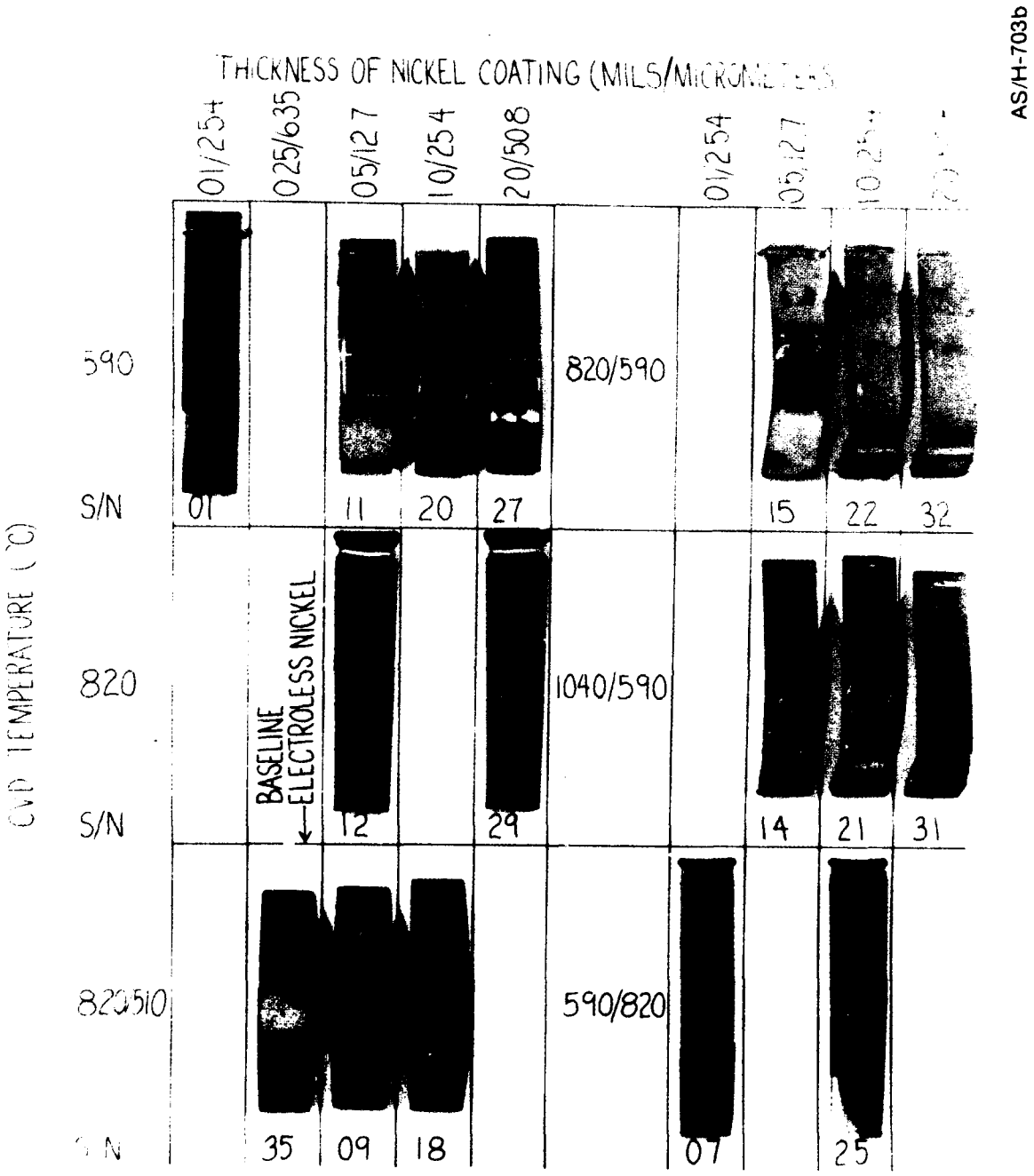

Figure 36. Composite photo of worst samples from the matrix in Table 6.

TABLE 7. RESULTS OF BONDING DEVELOPMENT STUDY

Serial Number	Initial CVD Temperature (°C)	Final CVD Temperature (°C)	Nickel Thickness (mils/micrometers)	Tungsten Thickness (mils/micrometers)	Prebend Condition	Postbend Condition	Postprocess Hardness (R_c)
01	590	590	0.1/2.54	52/1321	Debonded	--	34
02			0.1/2.54	49/1245	Debonded	--	32
10			0.5/12.7	48/1219	Large crack	--	35
11				35/889	Excellent	Debonded	35
16[a]				6/152		Debonded	23
17[a]				8/203		Minor debonding	32
19			1.0/25.4	20/508		Excellent	33
20			1.0/25.4	20/508		Minor debonding	35
27			2.0/50.8	16/406		Debonded	33
28			2.0/50.8	22/559		Excellent	34
12	820	820	0.5/12.7	--	Nodules	--	31
13			0.5/12.7	--		--	34
29			2.0/50.8	--		--	32
30				--		--	31
33[a]				7/178		--	34
34[a]				7/178		--	34
03	590		0.1/2.54	--		--	37
04				--		--	35
07[a]				--		--	35
25[a]			1.0/25.4	--		--	35
35	820	510	0.25/6.35[b]	13/330	Excellent	Debonded	32
36			0.25/6.35[b]	13/330		Debonded	35
09			0.5/12.7	15/381		Minor debonding	34
18			1.0/25.4	18/457		Excellent	36
15		590	0.5/12.7	23/584		Excellent	33
22			1.0/25.4	14/356		Excellent	35
24			1.0/25.4	13/330		Not tested	37
32			2.0/50.8	15/381		Excellent	35
14	1040		0.5/12.7	17/432		Minor debonding	34
21			1.0/25.4	17/432		Excellent	39
23			1.0/25.4	11/279		Not tested	34
31			2.0/50.8	14/356		Excellent	37
05	Unplated spare		0.1/2.54	--	--	--	--
06				--	--	--	--
08[a]				--	--	--	--
26[a]			1.0/25.4	--	--	--	--
37			0	--	--	--	--
38			0				34[c]

[a]Originally planned for CVD setup/checkout
[b]Electroless nickel
[c]Maximum R_c equal to 38 expected for untreated bar

of these results, the liner failures at AEDC are not surprizing. Only one of the samples from 90° bend tests that was also processed at elevated temperature showed significant failure at the bondline -- the sample with electroless nickel. Since this was the type of nickel and of the same thickness used for the 8 ft tube and the AEDC tubes, it is reasonable to conclude that these liners would have failed even if they had been processed at elevated temperature.

From the results so far, it is not clear that electroless nickel is an inherently poor bonding medium. Note that sample 9 (see Table 7) with double the nickel thickness, but deposited electrolytically, showed only minor debonding (to be defined). All high temperature bend samples with nickel thicknesses of at least 25 microns were in excellent condition (to be defined) subsequent to the bend tests. So the failure of the electroless nickle sample may be due at least in part to the thinness of the nickel

Sample 17 is not included in the samples shown in Figure 36 since only the worst looking samples were selected for the presentation. In addition, sample 17 has only a thin layer of tungsten, approximately 200 microns (8 mils). The sample was subjected to the 90° bend test, showing only minor debonding even though the results in Figure 32 indicate minimal diffusion at the bondline. Sample 16, with identical history to sample 17 showed significant debonding after the 90° bend test. A postbend photomicrograph of sample 17 is shown in Figure 37. The photo shows that the tungsten is bonded very well to the substrate -- so well that the yielding in the steel during the bend test occurs between the cracks in the tungsten. That is, the tungsten bond is sufficiently good that yielding of the steel is locally prevented by the bonded tungsten.

The "minor debonding" on sample 17 is shown in Figure 37. The view is on the opposite side of the sample from that in Figure 37. It is difficult to obtain a good picture of how the sample really looks, but the tungsten "tiles" can be seen to be pulled away from the substrate, and the exposed steel substrate can be seen normal to the line of sight.

By way of contrast, the "excellent" condition of sample number 32 is also shown in Figure 38. This sample is photographed in the same way as the companion photo of sample 17 in Figure 38. Here, the exposed surface that is normal to the line of sight is tungsten. A thin layer of

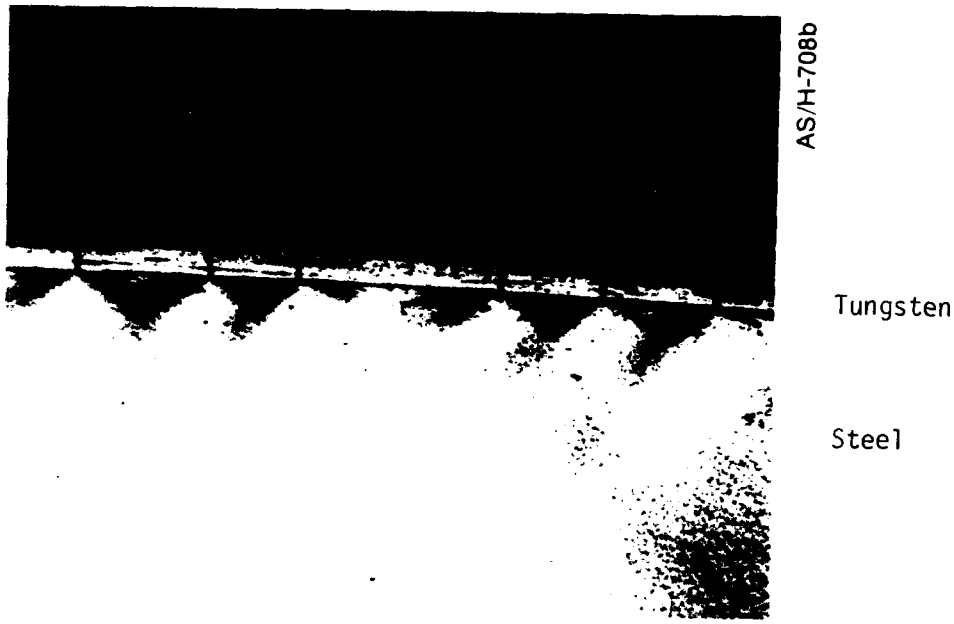

Figure 37. Post-bend photomicrograph of sample S/N 017 showing bond retention during substrate yielding, 20X.

AS/H-704b

S/N 017, bond failure, showing exposed substrate, example of "minor debonding"

S/N 032, bond retention, showing exposed tungsten layer, example of "excellent condition"

Figure 38. Photomicrographs of corners of bent samples, 20X.

tungsten is still bonded to the substrate in spite of the yielding of the substrate. Any tungsten missing from the sample is due to tensile or shear failure of the tungsten, rather than bond failure.

All tungsten missing from the sample was forcefully removed after the bend test. A plan view of the tungsten surface of sample 32 is shown in Figure 39. The light areas between the cracks are reflections, probably off the remaining thin tungsten layer.

These latter results are exactly what we wanted -- retention of the tungsten even if it cracks. The cracks obtained in the bend tests are gross exaggerations of what might appear within the launch tube.

4.4 CONCLUSIONS FROM LAUNCH TUBE THERMAL PROTECTION STUDIES

From the beginning of this program, the very severe heat transfer conditions implied by the hybrid launcher concept have been recognized. Detailed heat transfer calculations were carried out during the design of the hybrid internal ballistic cycle. The limitations in the design that are imposed by the properties of the launch tube thermal protection materials have been estimated. It is clear that reliable tungsten liners are essential to realizing the full potential of the hybrid launcher concept. Conclusions from the tungsten liner development studies are:

- Thin tungsten liners can be formed successfully by the CVD process in high L/D tubes
- A thin, high quality tungsten liner will not survive representative internal ballistic loads when it is not well-bonded to the launch tube
- Nickel forms a good diffusion bond with steel
- Liners that are deposited at temperatures below 600°C do not form reliable bonds with nickel
- Liners that are deposited at temperatures greater than 800°C form tungsten nodules that are unacceptable
- Bond reliability improves by increasing the thickness of the nickel that is plated on the steel substrate
- Electroless nickel does not form a good bond with tungsten, at least for the thicknesses considered under this program
- CVD of tungsten on electrolytic nickle forms reliable bonds and a high quality tungsten liner, if the CVD process starts at

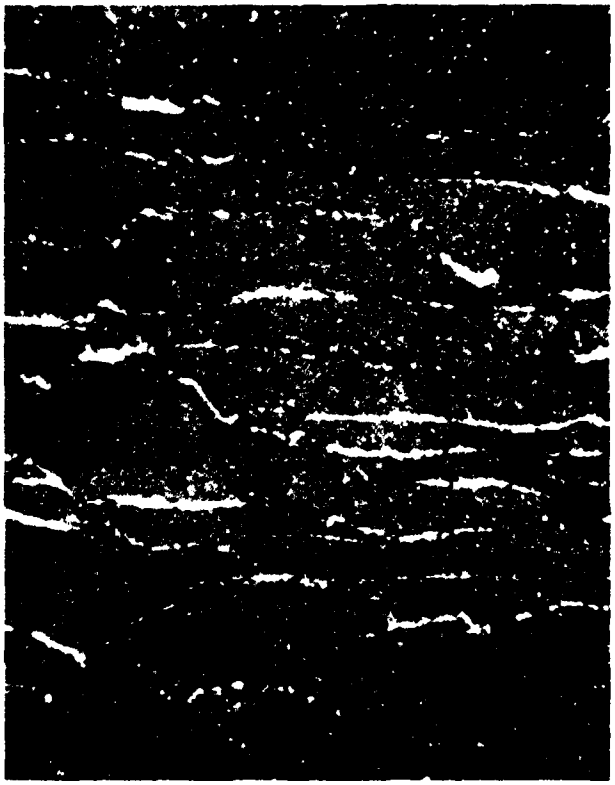

AS/H-706b

Figure 39. Plan view of sample S/N 032 showing well-bonded "tiles," 10X.

high temperature but obtains most of its thickness by deposition below 600°C

- Cracks are formed in the tungsten layer if CVD starts at high temperature and is completed below 600°C
- The failures that have been experienced under this program using tungsten lined launch tubes are attributed to a nickel layer that was too thin, CVD at temperatures that are too low, and possibly a poor choice of nickel type
- The probability of a tungsten liner surviving the hybrid launcher internal ballistic loads is very high based on the recent results of this program

SECTION 5
DESIGN AND FABRICATION STATUS

This section summarizes the status of the 1/4-scale launcher design and fabrication. For convenience, it is divided into two subsections, "gun" components and gun mounts.

5.1 GUN COMPONENTS

As discussed in Section 2, the basic design of the 1/4-scale launcher was completed in April 1977 (Reference 3). This original design was subject to a number of design constraints, which arose due to various materials and launch cycle physics limitations. These constraints include the following:

- Model base pressure $\leq$ 5 kbar
- Reservoir pressure $\leq$ 8 kbar
- Liner surface temperature $\leq$ 4153°K (TaC/W/Steel)
- Reservoir gas temperature $\leq$ 5800°K
- Design launch tube length $\leq$ 300 times its diameter

To remain within these constraints, the original gun design proposed the following design features:

- First stage M68 honed to a 10.8-cm (4.25-inch) diameter
- Polyethylene/delrin piston*
- Four (or six) nitromethane explosive drivers injecting 50 grams of hydrogen each
- 30.5-cm (1-foot) diameter injection block with replacement rods opposite each injection port for refurbishing
- 40.6-cm (16-inch) OD (10.8-cm ID) compression section

---

*The piston mass and velocity would be modified during testing to optimize the launch cycle performance and to remain within design constraints.

- 40.6-cm (16-inch) OD compressor throat with a TaC-over-tungsten liner on ID to prevent surface melting
- Split launch tube with a 2.54-cm (1-inch) diameter TaC-over-tungsten liner clamped between halves

An assembly drawing of the launcher design as of April 1977 is provided in Figure 40.

New design work on the launcher began in September 1977. This included a more detailed stress analysis of the April 1977 design. As a result of this work, several of the gun component outer diameters were increased and the driver coupling system was made much stronger.

It was also decided that the launch cycle should be modified to allow use of bare tungsten liners in the launch tube, thus eliminating the TaC layer on top of the tungsten. This allowed a reduction in the liner development effort, so that emphasis could be placed on perfecting the tungsten liners. The launch tube inside diameter was increased to 3.18 cm (1.25 inches) to achieve this launch cycle.

A revised launch tube design was developed after considerable work with the two major suppliers of CVD tungsten.* As a result of careful consideration of the various methods of fabricating the tungsten liners and the launch tube, it was concluded that the launch tubes should be monolithic. Thus the original design with the tungsten liner clamped between two launch tube halves was replaced by a simpler and mechanically stronger design.

An assembly drawing of the launcher design as of November 10, 1977 is shown in Figure 41. This design was sent out for quotes and, in December 1977, Caral, Inc. in Albany, California was selected as the major fabricator of hybrid launcher parts.

Caral began fabrication of the launcher in January 1978 based on the design shown in Figure 41. However, on February 22, 1978, the I-1 test revealed that the injection block design may be inadequate. Caral was asked to halt all fabrication on the gun at that time. Subsequent

---

*The selection of CVD tungsten is described in Section 4.

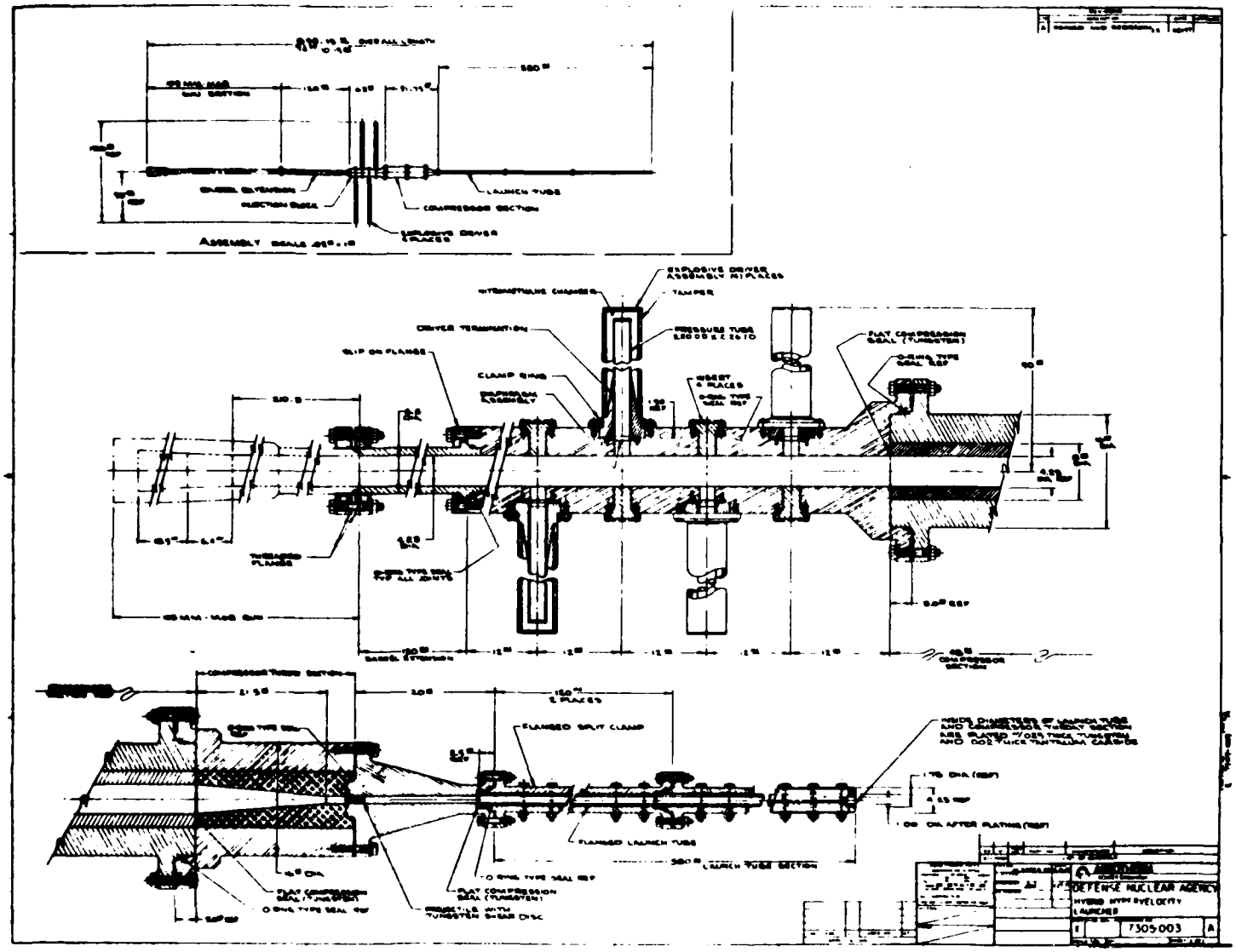

Figure 40. One-inch bore (1/4-scale) hybrid launcher assembly drawing (April 1977).

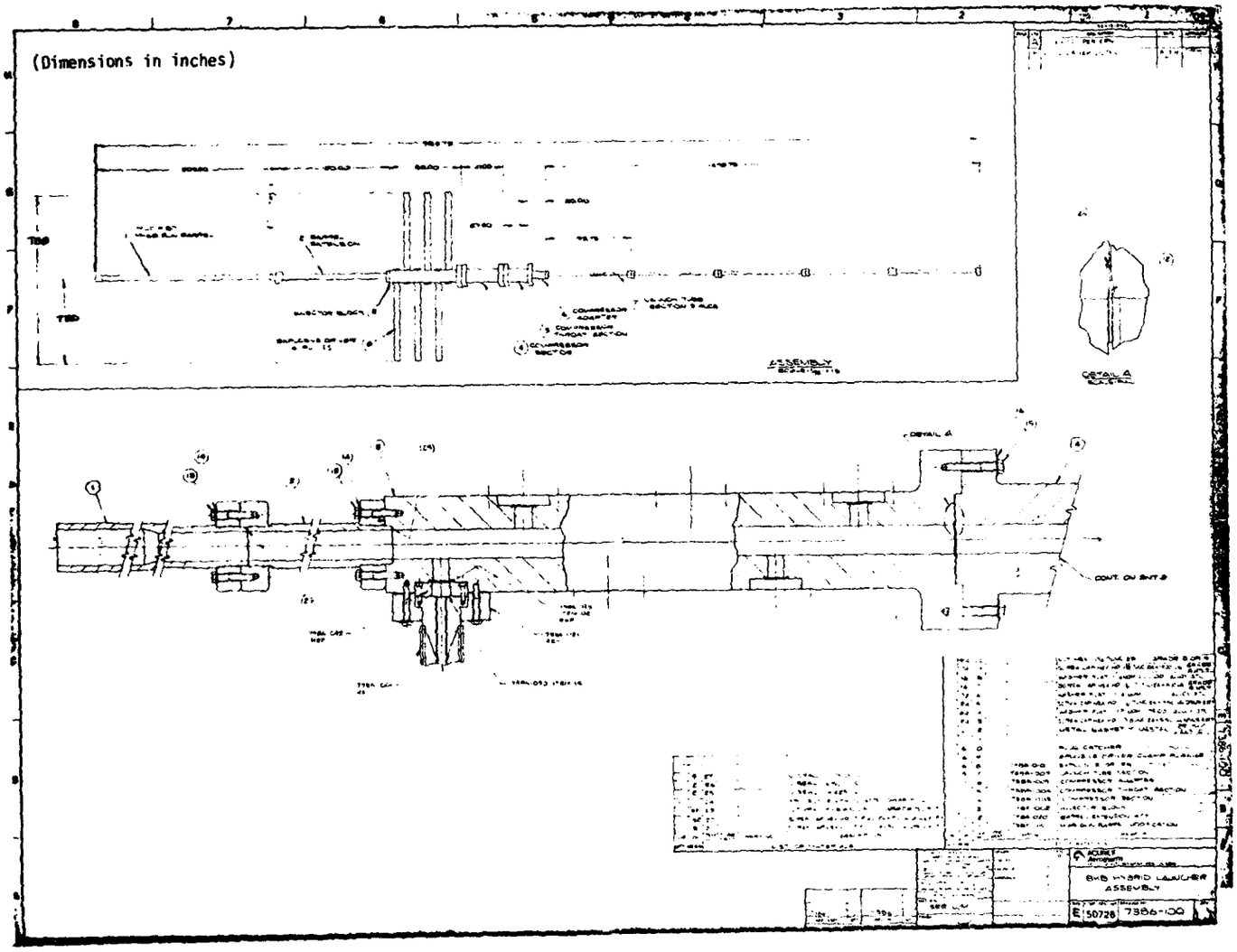

Figure 41. One and a quarter-inch bore (1/4-scale) hybrid launcher assembly drawing (November 10, 1977).

tests, which culminated with the successful March 1979 I-5 injection test, resulted in an adequate injection block design. As these tests progressed, changes were made to the design. These changes are summarized below:

- For the injection block:
  - -- Replacement rods were eliminated
  - -- Number of injection ports were increased to allow for 10" drivers
  - -- Injection ports were flared
  - -- Corners were rounded at intersection of bore with injection ports
  - -- Hardness specification was lowered
- For the driver:
  - -- Dimensions were decreased 30 percent
  - -- Distance between nitromethane and the injection block was maintained (while reducing overall driver size)
  - -- Driver contact area with the injection block was reduced to a lesser extent than overall driver dimensions to achieve a relative increase in contact area
- For the seals
  - -- Seal designs were modified to incorporate improvements developed during the injection block tests series

An assembly drawing of the present launcher design is shown in Figure 42. Most of the drawings for the launcher components have been "red lined" to incorporate all changes made between November 1977 and March 1978. These changes will be made to the original design drawings as soon as design and fabrication activities are resumed. The injection block, driver, and driver coupling system drawings already incorporate all changes since these drawings had to be updated to fabricate the I-5 test components.

The fabrication status of the gun components is summarized in Table 8. For the most part, components reflect the amount of machining performed at the time of the I-1 failure. Some of the parts (such as the drivers and driver coupling flanges) will require replacement due to design changes.

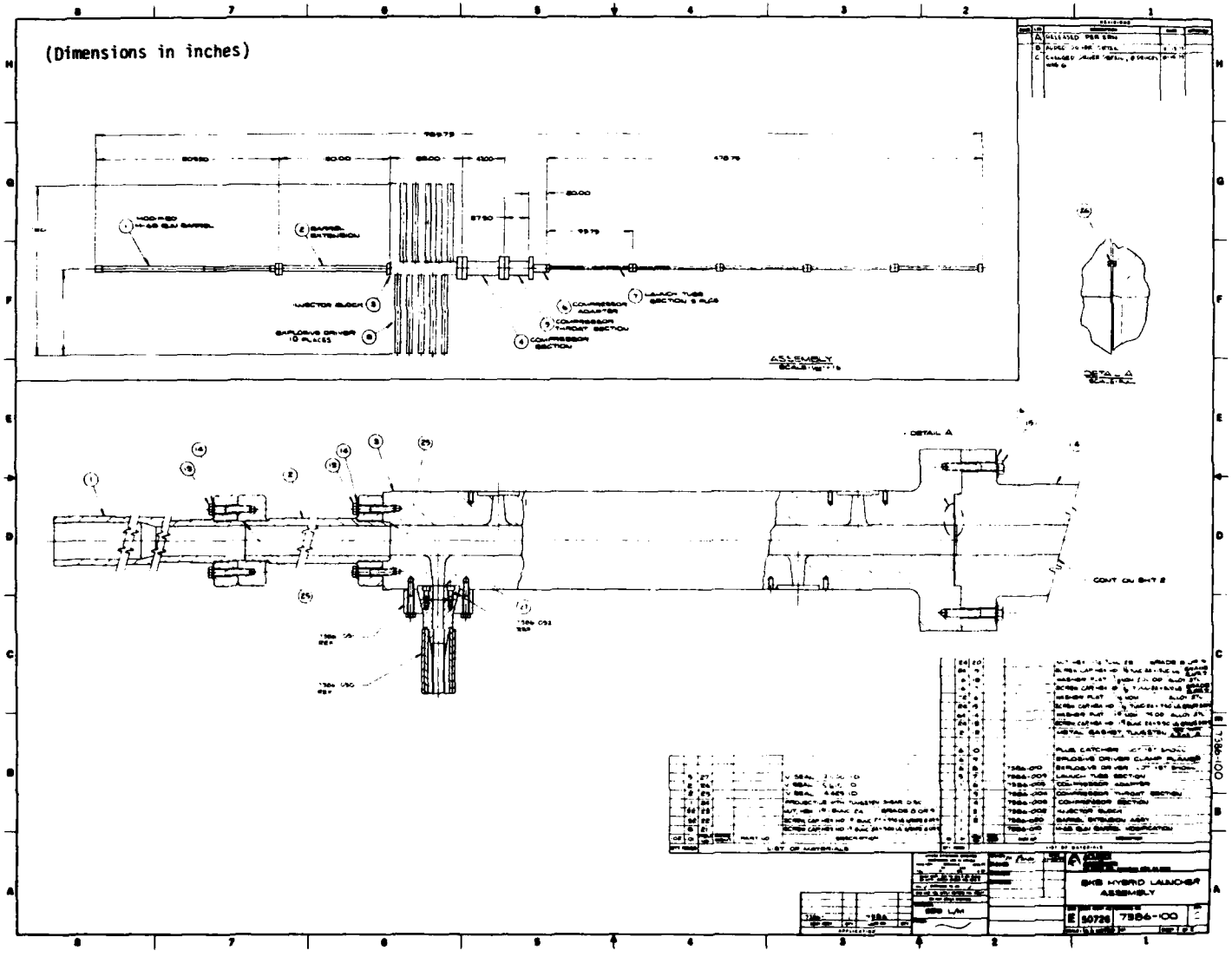

Figure 42. One and a quarter-inch bore (1/4-scale) hybrid launcher assembly drawing (March 1979).

TABLE 8. LAUNCHER FABRICATION STATUS

Name	Present Fabrication Status	Fabrication Remaining to Complete
Injection block	Partially machined and heat treated	• 8 additional ports • Sealing grooves • Bolt patterns for coupling with adjacent gun components • May require annealing prior to finish machining, followed by a new heat-treat cycle
Compressor section	Partially machined	• Central bore • Bolt pattern for coupling with injection block • Sealing grooves • Heat treatment
Compressor throat and insert	Compressor throat partially machined, insert machined and CVD W-liner added, but liner not adequate	• New insert on which to CVD W-liner • Sealing grooves • Bolt patterns • Heat treatment
Compressor to launch tube adaptor and insert	Tube partially machined, insert machined and CVD W-liner added, but insert was used as launch tube in I-2	• New insert • Bolt patterns • Sealing grooves • Heat treatment
Launch tube casings and flanges	For the casings: • 5 casings trepanned and electroless nickel plated • One of the 5 has had CVD W-liner deposited and has been cut in sections for testing For the flanges: all flange machining complete	For the casings: • Trepan new casing to replace sectioned tube • Strip electroless nickel and replace with electrolytic nickel • CVD • Thread ends to accommodate flanges For the flanges: heat treat

TABLE 8. Concluded

Name	Present Fabrication Status	Fabrication Remaining to Complete
First-stage barrel assembly	• M68 honed to final ID • Propellant exhaust vents welded shut • Flange machined	• Inspect weld -- improper weld may crack gun steel • Heat treat flange
First-stage barrel extension, flanges, and tube	• Flanges machined • Partial machining of tube	• Thread tube for flanges • Add vent to tube for flushing launcher with H_2 prior to each shot • Heat treat tube and flanges
Driver assembly	• Partial fabrication of drivers using old design • 6 coupling rings complete	• Make all drivers from scratch using new design • 10 new coupling rings and heat treat • New diaphragm ring for each driver

The injection block itself has had additional machining (since the I-1 test) to prepare it for the I-5 test. It will require final machining to add eight more injection ports and to add the bolt patterns necessary to couple it with adjacent gun sections.

5.2 GUN MOUNTS

During the spring of 1979, work began on the gun mount design. A fixed-mount system was used. The overall layout of the gun mount is shown in Figure 43. All components are rigidly fixed to a central steel I-beam which is anchored into a concrete foundation. First stage recoil imparts loads approaching a million pounds, requiring the heavy structures shown in the figure.

The injection block and compression section are the only components with fixed orientation. Mounts for all other components have adequate provision for adjustments in three dimensions. The ranges of adjustments and movements are sufficient to allow moderately rapid disassembly for inspection and model placement. Weldments are provided to support most of the components so that they can be rolled away from the launcher centerline for inspection and refurbishment.

The gun mount component drawings were completed and reviewed with the major fabricator (Caral, Inc.) in March 1979. Based on this review, a number of modifications were identified which will significantly reduce costs. These changes have been incorporated into "red lined" drawings of the original mount design. When design activities are resumed, the mount component designs will be revised and will reflect these changes. An additional design review will be made at that time, involving more fabricators to define any final cost saving changes before issuing a purchase order for their fabrication.

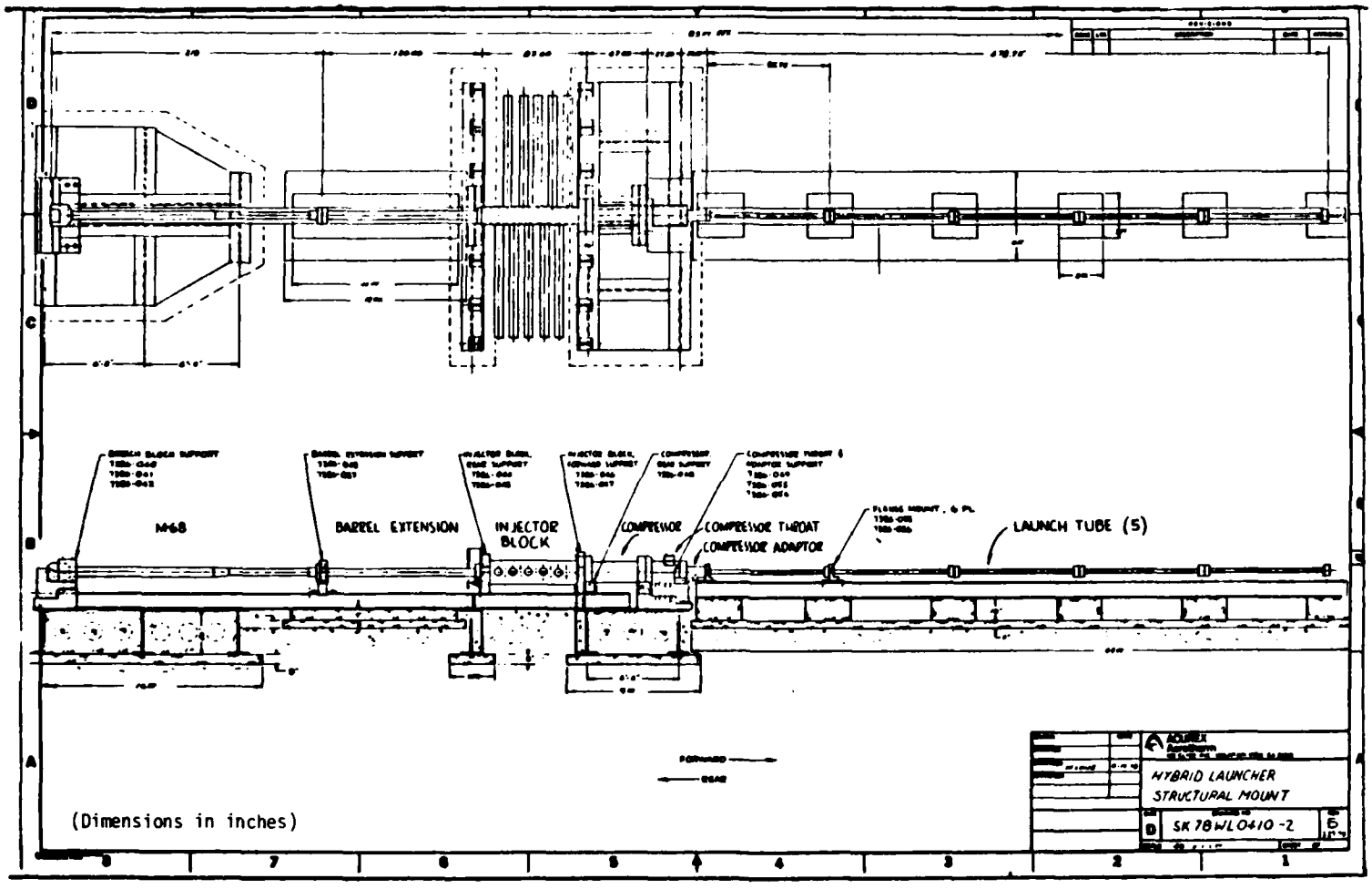

Figure 43. Launcher mount layout.

SECTION 6
SUMMARY AND CONCLUSIONS

The final design of a two-stage hybrid launcher for the soft launching of high-" models at 6.1 km/sec (20,000 ft/sec) has been completed. The launcher represents a 1/4-scale proof-of-concept of a launcher for the soft launch* of 5.50-kg (12-pound), 10.2-cm (4-inch) diameter models at 6.1 km/sec (20,000 ft/sec).

Major issues addressed during the current program effort were:

- Critical analysis and redesign of a preliminary design (reported in Reference 2) based on static structural requirements, costs, and fabrication limitations
- Testing of key components of redesigned components of the gun, including explosive drivers, diaphragms, injection block, and launch tube thermal liners
- Analysis, redesign, and further testing of these components to develop needed performance improvement

The primary design changes resulting from these component testing and analysis efforts were the following:

- Drivers
  - -- Tampers were increased to prevent overexpansion of the pressure tubes and sphincter
  - -- Sphincter/pressure tube assemblies were modified to eliminate debris in the injection gas
  - -- Pressure tubes were normalized to improve their allowable expansion during driver operation
  - -- Dimensions of the original driver design were reduced to lower driver termination loads on the injection block

---

*The model base pressure is to be maintained below 5 kbar.

- Diaphragms
  - -- Mylar diaphragms proved to be the best and simplest system of sealing drivers
- Injection block
  - -- Injection ports had to be flared to prevent pressure-formed craters in the bore wall
  - -- The hardness had to be reduced to improve material toughness
  - -- The port design had to be changed to allow more, but smaller, drivers and to minimize stress concentrations at the bore-port intersection
- Launch tube thermal liners
  - -- A monolithic launch tube/tungsten liner design was developed which meets thermal, mechanical, and fabrication requirements
  - -- Liners to be a CVD tungsten layer honed to proper ID
  - -- Tungsten to be deposited on electrolytic nickel which itself is plated onto the launch tube bore walls
  - -- Simple flat-plate tests have identified the optimum liner/launch tube bonding conditions

These changes were identified as necessary for a successful hybrid launcher design. The completion of the component tests during the reporting period verified that the final redesign configurations of these components are adequate. The components tested represent the major items of uncertainty prior to August 1977.

The following items remain to be completed before the hybrid cycle can be considered verified:

- Complete fabrication of remaining gun parts
- Review gun mount design and initiate fabrication
- Complete construction of gun mount pads
- Design and fabricate a vent system to reduce piston rebound in the first stage
- Perform first-stage (M68) test to define piston velocity as a function of propellant load (and check M68 mounts)
- Install launcher on mounts and test fire second stage to begin performance workup tests (and check gun mounts and thermal liner integrity)

- Connect first and second stages and begin test matrix to identify optimum piston velocity and mass
- Analyze performance and determine launcher efficiency

REFERENCES

1. Seifert, K., "Hypervelocity Launcher Design," PIFR-708, Final Report prepared for DNA by Physics International Company, May, 1976, DNA 3869F.

2. Cohen, L. M., et al., "Feasibility of a Hybrid Hypervelocity Launcher," Aerotherm Final Report TR-77-238, January 1977, DNA Report 4226F.

3. Dahm, T. J., and Watson, J. D., "Analysis and Design of a Two-Stage Hybrid Launcher," Aerotherm Report TR-77-245, May 1977, DNA Report 4334F.

4. Anderson, A. D., and Dahm, T. J., "Boundary Layer Closure and Heat Transfer in Constant Base Pressure and Simple Wave Guns," Transactions of the ASME Journal of Heat Transfer, Vol. 100, November 1978.

5. Hofmann, R., "STEALTH: A Lagrange Explicit Finite Difference Code for Solids, Structural and Thermohydraulic Analysis," EPRI Technical Report NP-176, Project 307, June 1976.

6. Canning, T. N., et al., "Ballistic Range Technology," AGARD-AG-138-70, Chapter 2.

7. Trimble, M. H., et al., "AEDC High-Temperature Testing Capabilities," AEDC-TR-78-3, April 1978.

APPENDIX A
HYBRID LAUNCHER DEVELOPMENT SUPPORTING ANALYSES

Throughout development of the hybrid launcher, a large number of background calculations were made to select the optimum launch cycle and configuration (Reference 2), to size and design gun components, and to analyze component testing results. This appendix is a brief summary of some of the key analyses made during the period of September 1977 to March 1979. The analysis of the injection block structural failure which led to the final injection block design is emphasized.

A.1 COMPONENT SIZING

Immediately upon resumption of work on the launcher, the components of the Reference 3 design (shown in Figure 17) were sized based on a static analysis. The peak pressure loads predicted for each component in the Reference 3 design effort were applied to the respective components as static loads. Thick wall pressure vessel formulas were applied to size components. In addition, the size of bolt circles and bolt diameters were re-examined to determine their ability to withstand both their respective pressure loads and a $8.9*10^{11}$ dynes (2 million-lb_f) thrust generated in the first stage during firing. Based on these calculations, a number of components were "beefed-up" as described in Section 5.1. The peak loads, materials, yields strengths, and safety factors assumed in the design of each component are summarized in Table 9.

A.2 HYDROGEN EQUATION-OF-STATE

The extreme pressures experienced in the hybrid launcher make it necessary to use an accurate equation-of-state for hydrogen. This is especially important for accurate gas dynamics calculations. The equation-of-state must account for:

- Intermolecular attraction
- Molecular covolume effects
- Dissociation of H_2 to H

TABLE 9. COMPONENT SIZING PARAMETERS

Component	Material	Yield Strength[a] (kbar)	Safety Factor[b]	Maximum Pressure Load (kbar)
Barrel extension	4340	9.3	1.4	3.5
Injection block	4340	9.3	1.4	8
Compressor	4340	9.3	1.4	8
Compressor throat and insert	4340/17-4 ph	9.3	1.4	8
Compressor to launch tube adaptor and insert	4340/17-4 ph	9.3	1.4	6.5
Launch tubes	17-4 ph	8.6	1.1	6.5
Bolts and flanges	--	--	1.25	Sized for maximum pressure and for $8.9*10^{11}$ dynes (2 million-lb_f) thrust (as appropriate)

[a]Yield strength may be modified slightly to improve material toughness.
[b]Based on yield strength.

Such an equation was developed for use in hybrid launcher analyses (Reference 3). The equation consists of a Van der Waals equation with adjustments to account for dissociation. This equation is:

$$p = \rho RT \left\{ 2\alpha + (1-\alpha) \left[\frac{1}{1-(1-\alpha)\rho b} - \frac{a(1-\alpha)\rho}{RT} \right] \right\} \qquad (1)$$

where:

T = temperature

α = degree of dissociation

a = intermolecular attraction parameter

b = molecular covolume parameter

R = gas constant per gram for molecular hydrogen

The degree of dissociation is predicted from free energy considerations.

In all previous studies of the hybrid launcher, the parameters (a) and (b) were evaluated from hydrogen critical point data. An equation-of-state based on a covolume parameter (b) calculated from critical point data is not necessarily accurate at the high-temperature, high-pressure conditions occurring in the hybrid launcher. Therefore, a better value of b was inferred from driver shock data. These data indicated that the covolume parameter (b) had to be reduced by 25 percent from the value (11.52 gm/cc) used (Reference 3) (to 8.64 gm/cc) in order to predict the measured shock velocity from the initial driver gas temperature and pressure and the measured nitromethane detonation velocity.

This new value of the covolume parameter was used in all gas dynamics calculations made since the first driver test (D-1).

A.3 DRIVER GAS STAGNATION PRESSURE

As noted in the I-1 post-test description (Section 2.3.1), a large crater was observed in the test injection block bore opposite each injection port. It was speculated that these craters were generated by the high stagnation pressures occurring during driver gas injection.

Calculations were made to estimate the pressure adjacent to the bore wall using the 1-D version of STEALTH* (Reference 1) to verify that

---

*The hydrogen equation-of-state described in Section A.2 was incorporated into the STEALTH code prior to these calculations.

the craters were indeed the result of pressure forming. This version can be used on 1-D hydrodynamic flow calculations, allowing for relative area changes in the streamwise direction. The analyses considered the slug of gas behind the shock wave from the time the shock first reached the diaphragm location until the time it impacted the bore and eventually reached a maximum stagnation pressure at the wall. To approximate the relative area change upon entering the injection block bore, radial zone boundaries were allowed to expand at a rate of 10 percent of the zone sound speed in the bore region. While this is a crude approximation of the effect of blowoff, it was still possible to make reasonable estimates of the bore wall pressure history. The computational model is illustrated in Figure 44.

The results of this computation indicate that pressures of 18.3 kbar (265 ksi) and higher are possible with the I-1 test configuration. From these calculations, it was concluded that pressure forming was indeed responsible for the craters observed in the soft I-1 mild steel injection block. Furthermore, these calculations revealed that even if the I-1 injection block had been a high strength steel such as 4340 (which was selected for the actual 1/4-scale injection block), pressure forming would still have occurred.

Additional calculations were made to select a port configuration which would reduce the stagnation pressures to below 10.3 kbar (150 ksi). These calculations suggested that increasing the injection port diameter to 4 inches by flaring the injection port could lower the stagnation pressures to approximately 9.3 kbar (135 ksi), which is in the yield strength range of 4340. This design, shown in Figure 45, was selected as the new driver port design.* In later tests using 4340, minor pressure forming has been detected in those tests where the 4340 yield strength was under 8.6 kbar (125 ksi), supporting the analysis conclusions.

---

*The 4-inch dimension at the bore entrance was scaled down when the driver size was changed in I-3, I-4, and I-5.

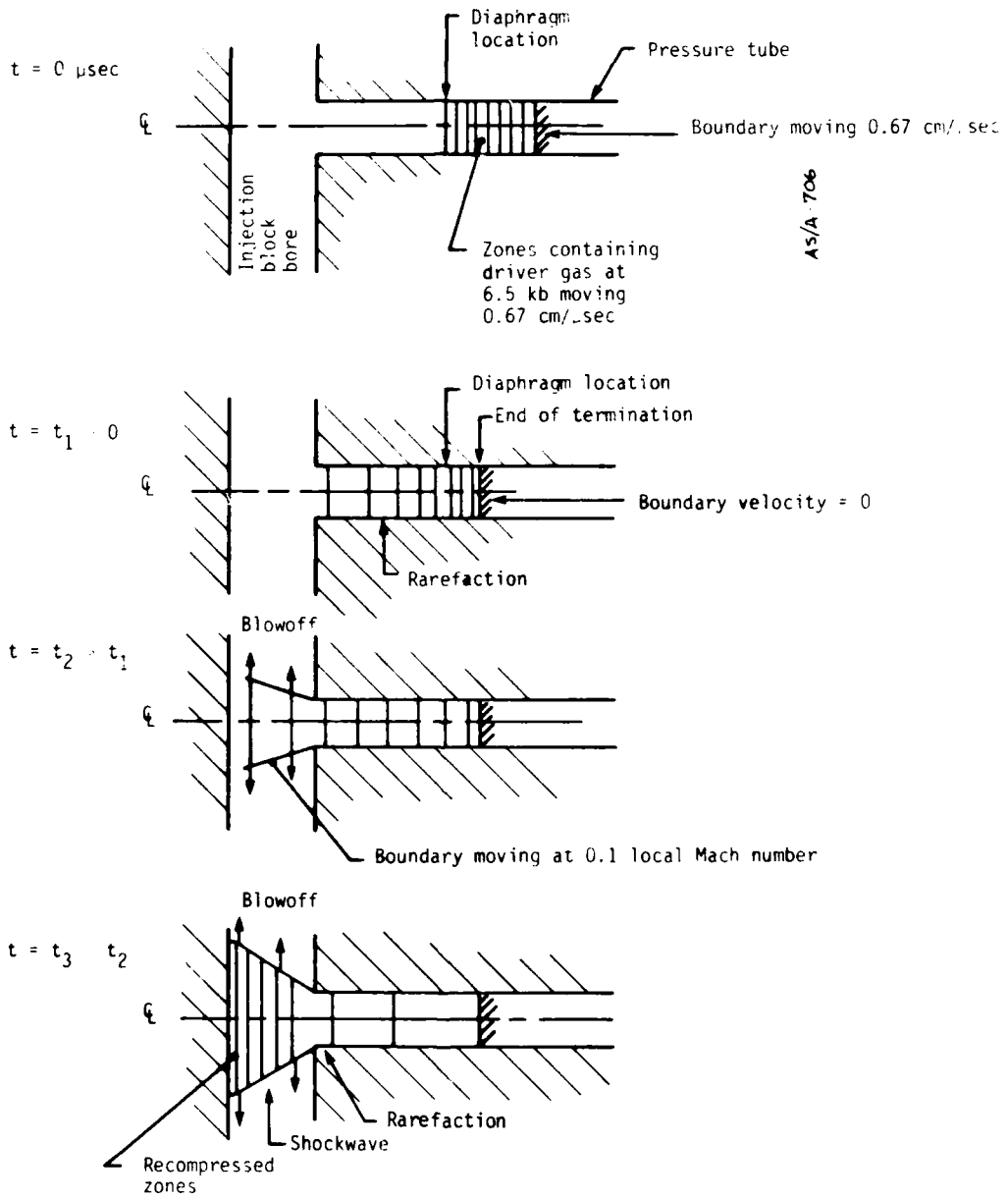

Figure 44. Schematic of STEALTH model of I-1 injection test.

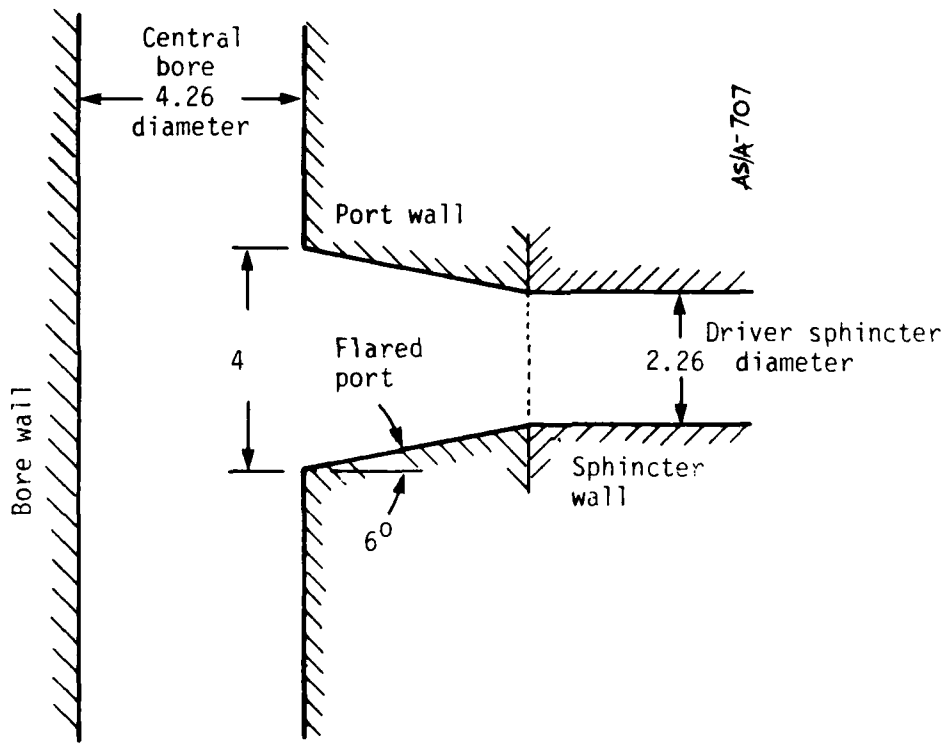

(Dimensions in inches)

Figure 35. I-2 test configuration.

A.4 TEST PROJECTILE LAUNCH CYCLE

Tests I-2, I-3, I-4, and I-5 used short launch tubes loaded with teflon projectiles to monitor internal pressures. These pressures themselves answer an important question in that they reveal the fraction of the driver gas injected into the injection block. The exit velocity of these projectiles is related to their base pressure by:

$$V = \frac{A}{m} \int_{o}^{t_{exit}} P \, dt \tag{2}$$

or:

$$\frac{V^2}{2} = \frac{A}{m} \int_{o}^{L} P \, dx \tag{3}$$

where:

V = exit velocity

A = base area of projectile

m = projectile mass

P = base pressure

t = time

x = distance along launch tube

L = distance traveled to exit launch tube

As an estimate of the velocity, the equilibrium pressure (for 100-percent hydrogen injection) was assumed as the base pressure in Equation (3). These pressures predicted the projectile exit velocity to within 5 percent for all tests (except I-2 where the exit velocity was overpredicted by 15 percent). Based on this simple analysis, it could be concluded that nearly 100 percent of the driver gas was injected in I-3, I-4, and I-5.

To determine more accurately whether these measured velocities truly indicated that nearly 100 percent of the hydrogen was being injected, 1-D STEALTH solutions with area changes were run for the I-2 and I-3 launch cycle. In these runs, 100 percent of the driver gas was assumed to be injected into the bore as a central high-pressure fireball. The internal energy of this fireball was equal to the total energy of the gas ejected by the driver(s). The pressure of the initial fireball was assumed to be the bulk pressure of the gas predicted in the Section A.3

injection calculations (at a time when nearly all the driver gas had been injected). Figure 46 illustrates this model for the I-2 analysis. The projectile base pressure predicted for I-2 by STEALTH is compared with the equilibrium pressure in Figure 47. Figure 47 illustrates that the equilibrium pressure is a good time-averaged estimate of the base pressure. The peak pressure predicted for the base pressure 6.6 kbar (95 ksi) is in fair agreement with the pressure transducer indications. The STEALTH predicted I-2 projectile exit velocity is close to that predicted using the equilibrium pressure. Figure 48 compares the projectile velocity predictions as a function of time. Both of these predictions are approximately 15 percent higher than the measured velocity.

Similar calculations were performed for I-3, however, the STEALTH prediction and equilibrium pressure predictions were 2 percent lower than the observed exit velocity. The I-4 prediction using the equilibrium pressure was 5 percent lower than observed, while I-5 velocity was exactly as predicted.

A.5 I-2 FAILURE STRUCTURAL ANALYSIS

The I-2 failure analysis represents the most important set of calculations performed during the development period covered by this report. As noted in Section 2.3.3, the I-2 failure revealed the necessity for design changes to the injection block. Resolution of the mechanism which caused the I-2 failure was required to define what these changes must be.

As noted earlier in Section 2.3.3, four hypotheses were set forth as causes of the failure: These were:

- Poor material properties
- Injection gas loads or subsequent equilibrium pressure loads
- Driver termination loading
- A combination of two or more of the above

A detailed analysis effort followed the I-2 test to deduce which of these hypotheses is correct and to determine what design changes would prevent injection block failure. The results of these analyses follow. The results of the metallurgical study are reported in Appendix B. These results indicated that the I-2 forging was of substandard quality and that it had been overhardened (i.e., low toughness). The metallurgical data indicate hypothesis 3 to be a contributing factor to the I-2 failure.

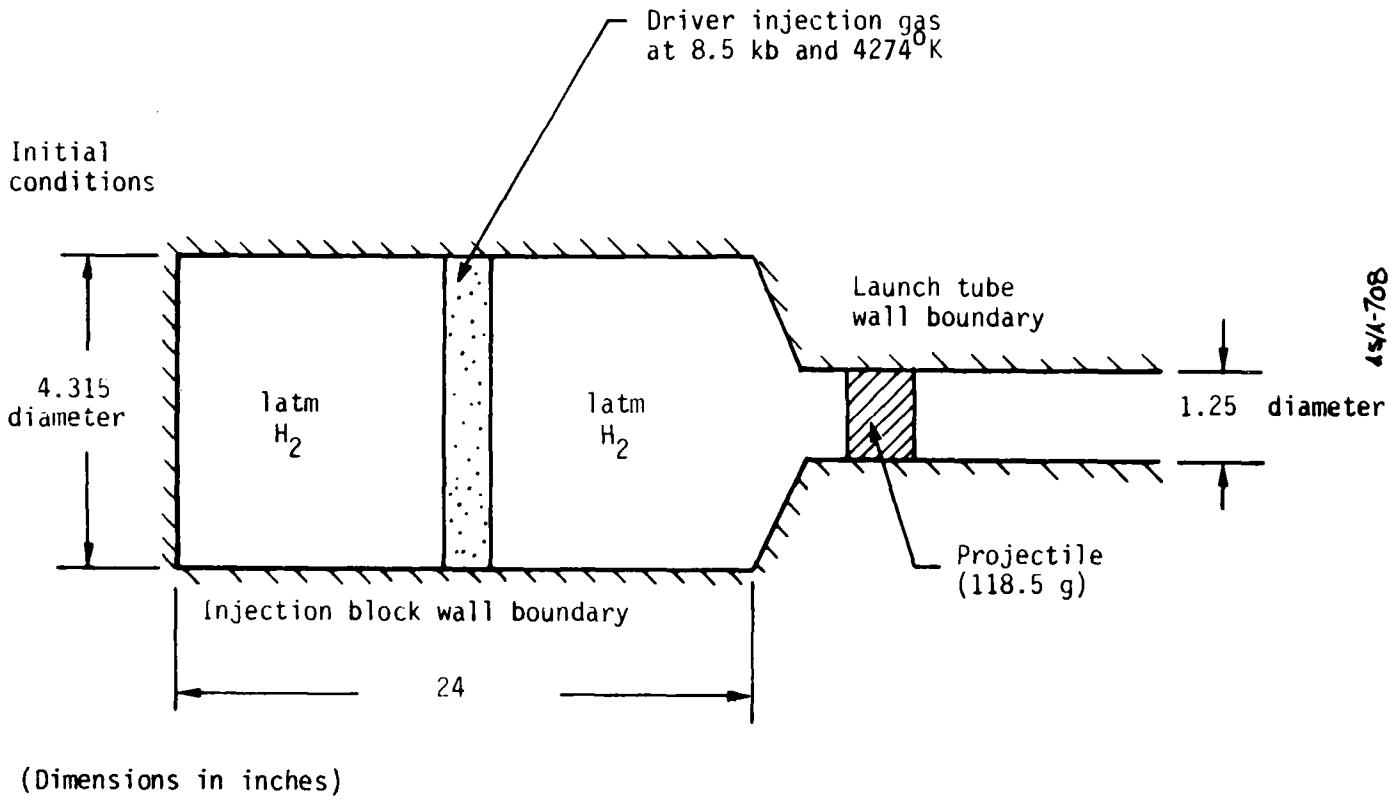

Figure 46. STEALTH model of I-2 launch cycle/pressure history.

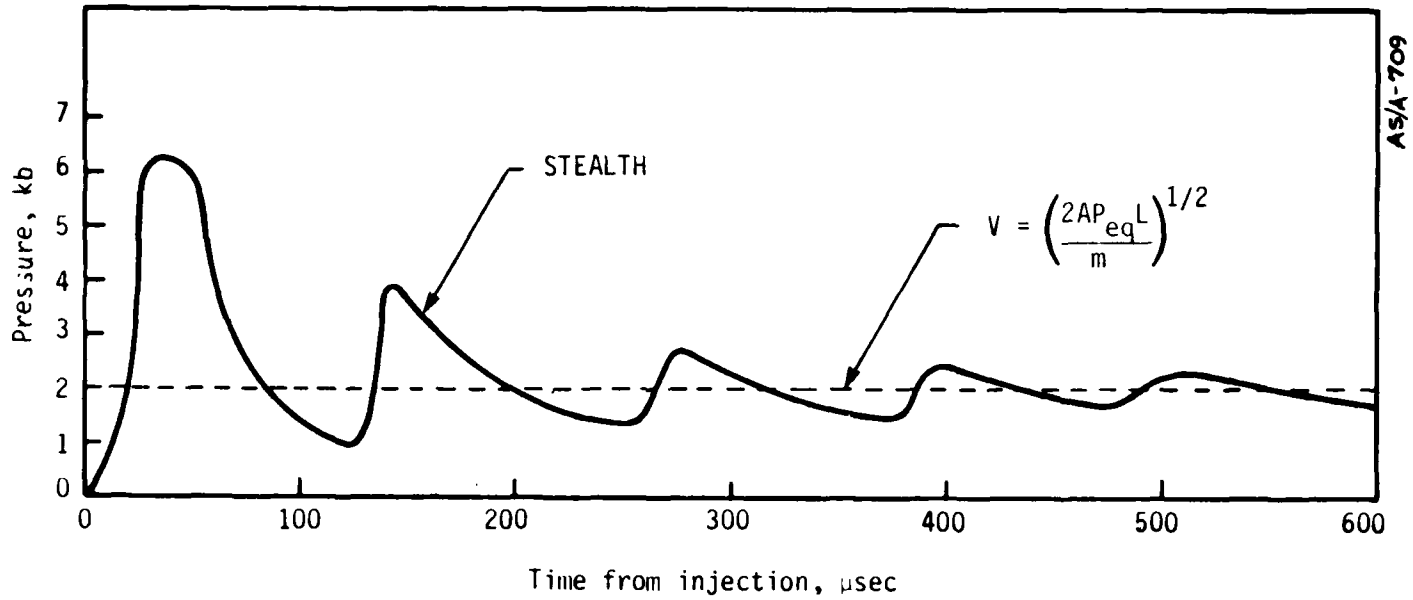

Figure 47. Pressure history at base of I-2 projectile.

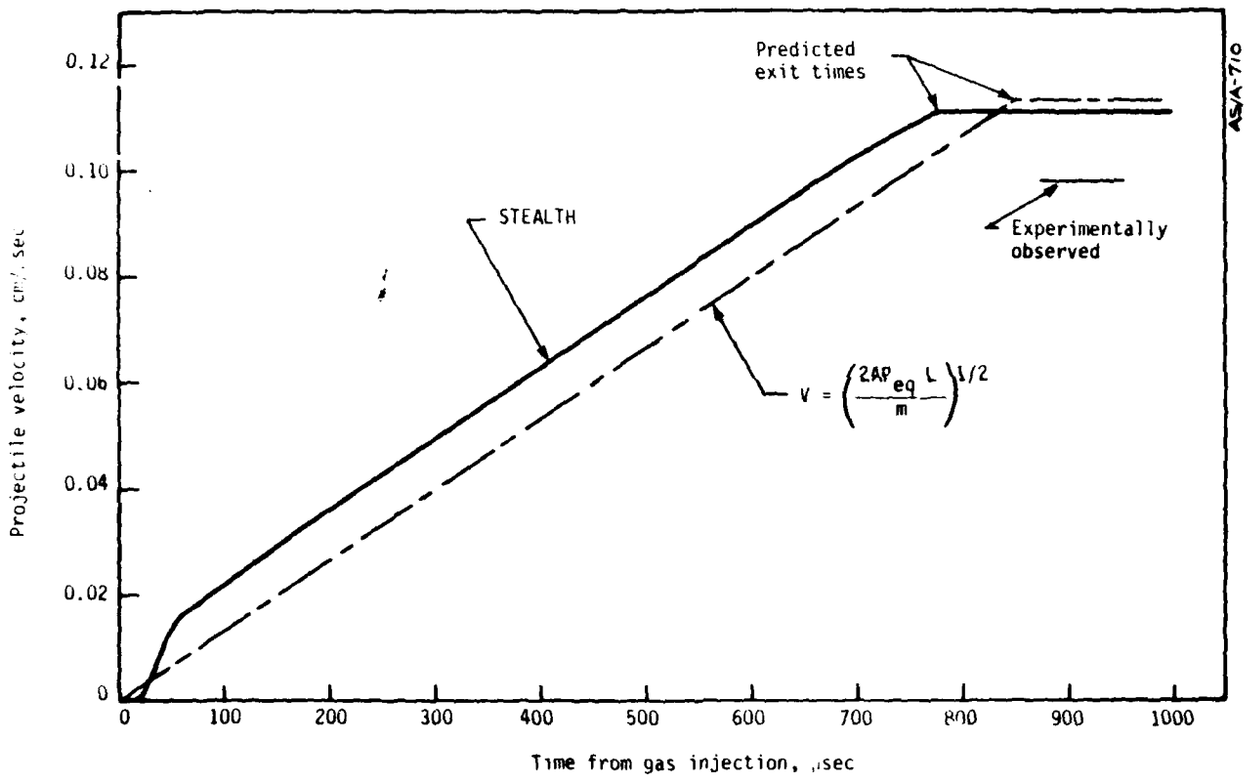

Figure 48. I-2 projectile launch cycle velocity history.

Pressure Vessel Computations. The first step in the failure analysis was to verify the I-2 injection block as a sound pressure vessel for holding the equilibrium 2-kbar (29-ksi) pressure. Thick wall formulas predict hoop stresses in I-2 to approach 2.2 kbar (32 ksi). Textbook formulas indicate a 2.8 stress concentration factor at the intersection of the port with the bore, which infers a 6.2-kbar (90-ksi) hoop stress at this location. These are far below the 12.1-kbar (176-ksi) yield strength measured in the circumferential direction.

As an additional check on the injection block pressure vessel design, a static 3-D finite element analysis was performed on the I-2 design. The grid used to describe the injection block is shown in Figure 49. Again an internal pressure was specified as 2-kbar (the equilibrium gas pressure). The results of this calculation are shown in Figure 50. The highest principle stress computed was 6.6 kbar (95 ksi) at the port/bore intersection in the plane of the observed failure. The solution suggests that this stress concentration can be reduced by machining a radius at the port/bore intersection.

Gas Impact Calculations. As described in Sections A.3 and A.4, a number of 1-D STEALTH calculations were made of the injection gas impact pressures and the subsequent pressure loads during the projectile launch cycle. These pressure histories were used to estimate the dynamic response. STEALTH 1-D was used for these calculations with the I-2 block modeled as a 1-D cylindrical ring pressure loaded at the interior surface. These calculations predicted hoop tensions developing opposite the injection port as high as 75 percent of the material yield strength. This estimate was considered to be high, since 3-D relief was not considered.

The calculation was repeated using a 2-D version of STEALTH. The model used is shown in Figure 51. In this calculation, the I-2 block was again modeled as a ring, but with only a small stagnation region impact by the stagnating gas. The results of this calculation are presented in Figure 52 for the bore wall opposite the injection port. These results show that with only 2-D relief, the hoop stress in the dynamic load situation is reduced to 1 kbar (14.5 ksi). Therefore, gas impact and subsequent internal pressure loads must be considered, at most, as secondary contributing loads.

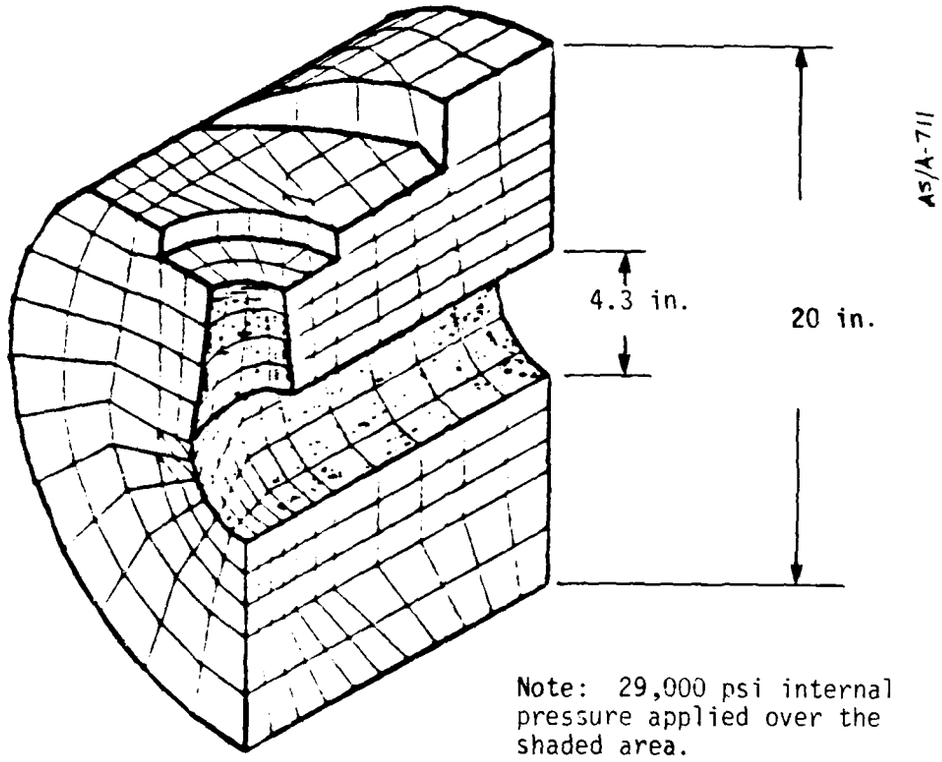

Figure 49. 3-D finite element grid.

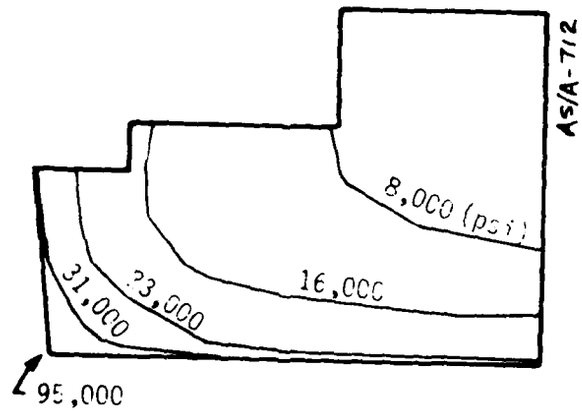

Figure 50. Stress contours on plane of symmetry of injection port and main bore.

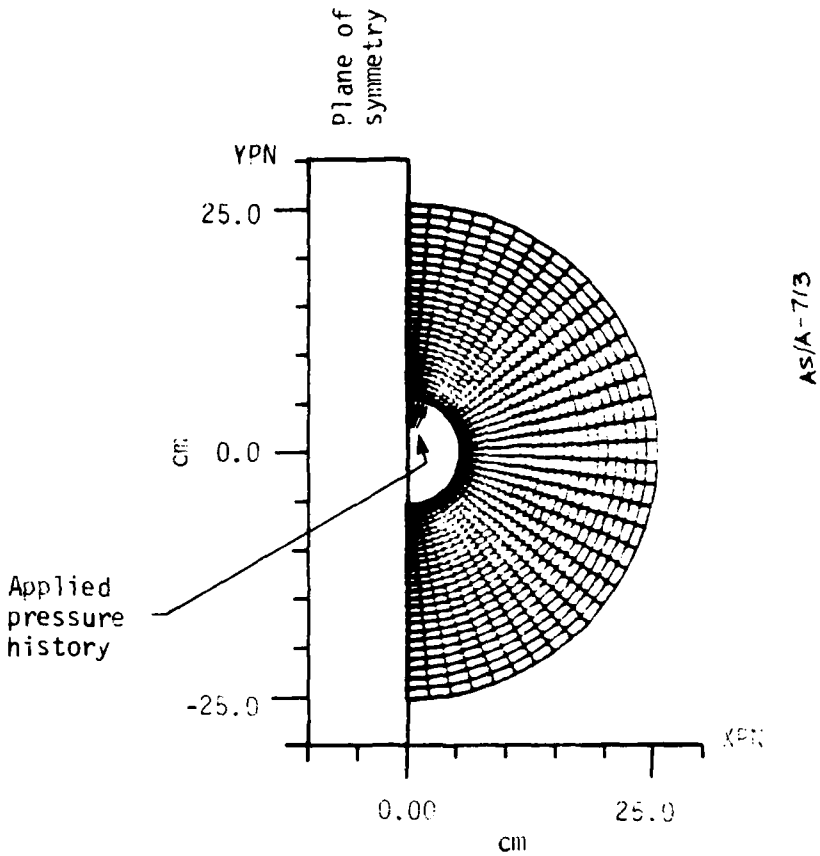

Figure 51. 2-D gas impact model.

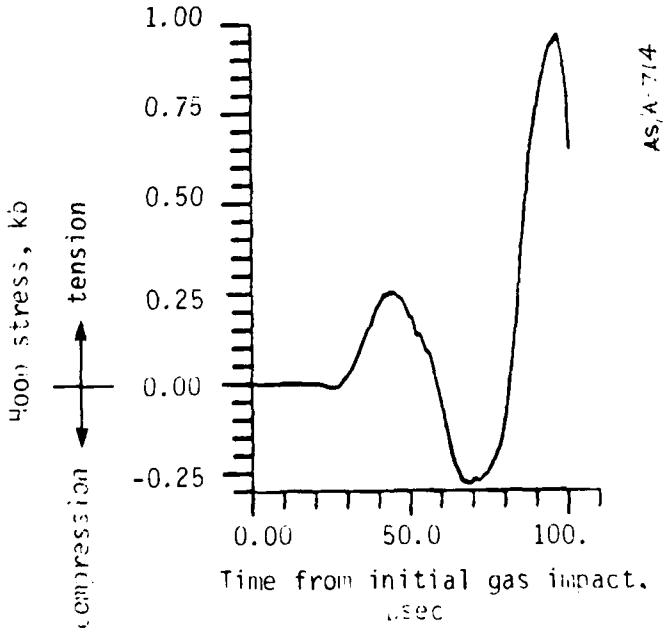

Figure 52. Main bore hoop stress opposite injection port.

Driver Termination Loads. A 2-D axisymmetric elastic-plastic finite difference calculation (using STEALTH) was made to determine the local effects of the driver termination process around the injection port. The model grid is shown in Figure 53. The injection port was selected as the axis of symmetry. The driver termination load was approximated by an exponential function initially at 70 kbar and decaying with an exponential time constant of -33 μsec^{-1}. The integrated momentum input to the grid is about $3*10^8$ dynes-sec (685 lb_f-sec) which is in accordance with the best estimate of driver termination momentum. This calculation neglects any very strong shock spikes because of grid zoning limitations. However, it is believed that such shock spikes would be diffused by the actual geometry of the driver termination process and would be smeared during passage through the mild steel of the termination section.

Analysis of the calculation reveals no harmful wave interactions (such as intersection of sharp shocks or rarefactions) and no regions of potential spall failure. However, the driver termination load tends to cave in the port area, and at approximately 100 μsec after initial loading, hoop* tensions of over 10 kbar are developed around the lower half of the port. The yield surface† of this region is pierced for about 20 μsec. This region is in the general proximity of the crack initiation point (based upon observations of fracture patterns).

Conclusion of the I-2 Analysis. Based on the I-2 analysis, it was concluded that:

- The driver termination load was the major contributing factor to the I-2 failure
- Other loads may have superimposed in a manner contributing to I-2 failure
- Poor material properties contributed to the I-2 failure, however, even with a much better forging and heat treatment (i.e., better toughness, etc.) the I-2 injection block would probably have failed

---

*Relative to port center line axis.

†The yield surface is defined by a Von Mises yield model with a material tensile yield strength of 200 ksi (13.8 kbar).

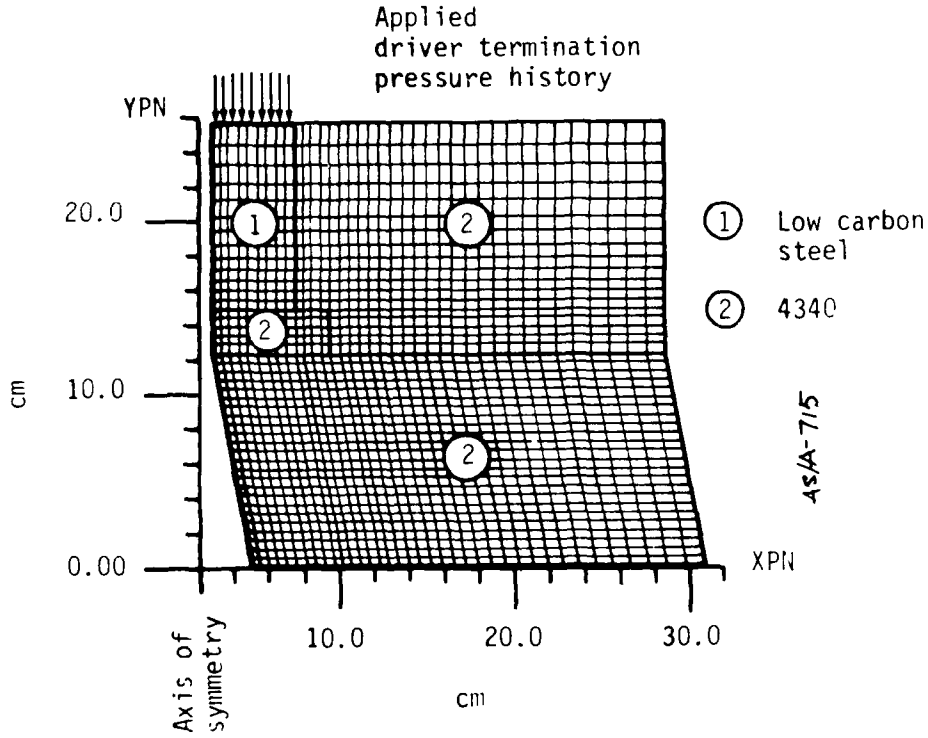

Figure 53. 2-D port model grid.

Continued analyses were made using the models developed in the I-2 failure analysis. Their primary purpose was to identify design modifications which would improve the injection block survivability. The conclusion of these analyses was that the most effective method to eliminate injection block failure was to reduce the driver size (i.e., use more, but smaller, drivers). In the calculation using smaller drivers, yielding in the bore region was eliminated. Other helpful design changes identified were:

- Increase distance between driver explosive and injection block face
- Increase contact area between driver and injection block
- Round the corner at the intersection of the port with the bore

Design changes based on these conclusions, along with a careful metallurgical program, were proven successful in the I-3, I-4, and I-5 injection block tests.

APPENDIX B
INJECTION BLOCK METALLURGY

This appendix summarizes much of the work and conclusions associated with the metallurgical analysis of injection block materials. Included is a description of why 4340 was selected for the injection block and 4340's properties, along with descriptions of the individual injection blocks used for tests I-2, I-3 (and I-4), and I-5.

B.1 BACKGROUND ON THE SELECTION OF 4340

Historically, 4340 steel has been used as a gun steel, as it combines good toughness and ductility with high strength and hardness. The alloy can be tailored to the desired degree of strength and hardness as a tradeoff for ductility and toughness. This is accomplished by heat treating as follows:

- The steel is austenitized (transformed to the austenite phase) by heating to approximately 843°C (1550°F), then cooling rapidly from the austenite phase by quenching in oil. This produces the martensite phase, which is hard and strong, in excess of 55 Rc and 19.3-kbar (280-ksi) yield strength, but with an elongation of less than 10 percent and Charpy impact strength below 6.8 Joules (5 ft-lb_f).
- The alloy is then tempered (i.e., heated to a temperature) generally in the range of 426°C to 649°C (800° to 1200°F), held at that temperature, then air cooled. This tempers the martensite and produces higher toughness and ductility with commensurate loss in hardness and strength. The specific tempering temperature is selected to produce the desired mechanical properties. For example, tempering at 538°C (1000°F) produces a yield strength of approximately 11.5 kbar (168 ksi) and 39 Rc with an elongation value of about 17 percent and a Charpy impact strength of approximately 47 Joules (35 ft-lb_f).

The above values are representative of bar stock. Thick sections exhibit somewhat lower strengths and hardness values.

The selection of 4340 steel is based on the fact that it is one of the most hardenable alloys available. This feature means that relatively thick sections can be hardened by transforming to martensite by cooling and quenching in oil. The more rapid water quench is not recommended, as it often results in cracking the steel as a result of the cooling stresses. In significantly thick sections, the center does not cool fast enough to transform to martensite, and, thus, the core of the material transforms to bainite, which is somewhat softer than martensite. In very thick sections, the cooling rate is not fast enough in the center to produce either martensite or bainite, so that some ferrite and pearlite are produced; these phases are considerably softer and weaker. To complicate matters, some residual untransformed austenite can remain on quenching 4340 steel, and this reverts to ferrite and pearlite when tempered. Techniques such as sub-zero quenching and double tempering are used to obviate this problem.

It must also be noted that the quoted mechanical properties are for the longitudinal direction in bar stock. Large forgings will not only have poorer values in the longitudinal direction, but will have significantly poorer values in the transverse direction, both radial and circumferential, especially with regard to ductility and toughness. This is because the structure of the metal is optimum in the longitudinal direction as a result of the "hot working" during the forging operation, producing elongated grains in the longitudinal direction with the resultant shortening of the grains in the transverse direction. The transverse strength of the grains may be increased by "hot upsetting" (pancaking) the forging, then reshaping the forging back to its original shape. The "hot working" in the transverse direction results in significantly improved transverse properties. The forging should also be homogenized (heated to 1038°C (1900°F)) and normalized (by cooling from 899° to 649°C (1650° to 1200°F) and slow cooling from 649°C (1200°F)) to remove any residual structure remaining from the as-cast condition. Localized differences in structure (and properties) are thus minimized. The degree of breaking down of the cast structure is a function of the amount of hot work introduced during forging. Ideally, a

reduction in excess of 10 to 1 is desirable in the forging process to remove all vestiges of the cast structure and the resulting brittleness.

One other factor of importance in the selection and processing of 4340 steel is the quality of the casting itself. The presence of inclusions may be very damaging to the properties of the final product. While hot working and especially hot upsetting help break up these inclusions, which tend to align in the longitudinal direction as long brittle stringers, their presence in significant numbers may cause the initiation and growth of cracks in the injector block. Consequently, 4340 relatively free of inclusions is obtained by specifying aircraft quality steel. Such steel is vacuum degassed and is relatively free of impurities. However, an air melted steel is not of as high a quality as a vacuum melted grade which can achieve very high toughness values at any given strength level.

B.2 I-2 INJECTION BLOCK

B.2.1 Summary

The I-2 injection block was made from a commercial grade 4340, 22-inch diameter forged round that was in stock locally. After the experiment, the material was tested for hardness distribution, yield and ultimate tensile strengths, elongation, and fracture toughness; was examined ultrasonically; and was etched for grain structure.

The near surface Rockwell hardness values were higher than specified (45 to 47 Rc versus 43 to 44 Rc). The material strengths in the three orthogonal directions were compatible with the measured hardness, but elongation and fracture toughness (measured by Charpy impact) were substantially lower than expected from the measured hardness. The etched specimens revealed that the dendritic cast structure was insufficiently broken down during forging, although the ultrasonic testing indicated good forging characteristics as opposed to casting characteristics.

The results of materials tests on the I-2 forging follow. The general picture that emerges is that of an injection block that had the required strength properties but inadequate elongation and fracture toughness.

B.2.2 Test Results

The resultant mechanical properties are listed in Table 10. Charpy values below 6.8 Joules (5 ft-lb_f) are completely unacceptable. Gun

TABLE 10. I-2 CHARPY IMPACT TESTS

Sample	ft-lb	Joules
Longitudinal	4.5	6.1
Longitudinal	4.0	5.4
Longitudinal	3.5	4.7
Short transverse	4.5	6.1
Short transverse	4.0	5.4
Short transverse	3.0	4.1
Transverse	3.5	4.7
Transverse	3.0	4.1
Transverse	3.0	4.1

steels are generally approximately 20.3 Joules (15 ft-lb) in impact strength. The critical flow size at this impact strength level for loads on the order of 10 kbar is only 0.009 inch. Inclusions significantly larger than this (up to 0.050 inch) may be expected in the material of this injection block. The analysis of the driver termination loads (Appendix A) projected that loads were in excess of 10 kbar. Consequently, the critical flow size was exceeded, and uncontrolled crack growth took place well below the maximum possible load. By contrast, a vacuum cast grade optimally heat treated has a critical crack size of about 7.1 mm (0.28 inch) (for a 10-kbar load) well above the size of anticipated inclusions.

Metallography was conducted on a sample of the I-2 test injection block material. This indicated a pronounced dendritic (cast) structure with an imperceptible grain flow. The conclusion was drawn that the forging was insufficiently hot worked, and that the forging reduction was very minimal, probably on the order of 4 to 1.

Additional mechanical tests were performed to determine the tensile properties of the I-2 injection block. These properties are listed in Table 11. It may be observed that the strength values are quite high and that the ductility in the transverse directions is quite low.

TABLE 11. TENSILE TESTS

	Longitudinal	Short Transverse	Transverse
Yield strength (lb /in^2)[a]	205500	176250	203330
Tensile strength (lb /in^2)[a]	233050	203330	230830
Elongation in 1.4 inches	0.14	0.06	0.06
Elongation, percent	10.0	4.3	4.3
Reduction of area, percent	36.8	12.5	13.5
Fracture	Cup and cone	brittle	Cup and cone

[a]bar = 14.5 lb_f/in^2

A hardness traverse was made on a fragment of the I-2 injection block. This fragment was broken loose during the test failure from one end of the block. Hardness data from this traverse are shown in a sketch of the sectioned fragment in Figure 54. The figure shows a large drop in the hardness with distance from the OD dropping from 47.5 to 39 Rc. Figures 55 through 58 compare test data for the I-2 injection block with AISI data of nominal 4340 variations of hardness with temper temperature, and variations of tensile strength, elongation, and impact strength with hardness. These nominal values represent values to be expected in the optimum direction. Indictions from Figure 55 are that the hardness range observed is somewhat low for the 371°C (700°F) temper, but that is to be expected for large forgings with thick sections which do not quench rapidly. Figure 56 indicates that the material in I-2 does follow the 4340 strength-hardness relationship. However, Figures 57 and 58 indicate that the ductility and impact strength were significantly substandard.

6.2.3 Conclusions

I-2 was poorly forged and was not tempered at a sufficiently high temperature to produce a relatively ductile material. Instead, the material proved to be excessively brittle, failing by catastrophic crack extension.

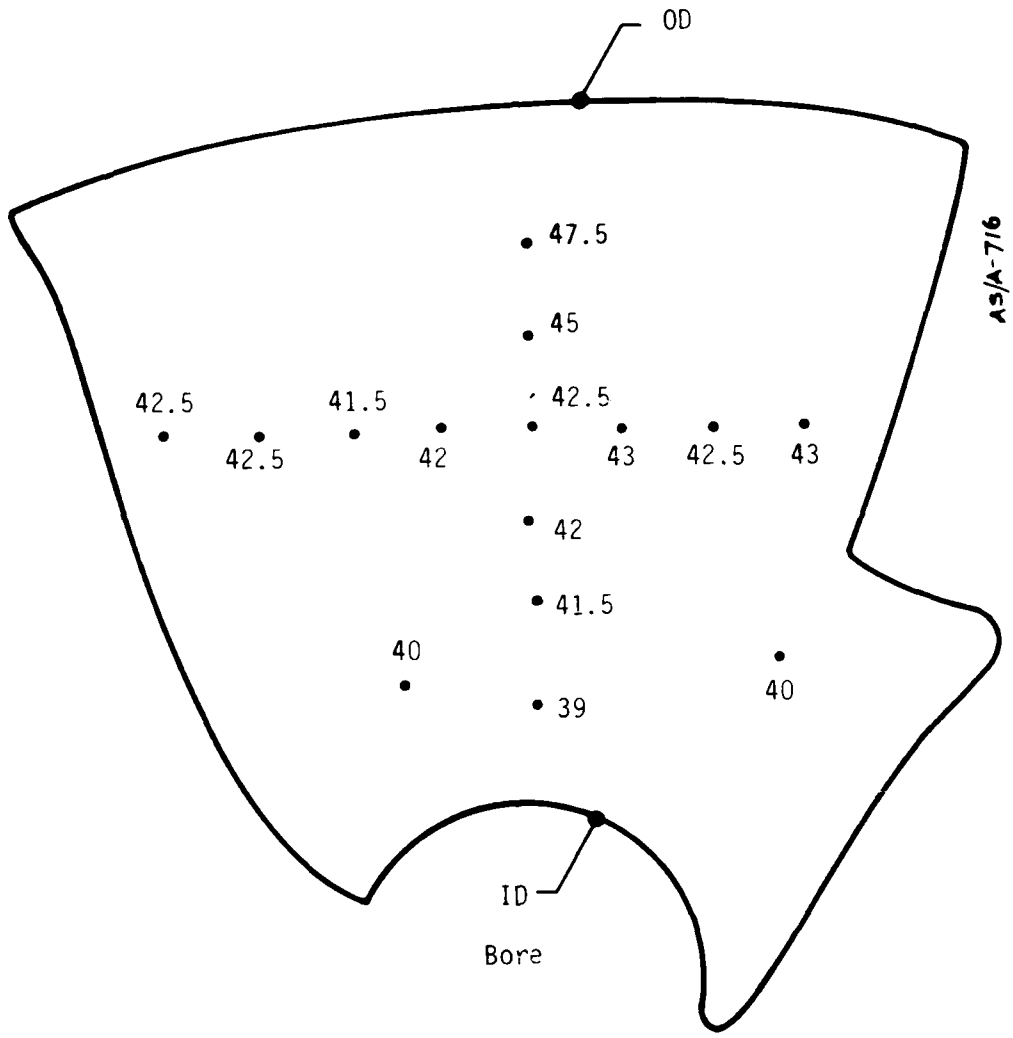

Figure 54. Rockwell C hardness measured on plane about 2 inches from end of injector block.

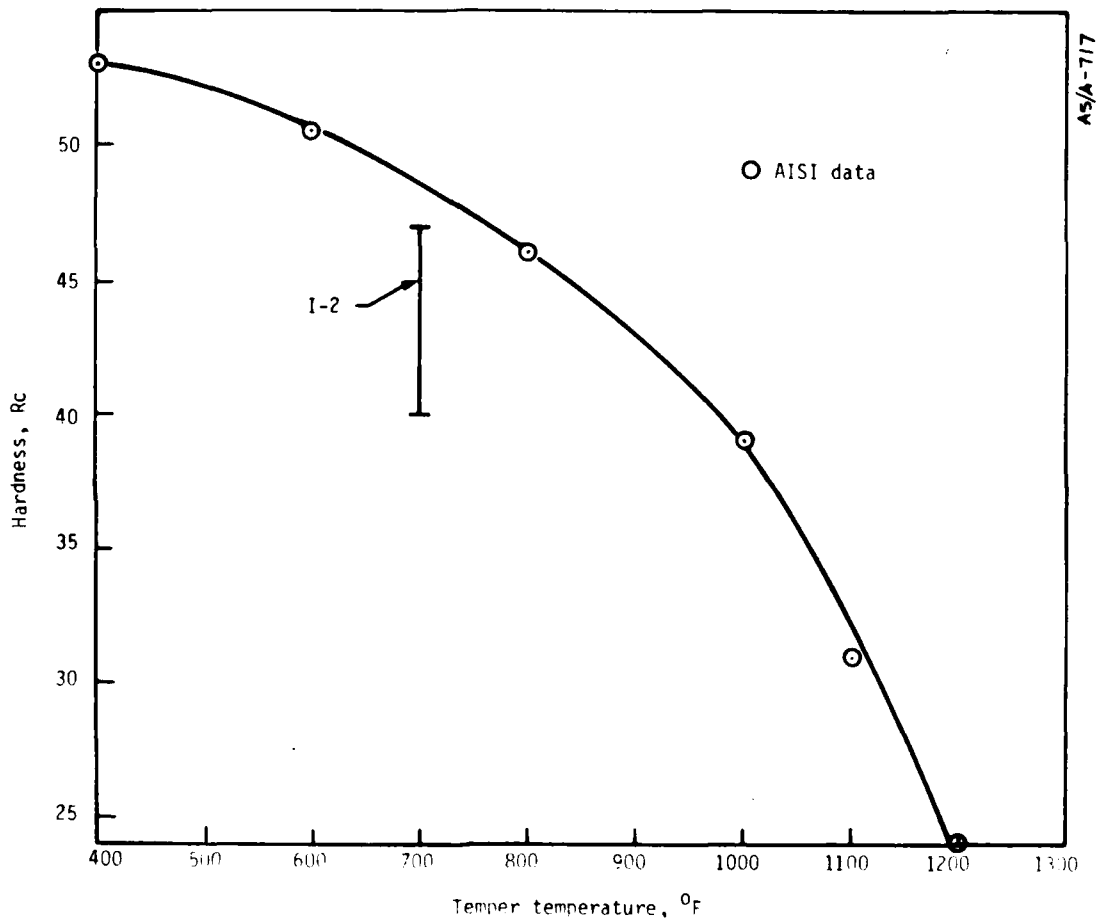

Figure 55. 4340 hardness versus tempering temperature.

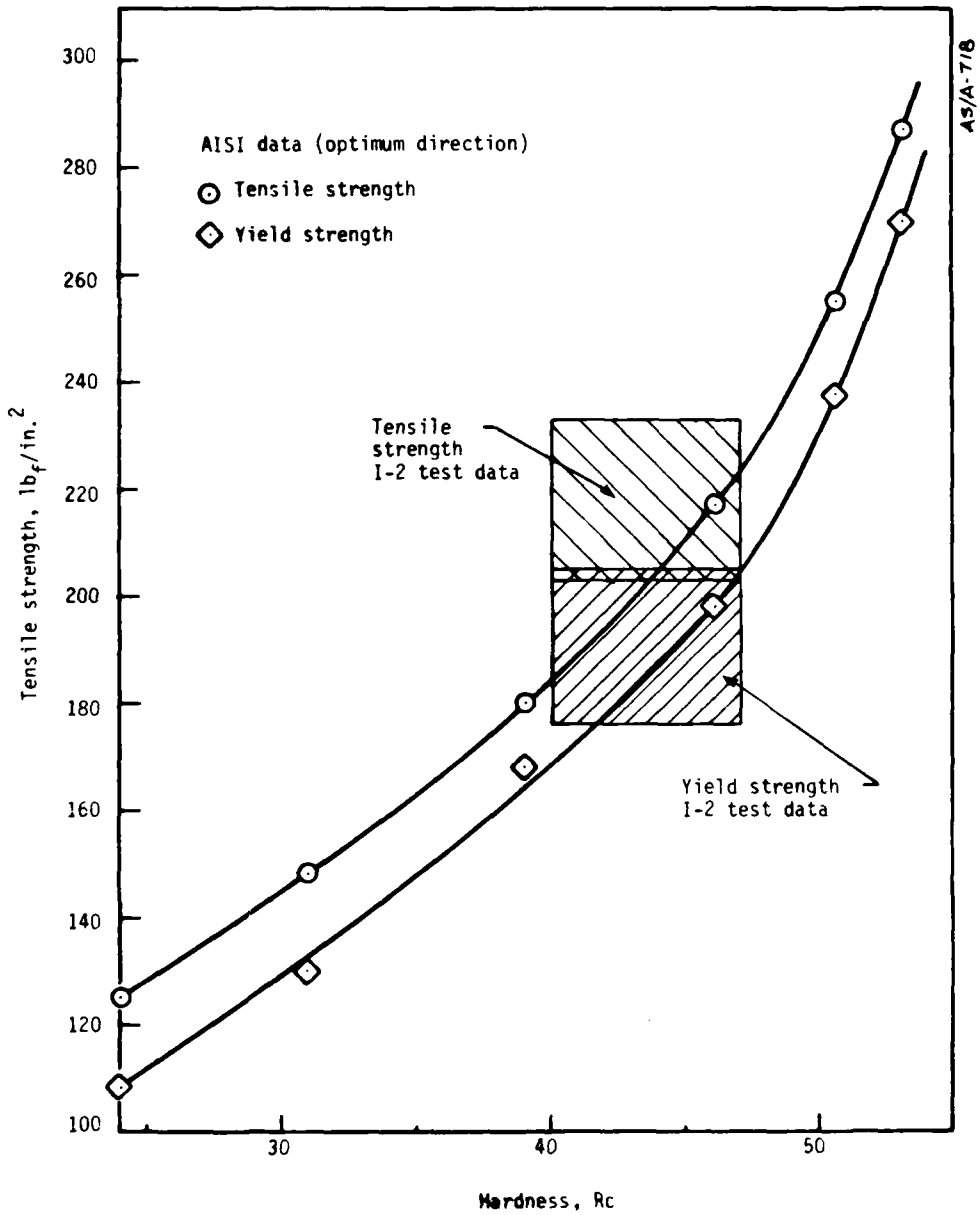

Figure 56. 4340 tensile and yield strength versus hardness.

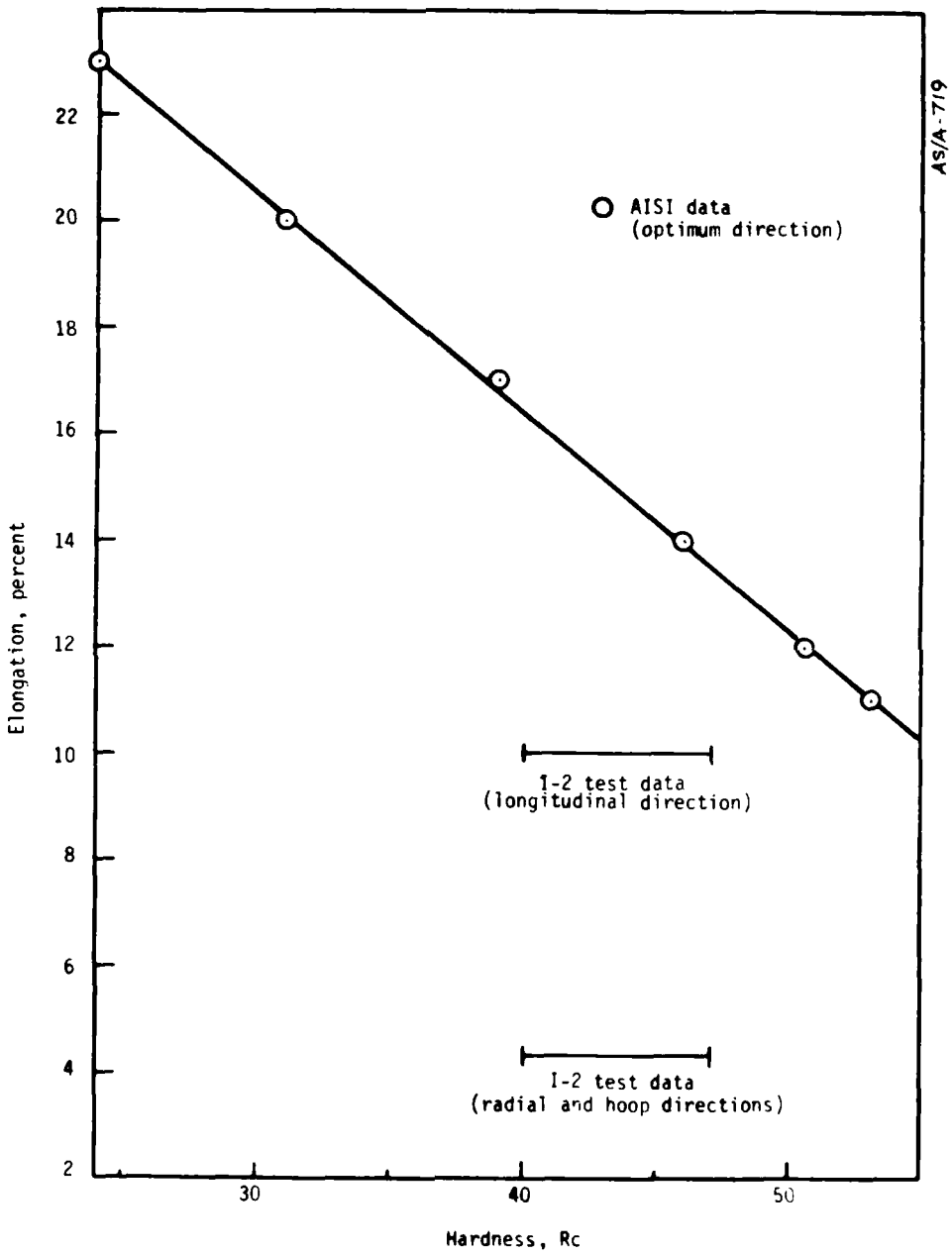

Figure 57. 4340 elongation versus hardness.

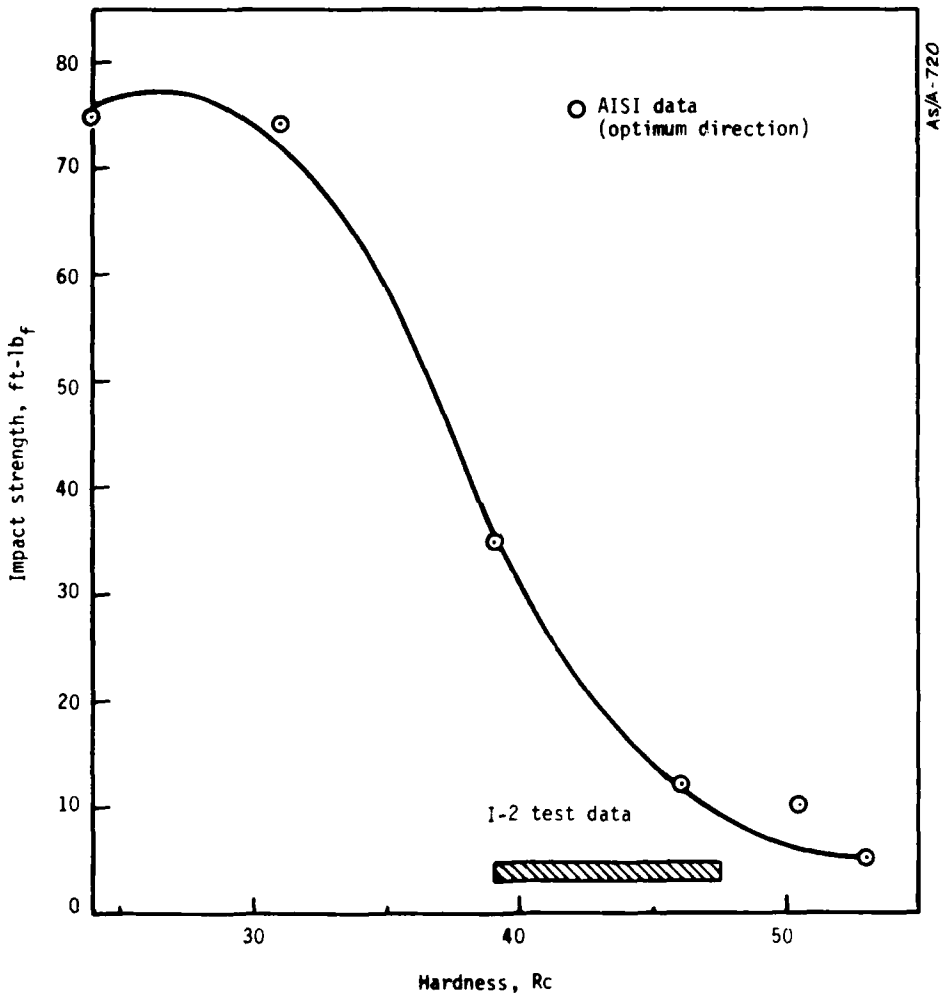

Figure 58. 4340 impact strength versus hardness.

B.3 I-3 INJECTION BLOCK

B.3.1 Summary

The forging purchased for I-3 was from a vacuum-degassed aircraft quality 4340 casting. The forging as purchased had undergone some reduction, but to improve its mechanical properties additional upsetting was performed to result in an 8 to 1 reduction. A 2.54-cm (1-inch) thick slab was cut from one end of the forging prior to the additional upsetting. The outer diameter was then turned down to 25.4 cm (10 inches) following the upsetting and a 5.48-cm (2.156-inch) bore was machined down the center. A 17.8-cm (7-inch) thick slab was cut from each end. The remaining forging material was machined into the I-3 injection block.

A piece of the 2.54-cm (1-inch) thick slab underwent metallographic examination to observe grain size and inspect for inclusions. Grain size was between ASTM 7 and 8, which is approximately the grain size specified when the forging was purchased. Several 0.4-mm (15-mil) inclusions were also observed.

Prior to heat treating the I-3 test injection block, it was decided to send the 17.8-cm (7-inch) thick end pieces through two different heat treatments. One end piece was sent through a conventional heat treat where it was austenitized, oil quenched, and tempered. The other end piece was sent through an unconventional heat treat in which it was austenitized, quenched in a hot salt bath, air cooled, and tempered. Charpy, tensile, and metallographic samples were cut from each piece.

Tests on the unconventional heat treat indicated that further development would be required if it was to be used for the injection block heat treat. Tests of the conventional heat treat (end piece 1) indicated that it produced satisfactory mechanical properties. Hardness traverses showed large variations due to an unhomogeneous forging possibly containing retained austenite.

It was decided to heat treat the I-3 test injection block by the conventional heat treat with a slight modification to freeze out retained austenite. A large piece of each of the 17.8-cm (7-inch) end pieces was sent through the heat treat with the I-3 injection block. Rc hardness traverses were made on the end pieces after reheat treat. Hardness variations were not as great as observed in the original conventional heat treat. Observed hardnesses were between 32 to 27 Rc.

Ultrasonic tests of the I-3 test injection block following heat treat showed that it was free of cracks. The injection block was magnafluxed. This revealed several inclusions approximately 1 cm long. The inclusions observed were not near critical port regions. Following the I-3 test, the injection block was again ultrasonically tested. No cracks were observed.

B.3.2 Upsetting and Forging Details

In order to improve the transverse properties, the forging was upset at 1204°C (2200°F) by a 3 to 1 reduction. The original size was a 61-cm (24-inch) by 30-cm (12-inch) square, upset to a 20-cm (8-inch) by 61-cm (24-inch) round, then forged to a 76-cm (30-inch) by 27.5-cm (10.5-inch) round. The upsetting was carried out at Western Forge. The basic forging was produced by Copperweld Steel from an air-melted casting which was vacuum degassed to produce aircraft quality 4340 steel. The casting size was a 152-cm (60-inch) by 69-cm (27-inch) square, reduced 5 to 1 to a 300-inch by 30-cm (12-inch) square, and a 61-cm (24-inch) length was cut off and sent to Western Forge. The overall reduction after upsetting was 8 to 1.

B.3.3 Experimental Heat Treatments

The two experimental heat treatments carried out on 7-inch thick test samples were as follows:

End piece 1: (conventional heat treat)
- Austenitize at 843°C (1550°F) for 2 hours
- Oil quench to room temperature
- Temper at 552°C (1025°F) for 3 hours

End piece 2: (unconventional heat treat)
- Austenitize at 843°C (1550°F) for 2 hours
- Salt bath quench (austemper) at 324°C (615°F) for 1.5 hours
- Air cool
- Temper at 552°C (1025°F) for 3 hours

End piece 1 was heat treated conventionally to produce an Rc value of about 35. End piece 2 was heat treated to produce more uniform properties thorough the thick section by quenching in a salt bath, thereby minimizing the cooling gradient but producing a bainitic steel instead of a martensic one. When tempered, tempered bainite is obtained.

Test results on end piece 2 showed the hardness values to be uniform but fairly low (26 to 29 Rc), strength to be uniform but moderate (7.2-kbar (105-ksi yield)) and good elongation (8 to 16 percent). However, the Charpy values were only fair (28 Joules (21 ft-lb_f) axially and 15 Joules (11 ft-lb_f) in the other two directions). The microstructure was uniform, fine tempered bainite. Consequently, the properties can be considered to be marginal, but may be improved by reduced tempering.

Test results on end piece 1 showed a nonuniform hardness profile (16 to 35 Rc), good strength (8.3 to 10 kbar (120 to 145 ksi)), and generally good elongation (8 to 14 percent except in the circumferencial direction where it was only 3.5 percent). The Charpy values were good (64 Joules (47 ft-lb_f) axially, 33 Joules (24 ft-lb_f) radially, and 20 to 24 Joules (15 to 18 ft-lb_f) circumferentially). The microstructure was martensitic with some bainite and ferrite in the regions away from the surface.

Test results of end piece 1 indicated that there were problems with the original forging quality. These are as follows:

1. Poor hardenability. The hardness drops rapidly with the distance from the surface to low values -- one traverse as low as 16 Rc, another traverse of 22 Rc. (These are even lower than the as-forged value of 26 Rc.) A more normal profile would drop down to around 29 Rc in the center. Consequently, interior regions of this 4340 steel are not as hardenable as they should be.
2. There are soft spots and hard spots in the material. Points close to each other (near the center) are as low as 16 Rc and as high as 33 Rc (surrounded by 24 Rc material). This indicates that there is alloy segregation and nonuniformity, with depleted regions behaving like carbon steel (yield of around 3.1 kbar (45 ksi)) and hard carbide regions which are brittle (and can account for the low elongation in one sample).

In view of the developmental nature of the unconventional heat treatment, it was decided to proceed with the conventional heat treatment modified by a subzero quench to transform the retained austenite and avoid deleterious ferrite formation.

B.3.4 I-3 Injection Block Heat Treatment

The I-3 injection block was heat treated as follows:

- Austenitized at 843°C (1550°) for 4 hours
- Oil quenched in agitated bath for 0.5 hours
- Low temper treatment at 204°C (400°F) for 4 hours
- Air cooled
- Quenched in a dry ice-alcohol mixture for 4 hours at -61°C (-77°F)
- Tempered at 538°C (1000°F) for 4 hours

Pieces of the 17.8-cm (7-inch) thick end pieces were sent through the heat treatment with the I-3 injection block for subsequent mechanical testing.

B.3.5 I-3 Injection Block Properties

Examination of the "as forged" microstructure indicated that the ASTM grain size had increased slightly to between ASTM 6 and 7 as a result of upsetting (it was originally between 7 and 8). Inclusion size appears to be under 0.4 mm (15 mils), well under the critical size.

Examination of the test pieces heat treated with the forging indicated that the ultrasonic tests were negative in picking up the presence of defects and magnafluxing resulted only in the observance of three inclusions (as long as 1.3 cm (1/2 inch)) near the center of the surface.

The hardness traverse averaged as follows: 31 Rc in the regions up to one-third the way in from any surface and 29 Rc in the interior. The highest reading was 35 Rc and the lowest was 26 Rc. The soft regions were eliminated by the subzero quench. However, the hardenability is still below standard, and there were both gross and local variations in hardness.

End piece 1 was quite erratic in hardness readings on a local scale and also did not harden as much as end piece 2, presumably because of compositional (alloy) differences since both pieces were identically heat treated. There appeared to be a loss of hardness (decarburization) at the surface of both pieces, with the hardness dropping down to approximately 29 Rc. A hardness of 36 Rc was requested.

B.3.6 Conclusions

The forging is substandard, with significant alloy segregation impairing uniformity in hardenability and in structure. Homogenizing and grain refining the structure prior to machining would have improved the

forging. But it must be emphasized that only a partial improvement would have resulted: local (but not gross) variations would have been somewhat reduced. Elimination of the soft spots in the I-3 injection block has been accomplished. Consequently, the main problems are:

- The presence of large inclusions
- Alloy variation in composition
- Probable surface decarburization

B.4 I-5 INJECTION BLOCK

B.4.1 Summary

The I-5 test injection block was machined from the actual forging purchased for the 1/4-scale launcher injection block. The forging was vacuum-degassed aircraft quality 4340.

Two injection ports were machined into the I-5 forging prior to heat treat. During machining, a trepanned core was removed from each port location. These cores were inserted into holes drilled into one of the I-2 injection block halves. With these cores in place, the I-2 half-block was sent through the same heat treatment as the I-5 injection block. At the end of the heat treatment, the cores were tested for metallographic and mechanical properties. Results indicated the I-5 injection block condition after heat treatment. Test results on the cores indicated the I-5 block to have a very uniform hardness. Material properties were good. The toughness was adequate, but still not as high as desired.

A description of the forging, heat treatment and metallurgical test results follows.

B.4.2 Forging

The forging was vacuum-degassed 4340 obtained from Armco Steel Corporation. It had been subjected to a postforge heat treatment of normalizing at 899°C (1650°F) for 12 hours and tempering at 649°C (1200°F) for 16 hours. However, the forging was not homogenized.

It was reduced 4.4 to 1 from a 125-cm (49-inch) round casting to a 61-cm (24-inch) round, and then 6 to 1 to a 48.9 (19-1/4-inch) round. These reductions are marginal as far as breaking down the cast structure. Furthermore, there has been no upsetting of the forging, resulting in somewhat poorer transverse ductility and toughness. However, the normalizing treatment should improve the uniformity of the forging.

B.4.3 Heat Treating

Two radial test bars were obtained from the forging for heat treating simultaneously with the forging. In order to be representative of the main body of the forging (away from the ends), the test bars were imbedded in large blocks of 4340 of roughly the same cross section as the forging.

The forging was heat treated at Certified Steel Corporation in Los Angeles. Handling of the 3400 kb (7500 lb_m), 213-cm (7-foot) long forging was carried out by threading in three stainless steel eye bolts to the small end (19-1/4-inch diameter) of the forging to a depth of 10 cm (4 inches).

The forging was first preheated 5 hours at 316°C (600°F) in air, followed by intermediate heating of 8 hours at 538°C (1000°F) in air. In this manner, the heating was gradual and thermal stressing of the 20-cm (8-inch) thick walls of the forging was kept low. The forging was then transferred to a 829°C (1525°F) furnace with endothermic (nonoxidizing) gas for 6 hours and then quenched in an agitated oil bath for 3 hours. The transfer time into the quench oil was less than 1 minute. All furnaces were electric with a fan circulating the air (or gas) and controlled to within 4°C (7°F) at all furnace height levels. The furnaces were 12-meter (40-foot) deep pit furnaces, and the top of the forging fit 224 cm (8 feet) below an extra door lid to which it was attached. (Door lids are switched on inserting the forging into the pit.) The forging was quenched with its top 183 cm (6 feet) below the surface of the oil until its temperature reached 66°C (150°F) (3 hours). The oil temperature simultaneously rose from 21° to 38°C (70°F to 110°F). The forging was then removed from the oil and washed at 71°C (160°F) in a caustic solution.

The first temper was in air at 510°C (905°F) for 8 hours and was preceded by a preheat at 316°C (600°F) in air for 5 hours. The part was air cooled to essentially room temperature prior to a second temper. The second preheat was 2 hours at 316°C (600°F) in air followed by a second temper of 6 hours at 538°C (1000°F) and 2 hours at 552°C (1025°F), both in air. The part was then air cooled.

8.4.4 Test Results

Hardness readings were taken on the top of the part after both tempers. The Rockwell hardness averaged 38 after the first temper and 36 after the second temper.

Test pieces (embedded in an 46-cm (18-inch) section of the I-2 injection block) were heat treated simultaneously. Hardness readings were taken after the quench and after both tempers. The data were used to help determine the tempering treatment on the large part in order to arrive at the desired hardness level. The Rockwell C data were as follows from OD to ID at 2.54-cm (1-inch) intervals:

After quench:	46.0, 37.5, 38.0, 37.5, 38.5, 39.5, 38.0, 39.5, 46.0
After first temper:	38.0, 35.0, 33.0, 35.0, 34.0, 35.0, 36.0, 36.0, 39.0
After second temper:	37.0, 34.0, 33.0, 35.0, 34.0, 35.0, 32.5, 32.0, 37.0

The (gross) hardness profile was remarkably uniform, achieving the desired narrow range of 5 points (32 to 37) along the 20-cm (8-inch) thickness, whereas 8 to 10 points is more commonly achieved. However, there were severe short-range variations in hardness. Segregation is present in the injection block in the order of 2.3 mm (0.091 inch). Specifically, there is banding (stringers) consisting of alternating regions of hard martensite (Y.S. ≈12.4 kbar (180 ksi)) and softer bainite plus ferrite (Y.S. ≈8.3 kbar (120 ksi)). Their diameters are approximately 0.25 mm (0.01 inch) wide for the martensite and approximately 0.5 mm (0.02 inch) (0.75 mm maximum) for the bainite plus ferrite. The lengths of these elongated stringers average 5 mm (0.20 inch), but some may be as long as 10 mm (0.40 inch). The stringers are oriented in the axial direction. Microhardness measurements on these stringers indicate that the martensite region hardness is 45 Rc and the bainite region hardness is approximately 33.5 Rc, which corresponds to the estimated 12.4- and 8.3-kbar) (180- and 120-ksi) yield, respectively.

This banding of alternating hard and soft regions has resulted in very poor Charpy impact values in the range 15 to 20 Joules (11 to 15 ft-lb_f), which makes the toughness of this forging marginal. At the existing hardness and strength level, the Charpy impact values for this forging should have been around 81 Joules (60 ft-lb_f) in the axial direction and on the order of 40 Joules (30 ft-lb_f) in the

circumferential and radial directions. The lower values measured reflect the segregated banded structure of alternating strength, which causes a notch effect. The causes of the banded structure relate back to the original forging which had only a 6 to 1 reduction, while at least a 10 to 1 reduction is desirable for breaking down the cast structure completely. Consequently, we have alloy segregation resulting from the remnants of the cast structure, and it is this segregation which is responsible for the banded structure: the regions higher in alloying elements form the harder martensite, and the regions lower in these elements form the softer bainite and ferrite.

The mechanical properties are shown in Table 12. The hardness profile is relatively even in a narrow range about 34 Rc (except for a skin hardness of 37 Rc at both the ID and OD).

Two radial tensile specimens were tested, with the test sections representative of regions 8.9 and 16.5 cm (3.5 and 6.5) inches, respectively, from the OD. Test results from the two specimens were essentially identical, confirming the results of the hardness tests. The ultimate tensile values were 10 kbar (145 ksi) at both locations, with a corresponding yield strength of 8.4 kbar (122 ksi) at each location. The tensile elongations were both 13 percent and the reductions in area were 37 and 35 percent, respectively. The strength values are in excellent agreement with the properties expected from a thick section of 4340, except that the elongation and reduction in area values are somewhat lower than the anticipated 16 and 44 percent, respectively. Fibrous fractures were observed.

Twin radial Charpy impact specimens were tested, each one with axial and circumferential notch directions at two locations 2.54 and 12.7 cm (1 and 5 inches) from the OD. The impact values were 19 and 16 Joules (14 and 12 ft-lb_f), respectively, in the axial direction, and 14 and 15.5 Joules (11 and 11.5 ft-lb_f), respectively, in the circumferential direction. Single radial Charpy specimens were tested with an axial notch direction 7.6 and 17.8 cm (3 and 7 inches) from the OD. The impact values were 17 and 20 Joules (12.5 and 15 ft-lb_f,) respectively. All of these values are considerably lower than anticipated values in excess of 68 Joules (50 ft-lb_f). Fibrous fractures were observed on all Charpy specimens, with the fibers running in the axial direction.

TABLE 12. I-5 TEST DATA

Distance from OD (inches)	Hardness (Rc)	Charpy Impact		U.T.S. (ksi)[b]	Y.S. (ksi)[b]	El (5)	R.A. (%)
		Axial (ft-lb_f)[a]	Circumferential (ft-lb_f)[a]				
0 (OD)	37	--	--	--	--	--	--
1	34	14	11	--	--	--	--
2	33	--	--	--	--	--	--
3	35	12.5	--	--	--	--	--
3.5	--	--	--	145.4	122.3	13	37
4	34	--	--	--	--	--	--
5	35	12	11.5	--	--	--	--
6	32.5	--	--	--	--	--	--
6.5	--	--	--	145.0	121.9	13	36
7	32	15	--	--	--	--	--
8 (ID)	37	--	--	--	--	--	--

[a]Joule = 0.7376 ft-lb_f
[b]kbar = 14.5 ksi

B.4.5 Conclusions

Large forgings present a significant problem in obtaining uniform mechanical properties. Control of inclusions requires that high quality vacuum-melted material be used. Uniformity of structure requires that the material be hot worked at least 10 to 1 and be upset, homogenized, and normalized. Homogenization of I-5 (at 1066°C (1950°F)) would have removed the remnants of alloy segregation present in the cast structure which had already been broken down by the hot forging (at 1204°C (2200°F)). The banding would not have been present and the toughness and ductility would have been considerably improved. Alternate "gun steels" to 4340 exist that are higher in alloys such as molybdenum, chromium, nickel, and vanadium, with superior fracture toughness. However, the success of the I-5 test verifies the injection block as adequate for the 1/4-scale launcher.

Heat treatment of forgings along with test specimens for mechanical testing provide a means for controlling the heat treatment and optimizing the mechanical properties.

Tests indicate that the designs that have evolved for the drivers, driver-to-injection-block diaphragms, seals, and injection block are adequate for the subscale demonstration. Injection timing has been established, and early problems concerning fluidynamic and structural dynamic performances have been resolved. The technical requirements to complete the demonstration of the hybrid launch concept are outlined.

DISTRIBUTION LIST

DEPARTMENT OF DEFENSE

Assistant to the Secretary of Defense
Atomic Energy
ATTN: Executive Assistant

Defense Advanced Rsch. Proj. Agency
ATTN: TIO

Defense Communications Agency
ATTN: CCTC

Defense Intelligence Agency
ATTN: DT-2
ATTN: DB-4D
ATTN: DT-1C

Defense Nuclear Agency
ATTN: STSP
ATTN: SPAS
ATTN: SPSS
ATTN: SPTD
4 cy ATTN: TITL

Defense Technical Information Center
12 cy ATTN: DD

Field Command
Defense Nuclear Agency
ATTN: FCTMOF
ATTN: FCTMD
ATTN: FCTMOT
ATTN: FCPR

Field Command
Defense Nuclear Agency
Livermore Division
ATTN: FCPRL

Joint Chiefs of Staff
ATTN: SAGA/SSD
ATTN: J-5 Force Planning & Program Div.
ATTN: SAGA/SFD
ATTN: J-5 Nuclear Division

Joint Strat. Tgt. Planning Staff
ATTN: JPTM
ATTN: JLTW-2

NATO School (SHAPE)
ATTN: U.S. Documents Officer

Undersecretary of Def. for Rsch. & Engrg.
ATTN: Engineering Technology, J. Persh
ATTN: Strategic & Space Systems (OS)

DEPARTMENT OF THE ARMY

BMD Advanced Technology Center
Department of the Army
ATTN: ATC-T, M. Capps

BMD Systems Command
Department of the Army
ATTN: BMDSC-H, N. Hurst

DEPARTMENT OF THE ARMY (Continued)

Deputy Chief of Staff for Ops. & Plans
Department of the Army
ATTN: DAMO-NCZ

Deputy Chief of Staff for Rsch. Dev. & Acq.
Department of the Army
ATTN: DAMA-CSS-N

Harry Diamond Laboratories
Department of the Army
ATTN: DELHD-N-TF
ATTN: DELHD-N-P, J. Gwaltney

U.S. Army Ballistic Research Labs.
ATTN: DRDAR-BLE, J. Keefer
ATTN: DRDAR-BLT, R. Vitali
ATTN: DRDAR-BL, R. Eichelberger
ATTN: DRDAR-BLV, W. Schuman, Jr.
ATTN: DRDAR-BLV
ATTN: DRDAR-BLT, J. Frasier

U.S. Army Material & Mechanics Rsch. Ctr.
ATTN: DRXMR-HH, J. Dignam

U.S. Army Materiel Dev. & Readiness Cmd.
ATTN: DRCDE-D, L. Flynn

U.S. Army Missile Command
ATTN: DRDMI-XS
ATTN: DRSMI-RKP, W. Thomas
ATTN: DRDMI-TRR, B. Gibson

U.S. Army Nuclear & Chemical Agency
ATTN: Library

U.S. Army TRADOC Systems Analysis Activity
ATTN: ATAA-TDC, R. Benson

DEPARTMENT OF THE NAVY

Naval Research Laboratory
ATTN: Code 6770, G. Cooperstein
ATTN: Code 2627
ATTN: Code 7908, A. Williams

Naval Sea Systems Command
ATTN: SEA-0352, M. Kinna

Naval Surface Weapons Center
ATTN: Code R15, J. Petes
ATTN: Code F31
ATTN: Code K06, C. Lyons

Naval Weapons Evaluation Facility
ATTN: P. Hughes
ATTN: L. Oliver

Office of Naval Research
ATTN: Code 465

Office of the Chief of Naval Operations
ATTN: OP 604E14, R. Blaise
ATTN: OP 604C
ATTN: OP 604C3, R. Piacesi

DEPARTMENT OF THE NAVY (Continued)

Strategic Systems Project Office
Department of the Navy
ATTN: NSP-272

DEPARTMENT OF THE AIR FORCE

Aeronautical Systems Division
Air Force Systems Command
2 cy ATTN: ASD/ENFTV, D. Ward

Air Force Flight Dynamics Laboratory
ATTN: FXG

Air Force Geophysics Laboratory
ATTN: LY, C. Touart

Air Force Materials Laboratory
ATTN: MBC, D. Schmidt
ATTN: MBE, G. Schmitt
ATTN: LLM, T. Nicholas

Air Force Rocket Propulsion Laboratory
ATTN: LKCP, G. Beale

Air Force Systems Command
ATTN: SOSS
ATTN: XRTO

Air Force Weapons Laboratory
Air Force Systems Command
ATTN: DYS
ATTN: DYV
ATTN: DYV, A. Sharp
ATTN: DYT
ATTN: SUL
ATTN: HO, W. Minge
2 cy ATTN: NTO

Arnold Engineering Development Center
Air Force Systems Command
ATTN: Library Documents
ATTN: VKF, G. Callens
ATTN: VKF, H. Ball
ATTN: VKF, Capt J. Scott
ATTN: G. Norfleet

Ballistic Missile Office
Air Force Systems Command
ATTN: MNR, Lt Col McCormick
ATTN: MNNXH
ATTN: MNRTE, Capt Wheaton
ATTN: MNRTE, Maj Yelmgren

Deputy Chief of Staff
Operations Plans and Readiness
Department of the Air Force
ATTN: AFXOOSS

Deputy Chief of Staff
Research, Development, & Acq.
Department of the Air Force
ATTN: AFRD
ATTN: AFRDQSM

Foreign Technology Division
Air Force Systems Command
ATTN: TQTD
ATTN: SDBS, J. Pumphrey
ATTN: SDBG

DEPARTMENT OF THE AIR FORCE (Continued)

Headquarters Space Division
Air Force Systems Command
ATTN: DYS
ATTN: YNAT

Headquarters Space Division
Air Force Systems Command
ATTN: RSS
ATTN: RST
ATTN: RSSE

Strategic Air Command
Department of the Air Force
ATTN: DOXT
ATTN: XPFS
ATTN: XPQM
ATTN: XOBM

DEPARTMENT OF ENERGY

Department of Energy
ATTN: OMA/RD&T

DEPARTMENT OF ENERGY CONTRACTORS

Lawrence Livermore Laboratory
ATTN: L-125, J. Keller

Los Alamos Scientific Laboratory
ATTN: J. Taylor

Sandia Laboratories
ATTN: H. Rarrick

Sandia Laboratories
Livermore Laboratory
ATTN: Library & Security Classification Div.

DEPARTMENT OF DEFENSE CONTRACTORS

Acurex Corp.
ATTN: C. Nardo
ATTN: R. Rindal
2 cy ATTN: K. Suchsland
2 cy ATTN: W. Lowe

Aerospace Corp.
ATTN: H. Blaes
2 cy ATTN: H. Dyner

Analytic Services, Inc.
ATTN: J. Selig

AVCO Research & Systems Group
ATTN: J. Stevens
ATTN: W. Broding
ATTN: Document Control
ATTN: J. Gilmore

Battelle Memorial Institute
ATTN: E. Unger
ATTN: M. Vanderlind

Boeing Co.
ATTN: B. Lempriere
ATTN: R. Holmes

California Research & Technology, Inc.
ATTN: K. Kreyenhagen

DEPARTMENT OF DEFENSE CONTRACTORS (Continued)

Calspan Corp.
ATTN: M. Holden

Effects Technology, Inc.
ATTN: R. Wengler
ATTN: R. Parisse

General Electric Co.
ATTN: D. Edelman

General Electric Co.
ATTN: P. Cline

General Electric Company—TEMPO
ATTN: DASIAC

General Research Corp.
ATTN: T. Stathacopoulos

General Research Corp.
ATTN: R. Patrick

Institute for Defense Analyses
ATTN: J. Bengston
ATTN: Library

Kaman Avidyne
ATTN: E. Criscione

Kaman Sciences Corp.
ATTN: T. Meagher
ATTN: F. Shelton

Lockheed Missiles & Space Co., Inc.
ATTN: F. Borgardt

Lockheed Missiles & Space Co., Inc.
ATTN: R. Walz

Martin Marietta Corp
ATTN: G. Aiello

McDonnell Douglas Corp.
ATTN: J. Garibotti
ATTN: H. Berkowitz
ATTN: E. Fitzgerald
ATTN: H. Hurwicz
ATTN: L. Cohen

National Academy of Sciences
ATTN: D. Groves

Pacific-Sierra Research Corp.
ATTN: H. Brode
ATTN: G. Lang

Payne, Inc.
5 cy ATTN: J. Huntington
5 cy ATTN: T. Dahn

Physics International Co.
ATTN: J. Shea

DEPARTMENT OF DEFENSE CONTRACTORS (Continued)

Prototype Development Associates, Inc.
ATTN: J. McDonald
ATTN: J. Dunn

R & D Associates
ATTN: P. Rausch
ATTN: F. Field
ATTN: C. MacDonald
ATTN: J. Carpenter

Rand Corp.
ATTN: J. Mate

Science Applications, Inc.
ATTN: D. Hove
ATTN: J. Warner
ATTN: G. Ray

Science Applications, Inc.
ATTN: G. Burghart

Science Applications, Inc.
ATTN: W. Layson
ATTN: W. Seebaugh
ATTN: J. Cockayne

Science Applications, Inc.
ATTN: A. Martellucci

Southern Research Institute
ATTN: C. Pears

SRI International
ATTN: G. Abrahamson
ATTN: H. Lindberg
ATTN: P. Dolan

Sverdrup/ARO, Inc.
ATTN: R. Smith
ATTN: H. Lewis

System Planning Corp.
ATTN: F. Adelman

Systems, Science & Software, Inc.
ATTN: G. Gurtman

TRW Defense & Space Sys. Group
ATTN: W. Wood
ATTN: P. Brandt
ATTN: D. Baer
ATTN: G. Arenguren

TRW Defense & Space Sys. Group
ATTN: L. Berger
ATTN: E. Wong
ATTN: V. Blankenship
ATTN: E. Allen
ATTN: W. Polich

EN

DAT

FILM

8—

DT